Sherry Stephanie Chan

The Effect of Osmotic Pressure on *Rigor Mortis* in Salmonids

Trondheim, June 2016

NTNU – Trondheim
Norwegian University of
Science and Technology

DTU
Technical
University of
Denmark

NTNU – Trondheim
Norwegian University of
Science and Technology

DTU Technical
University of
Denmark

The Effect of Osmotic Pressure on *Rigor Mortis* in Salmonids

Sherry Stephanie Chan

Master of Science in Aquatic Food Production - Safety and Quality
Submission date: June 2016
Supervisors: Rolf Erik Olsen, NTNU
Flemming Jessen, DTU
Co-supervisor: Turid Rustad, NTNU

Norwegian University of Science and Technology
Technical University of Denmark

Acknowledgements

First and foremost, I would like to express my heartfelt gratitude to my NTNU supervisor, Professor Rolf Erik Olsen, for his infinite support, enthusiasm and constructive advices during the development of my thesis. His continuous guidance has allowed me to understand the subject in a wider viewpoint and helped in presenting a good discussion in this study.

Special thanks to Erik Slinde from the Institute of Marine Research, who has also showed immense interest with regards to my research and for sharing his profound knowledge.

I would further like to thank my supervisor from DTU, Flemming Jessen, and co-supervisor from NTNU, Turid Rustad, for their valuable comments with regards to the improvements of my thesis.

My sincere gratitude goes also to senior engineer Tora Bardal from NTNU Sealab, for teaching me the different techniques in laboratory. In addition, a thank you to the staff from the Institute of Marine Research for permission and help with using the research facilities.

This period of my master study has been very insightful, not only as a professional experience but also as a great human exposure. This would not be possible without the endless love and support from my family, especially my parents, who continuously motivate me to achieve higher targets.

Abstract

Rigor mortis is a natural phenomenon caused by a series of complicated chemical changes in the muscles after the death of an animal. This concept is important especially in meat technology since it affects texture, yield and meat palatability. However, the understanding of *rigor mortis* in animals is currently not fully discovered, and research is still ongoing. The rigor process is frequently explained by the sliding filament theory, where actomyosin bridges form and cause stiffness during rigor. Yet adenosine triphosphate (ATP) concentration gradually depletes as the muscle enters rigor, so little or no ATP is available for rigor resolution and muscles remain stiff. Hence, this theory does not explain the rigor resolution process, where muscles eventually become soft and limp.

An alternative hypothesis of *rigor mortis* is postulated describing the rigor process via changes in osmotic pressure in muscle cells. Since catabolic reactions (glucose to lactate) predominate after death, the number of molecules inside muscle cells increase. This induces an increase in osmotic pressure and water flows into the cells to achieve osmotic equilibrium between compartments, thus creating stiffness. Therefore, this thesis investigates the hypothesis by analysing the movement of water in muscles immersed in solutes of varying salinities, together with texture and morphological analysis.

It was found that mass changes in salmonid muscles were significantly affected by the movement of water in different salinities, and were independent with the contraction rates. Rigor index measurements showed that the individual fish reached 63.2% of their maximum rigor within 4 to 6 hours *post mortem*. Shear force was expected to be highest at this time point but texture analysis did not follow the same trend and gave a general decrease in breaking force. Even so, there were high variations observed with the individual texture measurements explained by multiple reasons. The effect of formalin fixation also revealed that prolonged fixation of muscle tissues can lead to cell shrinkage. Morphological analysis of muscle cells by image processing in Matlab further showed that there were distinct differences in the amount of intra and extracellular spaces and inter-fibre distances from the tissue surface and center in the various solutions.

Contents

List of Figures

List of Tables

List of Acronyms

Ach acetylcholine

ADP adenosine diphosphate

ANOVA Analysis of Variance

ATP adenosine triphosphate

DFD dark, firm and dry

ECF extracellular fluid

ECS extracellular space

ICF intracellular fluid

ICS intracellular space

IR rigor index

MS-222 tricaine mesylate

NBF neutral buffered formalin

PAS Periodic acid-Schiff

Pi inorganic phosphate

PSE pale, soft and exudative

TN troponin

TM tropomyosin

TPA texture profile analysis

WHC water holding capacity

Chapter 1

Introduction

The general supply of seafood in the world is shifting towards aquaculture. Aquaculture production has been increasing at an impressive rate over the past decades and is now the fastest growing animal food production system in the world. At the same time, fish consumption has soared from 10 kg in 1960s to 19 kg per capita in 2012 (FAO, 2014). This change is due to higher demands from a growing population, better incomes and more efficient distribution networks.

Atlantic salmon *(Salmo salar)* is currently one of the most valuable and intensively farmed species in modern industrialized aquaculture, occupying 70% (2.4 million tonnes) of the market (Deike, 2014). The salmonid market has expanded geographically, with the EU and USA being the largest traditional markets (Möller, 2007). Norway is the world's largest producer of Atlantic salmon. In 2014, the total supply of all farmed salmonids has exceeded two million tonnes (Marine Harvest, 2015). As salmon is high in protein, omega-3 fatty acids and has low content of saturated fats, it is increasingly becoming a popular demand as nutritious food (Rahman, 2007). With this comes greater expectations from both producers and consumers to deliver and achieve fish products as high quality as possible. The producers have now shifted their industrial focus from a traditional quantity-driven production to a quality-driven production. It is therefore important to fully understand the different factors that determines fish quality and quantity, and one of them is the concept of *rigor mortis*.

Rigor mortis, or rigor, is a general phenomenon in all animals, and is defined as the stiffening of muscle shortly after an animal's death. This process converts muscle to meat. After the harvest of marine, freshwater or aquaculture fish, the fish undergo three stages of *rigor mortis*: pre-rigor, rigor maximum and rigor resolution. Immediately after death the muscles are soft and limp, where the flesh is said to be in the pre-rigor condition. Eventually the muscles start to stiffen and is said to be at rigor maximum. After some hours or days rigor resolution follows

where the muscles gradually begin to relax and pass through rigor.

For industrial meat producers, the concept of rigor is essential to optimise slaughter and processing procedures. The meat must undergo rigor in an optimal way to obtain the best meat quality. The state of rigor in fish has a vital influence on quality in that it influences gaping[1], excess thaw drip, meat toughness and gives rise to changes in texture (Lucas and Southgate, 2012). However, the main problem is that up to date all mechanisms and biochemical reactions involved *post mortem*, and how these affect meat quality and quantity, are complex and not fully understood (Devine et al., 1999; Skjervold et al., 2001; Slinde et al., 2003; Lynum and Rustad, 2005).

One of the many current challenges that needs to be done in the fish industry today is to provide a better scientific explanation of muscle contraction in fish (Balevik, 2004; Lynum and Rustad, 2005). Muscle contraction during rigor is commonly described by the sliding filament theory. This theory explains that contraction occurs via the formation of actomyosin bridges, using ATP in the process. As ATP is progressively used up after death, the actomyosin bridges cannot resolute and remain intact. Therefore this theory cannot justify rigor resolution when muscles have passed through rigor to become soft and limp again.

Since resolution of *rigor mortis* cannot be explained by the depletion of ATP, the alternative hypothesis is then that rigor and resolution is due to osmolar changes inside the muscle cells. Osmolarity is a numerical characteristic which results from the breakdown of cell material and the increased number of molecules/ions within the cell. This provides increased water transport into the cell and stiffness. When this water is leaking out, rigidity disappears. So *rigor mortis* resolves due to the rupture of the cell membranes and the tension disappears, leading to rigor resolution. Therefore, the development of rigor can possibly be explained by the changes in osmotic pressure ($\Pi = cRT$)[2].

1.1 Scope and Methodology

The aim of this project is to explore the alternative hypothesis of rigor and provide evidences that changes in osmotic pressure and flow of water into the cells is the main cause of the felt stiffness in *rigor mortis*. This was done by analysing the movement of water in salmonid muscles embedded in solutes of increasing salinity. Fish was selected as the animal model to study rigor as they have different muscle types that are well separated with low amount of connective tissues. Since rigor is a general phenomenon in all animals, the theory of *rigor mortis* can be applied for

[1] Gaping is a phenomenon where individual muscle flakes separate. This can result from high temperatures, especially if the glycogen content is high.

[2] Π is the osmotic pressure, c is the molar concentration of solute ions in solution, R is the gas constant and T is the temperature.

fish, reptiles, birds and mammals.

Experiment 1, a preliminary experiment, was carried out to analyse mass and contraction through the rigor process on small pieces of salmonid muscle in solutions of varying salinity. To increase the intracellular metabolite production, solutes containing glucose were also used.

In Experiment 2, whole muscle fillets were used for dimension and shear force measurements. The tail bending method was done to estimate the time of rigor. Muscle samples were sent for histology analysis for morphological examination.

To prevent build-up of intracellular pressure, some samples were treated with the detergent saponin to puncture cell membranes in Experiment 3. Histology analysis and cell morphology were also performed to measure the effect of solutes and rigor process on cell shape, appearance and the partition of solutes between intra and extracellular spaces.

Small adult fish were utilized in the experiments because they have less fat content. The white fibres of the fish were chosen for observation as they form the bulk of the musculature. They also display exceptional composite homogeneity, lessening the variation between muscle fibres. In the experiments, fillet skins were left on with the muscle during analysis to prevent errors from handling and sliding of muscle. The loss of osmotic properties that accompanies the onset of rigor is therefore independent of the anatomical arrangement of fibres in the muscle.

1.2 Organization of Thesis

A total of three experiments were done. The work for this thesis has been an incremental process, and is presented as such. Chapter 2 forms the background, offering mostly theoretical introductions to the topics covered in this thesis, including a thorough explanation of the alternative hypothesis. Chapter 3 covers the materials and methods while Chapter 4 gives the results obtained in each experiment. Next, Chapter 5 contains the discussion and evaluation of the experiments. As the concluding part of the thesis, Chapter 6 provides the conclusion of all the work done, with some additional reflections and suggestions for future work.

Chapter 2

Theoretical Background

This chapter introduces some background theory regarding this thesis and consists of five main sections. The first section gives a general introduction on fish quality while the second section illustrates the fish musculature in a macro and microscopic scale. The third section explains water in fish muscle and the principle of osmosis and Donnan equilibrium. Next, the fourth section describes the generally accepted sliding filament theory of *rigor mortis* and its challenges. This forms the basis of the alternative hypothesis in the final section.

2.1 Fish Quality

The term quality in fish is generally described by five components: healthiness (nutritional quality), safety (hygienic quality), serviceability (ease of use, prices), satisfaction (organoleptic quality) and animal welfare (ethical quality) (Listrat et al., 2016). Satisfaction is often driven by technological qualities like texture, pH value, colour, water holding capacity (WHC) and chemical composition (Sévon-Aimonen et al., 2007). The main quality characteristic in fish is usually associated with freshness. In salmonids, other quality parameters include white stripes (myocommata), marbling[1], bloodstains and melanin spots (Koteng, 1992; Sigurgisladottir et al., 1997).

There are at present various methods to measure quality like chemical analysis (Kent et al., 2004), sensory descriptive analysis (Gonzalez-Fandos et al., 2005) or instrumental analysis (Macagano et al., 2005; Casas et al., 2006; Mørkøre et al., 2009). Good technological qualities are often affiliated with low losses during processing. Thus to meet the increasing demands on product quality, a good knowledge

[1] Marbling refers to the amount and spatial distribution of visible white flecks of fat within the lean muscle, and is one of the most important traits in determining meat quality (ElMasry et al., 2012)

on *pre-* and *post mortem* factors influencing quality characteristics is needed.

The state of rigor and distribution of water in muscle have significant effects on meat quality, especially in terms of colour, firmness and amount of drip. After slaughter, the distribution of water in the muscle greatly changes. Muscle fibres shrink laterally while expelling intracellular water to the extracellular space (ECS), causing the size of ECS to increase. Consecutively, this water is expelled at the end of muscles (Guignot et al., 1993).

If fish are filleted pre-rigor, the fillets will shrink more as rigor develops since the muscles can contract freely. Hence the texture will be tougher. Pre-rigor filleting also gives changes in shape and certain operations like pin bone removal become more difficult (Sørensen et al., 1997; Skjervold et al., 2001; Kristoffersen et al., 2006). Moreover, it affects the water loss in fillets due to high drip loss (Kristoffersen et al., 2007; Skare, 2015). This practise has however some advantages like ensuring fresh processed fish with little or no gaping (Andersen et al., 1994; Mascheroni, 2012) and significantly thicker fillets (Skjervold et al., 2001). On the other hand, if the fish is frozen before rigor, the rigor process will take place slowly during the frozen storage. But if the frozen fish is cooked before rigor is resolved, the muscle will contract during cooking and lose cellular fluid. The meat in both cases will be tough. This is called thaw rigor which can be a problem with trawlers that freeze fillets on-board before the fish has passed through rigor. When a whole fish undergoes rigor, shrinkage is lessened as the muscles are anchored to the skeletal frame (Martin and Flick, 1990). Even so, pre-rigor filleting is now commonly practised in the farmed salmon industry. The extent of these practises can noticeably influence meat quality.

2.1.1 Fillet Texture

Fillet texture (firmness and resilience) is an important sensory quality for producers, processors and consumers (Haard, 1992). Muscle fibres, intramuscular connective tissue, and intramuscular fat have significant roles in determining fillet quality. Insufficient firmness of meat causes downgrading in the fish industry (Torgersen et al., 2014), thereby decreasing consumer satisfaction which can negatively affect the economy.

Texture can be influenced by various factors like fish species, age, size, fat content and distribution of muscle fat, amount and protein properties, and handling stress before slaughter. Water retention is also important for fish meat texture. Most of the water content is located in the myofibrils that occupy approximately 70% of the volume of lean muscle. A high water content in the muscle reduces the mechanical strength. Therefore the influence of water is related to muscle texture. (Hultmann and Rustad, 2002)

Texture is most often expressed in terms of flesh firmness and can be measured

by sensory or instrumental techniques. The ability to determine and improve the texture of fish products requires reproducible and reliable analytical methods. The most classical way in evaluating fish texture is by the "finger method", where a person presses the fish/fillet with a finger to evaluate firmness and elasticity. This method however is a subjective evaluation that depends on the person performing the measurement. Trained sensory panels can make more accurate evaluations on texture properties, but sensory evaluations are usually time consuming and costly.

Instrumental methods are more favoured over sensory evaluations since they minimize variations among measurements based on human factors and are more precise (Abbott et al., 1997). Different methods are available to measure specific texture properties. As compared to sensory methods, instrumental analysis is proven to be more precise due to reduction in variations arising from human factors (Cheng et al., 2014). The puncture, compression, shear and tension are four main techniques used to evaluate fish texture from the force-defamation curve, showing the force, defamation, slope and area (Casas et al., 2006).

2.2 Fish Muscle Structure

The skeletal muscle of teleost fish is a very dynamic and intricate tissue depending on immensely coordinated interactions between many myofibrillar, cytoskeletal and sarcoplasmic proteins for maintaining its integrity and function (Huff-Lonergan and Lonergan, 1999). It is the most abundant tissue, accounting for 65% of the total body mass in salmonids. The muscles are contractile tissues consisting of around 90% of muscle fibres and 10% of connective and fat tissues (Listrat et al., 2016). The nervous system controls the activity of skeletal muscle (Johnston, 2001). Typically, fish muscles contain approximately 66-81% water, 14-20% proteins, 0.2-20% fat and 1-1.8% ash, depending on the depth of water in which the fish is found. Since salmonid species are pelagic fish found in the middle and surface water layers of the sea, they contain high amounts of fats (10-20%).

2.2.1 Macroscopic Scale

The main purpose of fish muscle is locomotion. This differs from mammals where their muscles also give an additional purpose - to support the skeleton. The most distinct difference between fish muscle and those in higher vertebrates is firstly the anatomical separation of different fibre types into discrete layers in fish. Secondly, the growth in majority of the fish species is continuous throughout most of its life and this growth is a combined effect of the formation of more muscle fibres as well as the increase in size of existing fibres (Kiessling et al., 2006a).

Fish skeletal muscle contains short bundles of myotome (muscle blocks) and thin layers of myocommata (connective tissue). This unique structure contributes to the

soft flaky texture in fish meat. The connective tissue comprises mostly of collagen and proteoglycan, forming a scaffold supporting the muscle fibres and for transmission and absorption of force produced during muscle contraction (McCormick and Phillips, 1999).

The connective tissue in fish skeletal muscle is distributed into three levels of scale (Figure 2.2.1): the endomysium, that surrounds each muscle fibre; the perimysium, that surrounds bundles of muscle fibres; and the epimysium, that serves as the external envelope of the muscle (Astruc, 2014).

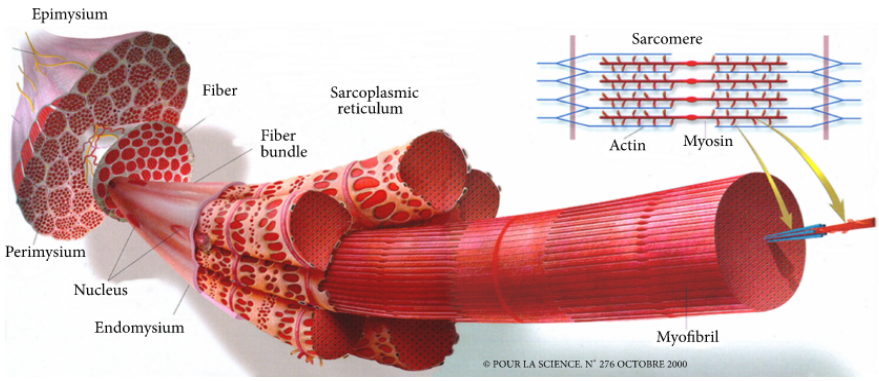

Figure 2.2.1: General organization of the muscle, showing the endomysium, perimysium and epimysium (Listrat et al., 2016).

Moreover, fish muscles consists of bundles of long, cylindrical muscle fibres organized into W-shaped myomeres to push the fish through water, giving fish energy for movement and the ability to swim (Figure 2.2.2). Myomeres are fitted into one another and separated by the horizontal connective tissue membrane called myosepta.

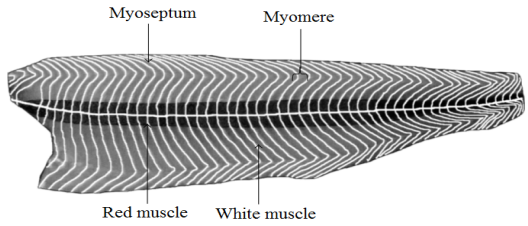

Figure 2.2.2: Structure of a fish muscle, consisting of muscle segments and connective tissue membranes where the segments are vertically W-shaped (Listrat et al., 2016).

The fish muscle organization is more complex in cross section. The two major masses of skeletal muscle lie on each side of the fish. The upper and lower pair of muscles are called epaxial and hypaxial muscles (Stead and Laird, 2002). Muscle fibre types present in fish can be divided into red, white and pink muscle (Figure 2.2.3). The dark aerobic red muscles have generally higher lipid content than white muscles. They are confined to a narrow strip beneath the lateral line close to the skin on both sides of the fish and is used mainly for sustained energy efficient swimming (Stead and Laird, 2002). These fibres are small in diameter (25-45 μm) and constitute less than 10% of the myotomal musculature (Kiessling et al., 2006a). Thus these muscles have high contents of mitochondria, myoglobin, lipid droplets and glycogen stores.

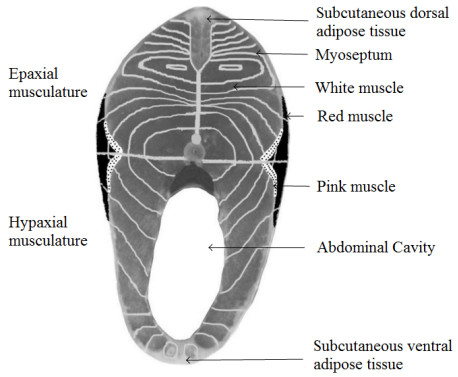

Figure 2.2.3: Cross-section of a fish showing the location of the red and white muscle. The muscle lying dorsally and ventrally from the horizontal septum are called epaxial and hypaxial musculatures (Listrat et al., 2016).

In contrast, the white muscles predominate in fish and constitute never less than 70%. These fibres have the largest fibre diameter of 50-100 μm or even more. The proportion of cross-sectional area that comprises of white muscle differs along the length of fish, being greatest at the anterior end and decreasing caudally (Sänger and Stoiber, 2001). They are dominated by myofibrils, occupying 75-95% of the fibre volume. Furthermore, they use anaerobic metabolism with low amounts of mitochondria and are hardly used up, remaining as energy storage in fish for agile swimming for prey capture and escape response. Last but not least, a thin, intermediate diffused layer of pink muscle occurs along the red-white boundary in most teleost species. Salmonids however do not seem to have pink fibres (Martinez et al., 1991, 1993; Kiessling et al., 1995).

2.2.2 Microscopic Scale

The muscle fibres are multi-nucleated and elongated as they are formed by the fusion of individual uni-nucleated cells called myoblasts. Enclosed by a plasma

membrane called sarcolemma, muscle fibres are where the action potential conduction triggering muscle contraction happens. Each fibre contains hundreds of cylindrical thread-like structures of myofibrils that are arranged in parallel. They are the contractile unit of the muscle fibre with 1.6-2 µm in diameter (Bear and Rintoul, 2014). The bundles of myofibrils occupy nearly the entire intracellular volume of muscle fibres (Listrat et al., 2016). Myofibrils have a diameter of rougly 1 µm and comprises of small subunits called myofilaments (Figure 2.2.1). Under high magnification electron micrographs, myofibrils can be seen to contain two kinds of myofilaments. The thick filaments comprise of mainly the protein myosin while the thin filaments of actin. A single thin filament has two chains of globular actin molecules intertwined around each other in a helix.

The basic repeat unit of a myofibril is the sarcomere (Figure 2.2.4). Each sarcomere is bounded at each end by the electron-dense structure called Z-line. A region of I-band surrounds the Z-line, which is the zone of thin filaments not superimposed by thick filaments. Next to the I-band is the A-band that contains the entire length of a single myosin thick filament.

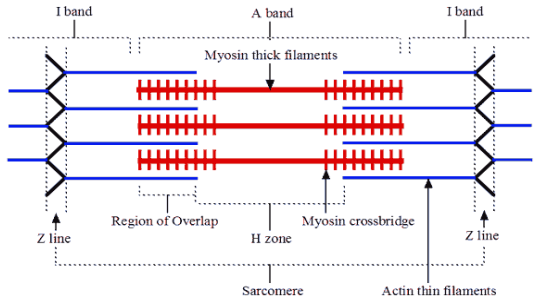

Figure 2.2.4: A schematic diagram of a single sarcomere (Retrieved from: `www.biophysicsandyourbody.wordpress.com` - last accessed 3 June 2016).

The myosin molecules contain projections called cross-bridges or heads. Each myosin head has two binding sites: one for actin and another for ATP. The ATP binding site is an ATPase with enzymatic activity, hydrolysing ATP to adenosine diphosphate (ADP) and inorganic phosphate (Pi) while capturing the released energy (Hill et al., 2012).

In the contraction process, the key physiological regulator are calcium ions, Ca^{2+}. The actin chains consist of two regulatory proteins, troponin (TN) and tropomyosin (TM), that are important in relation to Ca^{2+}. When a muscle is in the resting state, actin and myosin are kept separated by the regulatory proteins that blocks the binding sites. Tropomyosin prevents cross-bridge formation by blocking myosin binding sites on actin. This prevents muscle contraction. Troponin binds to tropomyosin and helps position it on the actin molecule. It also binds to Ca^{2+}, leading to muscle contraction (Bear and Rintoul, 2014).

Muscle fibre size increases with animal age and this is an important parameter in muscle growth. Simultaneous existence of small and large fibres are presented in the "mosaic" structures shown in fish (Figure 2.2.5). This fibre distribution in fish differs according to two growth stages: hypertrophic, where an increase in cell size is due to increase in volume, and the hyperplasic stage, where an increase in muscle volume is due to an increase in cell number (Listrat et al., 2016).

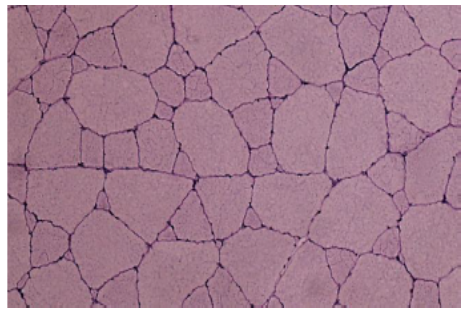

Figure 2.2.5: Histological cross section of Atlantic salmon. The white muscle is stained with PAS stain and consist of large and small fibres (Balevik, 2004).

2.3 Water in Fish Muscle

In farmed adult salmonids, muscles contain about 70% water. Approximately 85% of this are intracellular fluid (ICF), primarily in the spaces between actin and myosin. The remaining 15% of fluid are located in the ECS as extracellular fluid (ECF) (Høgåsen, 1998). Since myofibrils take up around 70% of the muscle volume, most of the tissue water is located within the three dimensional network of the filaments. Thus the amount of water immobilized depends on the space available between filaments. Any change in water distribution within the meat structure must originate from the myofilament spacings (Xiong et al., 1999).

2.3.1 Osmosis and Donnan Equilibrium

Osmosis is the transfer of solvent molecules through a semi-permeable membrane to achieve osmotic equilibrium. Two solutions of different concentrations allow solvent molecules to move from a region of lower to a higher solute concentration. This is termed a colligative property since it depends on the ratio of number of solute molecules over water molecules. The attraction property of solvents is called osmotic pressure ($\Pi = cRT$) and varies depending on the ions in the solution. If the osmotic pressure is known, the pressure difference needed to stop the flow of solvent is also identified.

Ions exert an effective osmotic pressure during rigor. The osmotic pressure in the intracellular space (ICS) increases by almost twice and has a close relationship with the change in pH. It was suggested that the pH drop was the major cause of the increase in osmotic pressure due to the alteration of proteins to which ions are normally bound (Ouali, 1990; Baumgarten and Feher, 2001). The distribution of ions affects water flow across cell membranes and thus cell volume. This phenomenon is called Gibbs-Donnan equilibrium, or simply Donnan equilibrium.

In a Donnan system, the semi-permeable membrane allows movement of small charged solutes (e.g.K^+ and Cl^-) between two compartments but impedes the movement of large ionic species like proteins, that are usually polyvalent and negatively charged at intracellular pH (Baumgarten and Feher, 2001; McCormick et al., 2013). The inability of one (or more) charged molecules to flow freely between the compartments influences the distribution of mobile ions and consequently, water. This osmotically unequal distribution of solute particles forces water molecules to move into the solution with higher osmolarity.

This effect can be correlated to living cells. Living cells contain impermeable anionic colloids, mostly made up of proteins and organic phosphates. These anionic colloids cannot cross the cell membranes, which are selectively permeable. Thus there is a high concentration of impermeable anions and this creates the Donnan equilibrium. This could cause water to continuously move into the cell and rupture. To prevent cell rupture, the sodium pump (Na^+-K^+-ATPase) in the cell membrane actively pumps K^+ out and Na^+ in the cell. Therefore, the cell can maintain and regulate the concentration of ions in the cytoplasm.

2.4 *Rigor Mortis*

In fish, the duration of *rigor mortis* is generally shorter than mammals (Sen, 2005). Stiffening usually starts a few hours *post mortem* and increases in intensity to a maximum rigidity around 12-24 hours *post mortem* (Stead and Laird, 2002). Resolution of rigor follows, using one or two days. Rigor development is generally dependent on the ATP level in the muscle, species, size, temperature, handling and biological status of the fish. Moreover, the onset of *rigor mortis* also depends on the red and white muscle, as rigor develops slower in white muscle compared to the red muscle (Kobayashi et al., 2004).

Different muscle groups in fish go into rigor at different rates depending on the depletion of ATP. It was observed in fish that stiffness generally starts in the head region and progressively spreads to the tail part (Riley, 2005), although the reverse sequence has also been observed (Rehbein and Oehlenschlager, 2009). It was further discovered that the dark muscle under the skin, muscles in the neck and near the bone in the ear enters rigor first in salmonids (Andreassen, 2012; Rehbein and Oehlenschlager, 2009).

2.4.1 The Sliding Filament Theory

The sliding filament theory describes the mechanism of muscle contraction by muscle proteins that slide past each other. To induce a movement, the muscle must receive a nerve impulse. This impulse comes from the brain and spinal cord, then managed by motor neurons to the muscle fibres. The action potential in the motor neurons trigger exocytosis of acetylcholine (Ach), which binds to ACh receptors that result in depolarization of the sarcolemma. The membrane potential becomes less negative due to Na^+ being pumped into the cell. This depolarization of cells induces the diffusion of Ca^{2+} from the sarcoplasmic reticulum to the sarcolemma. The concentration of Ca^{2+} in the sarcoplasma plays an important role for the development and duration of *rigor mortis* (Tsuchimoto et al., 1998). If the concentration of Ca^{2+} is low, the muscle relaxes. Otherwise, a high concentration of Ca^{2+} activates the contraction process. (Bear and Rintoul, 2014)

ATP is an important regulator of biochemical processes in all animals. The main functions of ATP in muscle are to provide energy for the Na^+ pump in sarcolemma, the Ca^{2+} pump in the sarcoplasmic reticulum and the myofibrillar contractile system (Hill et al., 2012). A high amount of ATP is generated when the muscle is active. This allows the released Ca^{2+} to adhere directly to TN. TM exposes the myosin-binding site of adjacent actin molecules. The myosin heads then bind to the actin sites and hydrolyses ATP, pulling the actin inwards. As actin is pulled, the sarcomere shortens and the muscle contracts. This cross-linkage is short lived. When ADP and Pi are released, the energy status of the myosin heads become low. However, the cross-bridge formed is still in place so actin and myosin are bound together. ATP can then attach to myosin, allowing the cross-bridge cycle to restart for further muscle contraction (Figure 2.4.1). When a muscle fibre contracts, thick and thin filaments do not shorten but instead slide along one another. After some hours or days, the muscles pass through rigor and gradually soften and become limp again. The duration in each phase can change or overlap depending on storage conditions like temperature.

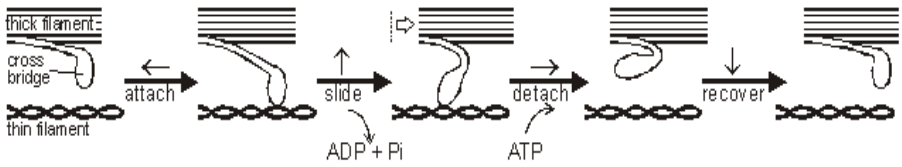

Figure 2.4.1: The cross bridge cycle showing only one myosin molecule for simplicity (Retrieved from: `www.mrothery.co.uk` - last accessed 19 March 2016)

2.4.2 Challenges

Many methods were done to study the development of *rigor mortis* like loss of extensibility (Bendall, 1973; Honikel et al., 1983), muscle shortening (Currie and Wolfe, 1979), tension development (Nuss and Wolfe, 1981), resistance to strain and combining muscle tension with shortening. Although the sliding filament theory explains the mechanisms of muscle contraction, there is still no good scientific explanation as to how muscle relaxes and goes out of rigor.

Some studies have speculated that the rigor development is not only due to actomyosin contraction. The current sliding filament theory of muscle contraction in *rigor mortis* is generally known that rapid *post mortem* glycolysis occurs and actomyosin bridges form during rigor development. After death, catabolic reactions predominate. The cytosol in cells switch from aerobic to anaerobic respiration which leads to the production of two lactate per pyruvate molecule. The muscle pH declines from 7.0 to a pH closer to the isoelectric point of most proteins (pH 5.4 to 5.6). This process of converting muscle to meat *post mortem* therefore creates a cellular environment that is greatly different from the cellular environment in a living muscle.

For muscle relaxation and transport of Ca^{2+} across the sarcoplasmic membrane to occur, ATP is required. But ATP is slowly depleted after death and reduces to almost zero, so myosin can no longer hydrolyse ATP and remains bound to actin. As the relaxation process needs ATP to break the actomyosin bonds, these bonds are deemed irreversible and remain contracted. In addition, it is agreed that stiffness resolves with no change in the actomyosin bridges (Balevik et al., 2004). For this reason *rigor mortis* cannot be explained by the resolution of these bridges, but by the proteolytic activity in the muscle and the destruction of the osmotic potential. These theories were widely discussed regarding the proteolytic activity in dead tissues (Tsuchiya et al., 1992; Hultin, 1984) and osmotic changes in cells (Slinde et al., 2003).

2.5 The Alternative Hypothesis

The alternative hypothesis was first discussed when cell morphological studies showed changes in cell sizes before, during and after rigor (Balevik, 2004). During rigor, number of molecules increase as glycogen is converted to lactate. This lactate increase raises the osmotic pressure in cells, causing water from the ECS to flow into the ICS. Moreover, proteolysis and lipolysis produce more amino acids, fatty acids and ions. The osmotic pressure within the different sub-cellular compartments of the muscle increases by nearly two fold, increasing intracellular osmolality (concentration of molecules). Hence the stiffness observed during rigor is due to the osmolarity change and water transport. The contours of cells undergo a change in fibre conformity to a more inflated shape (the cell border changes from

a wavy to a more streched appearance) to equalize the pressure (Figure 2.5.1). The semi-permeable membrane of the cells allows water to flow in but not out, making the cells stiff. This was calculated to be statistically significant (Slinde et al., 2001). This theory also explains why changes in ATP, Warner Bratzler, tension and contractions do not follow direct measurements of muscle stiffness during rigor (Slinde et al., 2001).

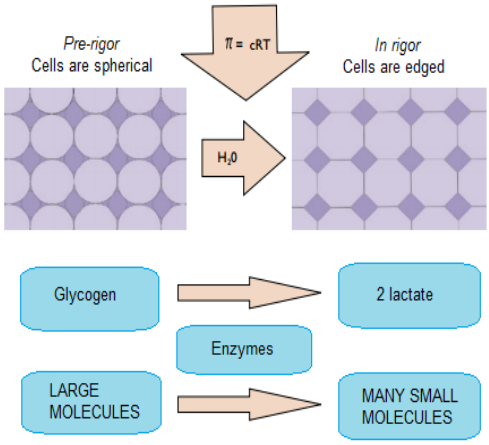

Figure 2.5.1: The biochemical process *post mortem* increases the number of molecules in the cell. The osmotic pressure increases, $\Pi = cRT$, and water flows in from the extracellular to the intracellular compartment in the cells. The cells will swell up and the shape becomes from a more spherical to a more edged form (Balevik, 2004; Slinde et al., 2003)

.

Research has explained that rigor resolution can be explained by the catabolic reactions, the lowering of pH and activation of all catabolic enzymes within the cell especially in the lysosomes (Balevik et al., 2004). This leakage breaks the osmotic potential and therefore the osmotic pressure that was created across the cell membranes is lost, leading to the resolution.

Winger and Pope (1980) also found that the osmotic pressure in beef muscle increased exponentially from 300 to 500 mOsm/L during the storage period. Veiseth et al. (2004) however showed an increase in osmolarity after death from 379 to 528 mOsm/L found in lamb muscle *M. longissimus dorsi*, and one-third of the increase took place within 24 hours, with a decrease in pH. This correlation between increased osmotic pressure and decrease in pH has also been observed by Bonnet et al. (1992). The conductivity also changed from 8.13 to 9.78 mS/cm during the first 12 hours (Veiseth et al., 2004), indicating that there are more charged molecules present in the solution. In some studies, it was further discovered that the intracellular volume of muscle cells has increased, which creates stiffness (Kobayashi et al., 2001; Veiseth et al., 2004).

Fishing trawlers usually gut the fish and chill them in ice immediately after harvest. This increases the fish weight as water flows into the cellular compartment of the fillets. When fish are thawed, cold shortening and weight loss takes place due to high drip loss. Previous studies have shown that muscle follows a contraction of up to 50% the original length (Slinde et al., 2001), making the meat stringy and dry in texture. Since water is one of the cheapest food ingredient that can be sold in the market, this brings forward to a question: Who is actually paying for the difference in yield when the initial half of the length is gone? This can influence WHC and lead to water loss. This is a serious issue in the economic point of view in minimising weight loss during processing as this directly represents economic loss.

The importance of *post mortem* changes in osmotic pressure has currently also not been linked to explain quality changes like pale, soft and exudative (PSE) meat, dark, firm and dry (DFD) meat, tenderness and WHC to meat in any kind of animal like fish, mammals, reptiles and more (Balevik et al., 2004). Knowledge about *post mortem* factors and *rigor mortis* is thus important both to the processing industry and to final consumers. Different methods could be discovered in ways of handling the products to decrease water loss and optimize quality. Therefore, a better understanding of water transport could increase the knowledge on rigor and potentially lower economic losses.

Chapter 3

Materials and Methods

This chapter describes the different materials and methods used in the three experiments. Experiment 1 served as a preliminary experiment to determine the effect of mass as muscles contract through the rigor process. Experiment 2 up-scaled the project to include texture and morphological analysis with the dimension measurements. The tissues from Experiment 2 were deemed unsuitable for histological analysis due to the presence of artefacts. Hence Experiment 3 was done to improve the tissue samples and for further observation in cell morphology.

One-way Analysis of Variance (ANOVA) was done for the dimension measurements using Microsoft Excel (Microsoft Incs, Redmond, USA) and compared with a self-written MatLab program (Appendix D.4). Samples were subjected to ANOVA since there were more than two groups of subjects to test if there were significant differences between the means. The alpha level was set to 5% ($p \leq 0.05$).

3.1 Experiment 1

Experiment 1 consisted of two trials with the salmonid brown trout (*Salmo trutta*). The experiment was carried out at around 10°C in NTNU Sealab, Trondheim. The fish were first anaesthesized using tricaine mesylate (MS-222), gutted then filleted into small pieces with the skin on to prevent flesh damage. The muscle pieces were immersed into solutions of varying salinity afterwards.

In Trial 1, four different solutions were used: 350 mOsm/L glucose, 0% NaCl (0 mOsm/L), 0.9% NaCl (350 mOsm/L) and 1.5% NaCl (500 mOsm/L). In trial 2, concentration of solutions used were the same as trial 1, except 1.5% NaCl that was replaced by a higher concentration of 2% NaCl (680 mOsm/L) to examine the difference more evidently. Triplicate fillet samples were used in each solution for both trials to ensure accuracy of results.

The dry mass, length and width were first measured before immersing them into different solutions. The fillets were taken out and dried consistently with an absorbent paper before measuring the dimensions at increasing time intervals. After measuring, they were then put back in the solutions, following through the rigor process. The percentage change for each measurement was calculated using the following formula

$$\text{Percentage change} = \frac{\text{fillet measurement at time t}}{\text{initial fillet measurement}} \times 100$$

where t = time of measurement *post mortem*.

In Trial 1, pieces of fillet slices of around $8 \times 2 \times 1$ cm^3 (length $\times$ width $\times$ height) were cut and immersed in the solutions. They were kept in ice to slow down the rigor process. Figure 3.1.1 shows an example on how the length and width were measured.

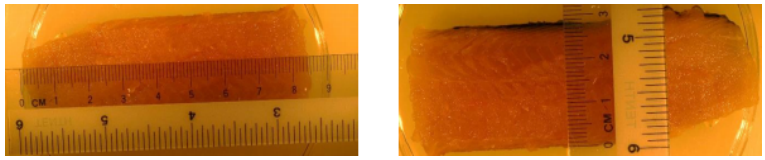

Figure 3.1.1: Sample measurement of length and width of fillet piece in Experiment 1.

In Trial 2, thinner fillet slices of $6 \times 1 \times 0.3$ cm^3 were cut and treated the same way as Trial 1. Thinner slices were used to increase the penetration rate of solution to the muscles. In addition, three dry fillet slices were cut, placed on a petri dish exposed to surroundings, and used as a control.

3.2 Experiment 2

Experiment 2 was done at the Institute of Marine Research in Matre Aquaculture Research Station, Norway. Farmed Atlantic salmons (*Salmo salar*) with an average body weight of 1 kg were caught in salt water bred at a temperature of 8.2°C from Masfjorden in Nord Hordaland. The fish were stunned with a strong cranial spike and transported to the research center, where they were bled, gutted and filleted with the skin on. The fillets were taken from the region behind the dorsal fin with the size of around $30 \times 10 \times 1$ cm^3.

3.2.1 Fillet Contraction

This experiment was carried out at an ambient temperature of around 14°C. Rigor development were recorded on 9 fish (18 fillets) during 25 hours. The right fillets

served as control samples and were placed on smooth plastic trays to allow free contraction. The corresponding left fillets were completely immersed in solutes of varying salinity (Figure 3.2.1). Three solutions were used and triplicate samples were carried out in each solution; 0% NaCl (Fillets 1 to 3), 0.9% NaCl (Fillets 4 to 6), and 1.5% NaCl (Fillets 7 to 9).

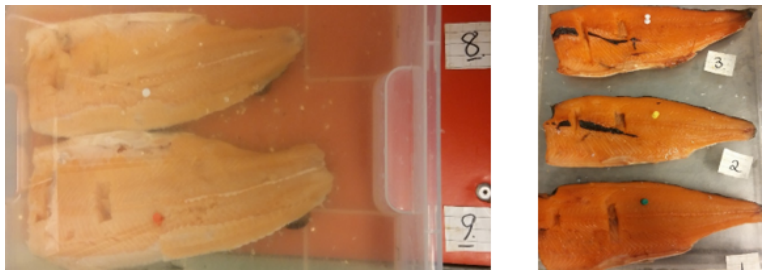

Figure 3.2.1: Examples of samples immersed in solution (left) and samples kept dry (right).

As with Experiment 1, the mass was recorded at each time interval with a mass balance. The rigor contraction rate was evaluated by measuring the change in length and width for each fillet, both dry and in solution at 0, 1, 5, 8, 21 and 25 hours *post mortem* (Figure 3.2.2).

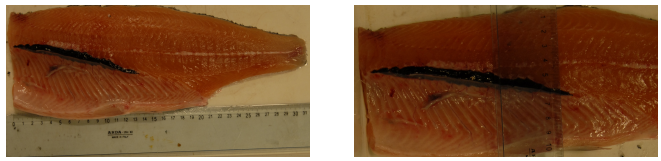

(a) length measurement (b) width measurement

Figure 3.2.2: Example on method used for length and width measurement in Experiment 2.

The length measurements were taken at the middle points from the anterior and posterior end while width measurements were taken at the highest point at the dorsal and lowest point at the ventral end. A decline in fillet length indicated a fillet contraction.

3.2.2 Rigor Index

In this part of the experiment, six whole fish were used for the "tail bending" method kept at a temperature of around 14°C. The fish were placed on a plane surface with their lengths beyond the dorsal fins to the tails placed beyond the edge of the surface (Figure 3.2.3). The sag of the tail from the horizontal plane

was measured and the rigor index (IR) was calculated by the following formula

$$\mathrm{IR} = \frac{L_0 - L_t}{L_0} \times 100$$

where L_0 and L_t are the height measurements at time 0 and 1, 2, 4, 6, 9, 22, 26 and 50 hours *post mortem* (Korhonen et al., 1990; Bito et al., 1983). Each fish was carefully placed on a flat dry surface after each measurement.

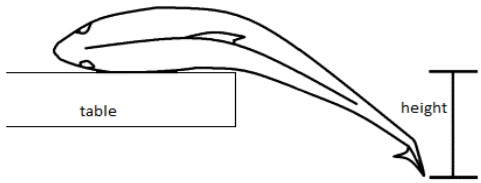

Figure 3.2.3: A schematic drawing (edited from Kiessling et al. (2006b)) on procedures used to measure development of rigor process and disappearance of stiffness as an index by the technique described (Bito et al., 1983) as tail bending.

From the data obtained it was observed that the rigor indices were following an exponential curve (Figure 4.2.3), so an exponential growth model was further used to curve fit the rigor index data. This was done to give an overall prediction of the measurements with reasonable accuracy and explain the rigor response. The formula used for exponential growth model of rigor index is

$$\mathrm{IR(t)} = \mathrm{N}_0 + \mathrm{N}_{\max}\left(1 - e^{-\mu_{\max}\mathrm{t}}\right)$$

where N_0 is the initial rigor, $\mathrm{N}_{\max}$ the rigor maximum and $\mu_{\max}$ the maximum specific growth rate of rigor. A non-linear in-build solver with the set-up of residual sum of squares (RSS) in Microsoft Excel was used to predict the parameters N_0, $\mathrm{N}_{\max}$ and $\mu_{\max}$ (Appendix B.2.2). RSS is used as an optimal criteria in parameter and model selection. The smaller RSS value, the closer the fitted values are to the observed values. The equation of RSS is given as

$$\mathrm{RSS} = \sum_{i=1}^{N} (\text{predicted value} - \text{observed value})^2$$

where $i = 1, 2, \ldots, N$ data samples. The time constants for the models were then calculated by the following formula

$$\mathrm{T} = \frac{1}{\mu_{\max}}$$

These constants revealed how fast the response will reach 63.2% ($1 - e^{-1} \approx 63.2\%$) of the total response, and helped to determine the time for histological sampling collection.

3.2.3 Texture Analysis

Instrumental texture analysis was done after each dimension measurement of the fillets with a *TA.HD Plus* texture analyser (Stable Micro Systems, Surrey, England). There were 5 measurements conducted in each fillet at locations 1-5 with the ascending time points of 0, 5, 8, 21 and 25 hours *post mortem* (Figure 3.2.4).

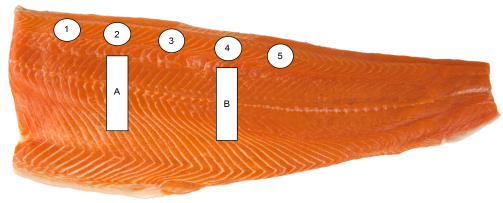

Figure 3.2.4: Texture measurements performed on locations 1-5 marked on the fillet. A and B were positions where samples were cut for histology at 5 and 21 hours (edited from: `http://www.europasalmon.com.au/` - last access 12 June 2016).

The average results were calculated and converted to percentage using the following formula

$$\text{Percentage change} = \frac{\text{measurement at time t}}{\text{initial measurement}} \times 100$$

The instrument was equipped with a 10 mm diameter flat-ended cylindrical plunger and operated with the computer software Texture Exponent Light Windows version 5.1.1.0 to generate a one cycle compression texture profile analysis (TPA) in each fillet. The probe was pressed down to 80% of the fillet thickness in the area of pin bones dorsally, perpendicular to the muscle fibers. The trigger force used was 5.0 g. A constant test speed of 1.0 mm/sec was used until the plunger returned back to the starting position. The sample was registered at 200 points per second and the plot was directly in force/time (kg/s) curve (Figure 3.2.5). The breaking force (F_{break}), time to F_{break} and force when time was at 5 seconds (F_5) were recorded.

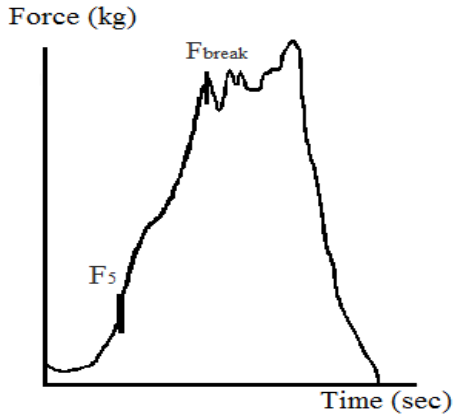

Figure 3.2.5: A typical force time curve (edited from Mørkøre and Einen (2003)) where F_{break} denotes the force required for breaking through the surface, and F_5 denotes the force when time = 5 sec.

3.2.4 Microstructure/Histology

Muscle samples of approximately 1 cm thick were collected for histology from each fillet (both right and left) right below the puncture from texture measurements at 5 and 21 hours *post mortem* with a sharp scalpel (Figure 3.2.4). A muscle sample was also cut randomly from a fish used in the tail bending experiment at 0 hour to serve as the control sample and at 5 and 21 hours for comparison.

The collected samples were immersed in 10% neutral buffered formalin (NBF) (4% formaldehyde in phosphate buffer) and kept at 14°C in Matre. They were then transported to NTNU Sealab in Trondheim after a day. Morphological analysis of the tissue samples was done a week later. The samples were kept in a 4°C refrigerator prior to the analysis. Grossing was done to cut the muscle samples transversally into thin slices of around 3 mm thick, placed in histology cassettes and embedded in NBF. The cassettes were processed using a Leica TP1020 tissue processor (Leica Biosystems, Wetzlar, Germany) where dehydration took place by immersing the specimens in increasing concentrations of alcohol. This was done to remove all extractable water and formalin from the tissues. Clearing was followed in which the organic solvent xylene was used to remove the remaining alcohol. Infiltration of the tissues in paraffin wax followed where liquid paraffin penetrated the tissues. Afterwards the embedding procedure began using a Leica EG1120 paraffin dispenser (Leica Bioystems, Wetzlar, Germany) where specimens were infiltrated with molten paraffin wax at 60°C. The samples were left to cool for solidification to occur.

Muscle sectioning of the embedded samples was carried out with a Leica Jung

Autocut 2055 power microtome (Leica Microsystems, Wetzlar, Germany). The samples were trimmed at 10 µm and then sectioned for 4 µm sections that were mounted on clear glass slides. The slides were dried at 60°C for 10 minutes prior to histochemical staining with haematoxylin and eosin (H&E), a routine dye that stains nuclei blue and cytoplasm of cells pink to red. Microscopy images of H&E stained muscle sections were obtained using a Zeiss Plan-Apochromat light microscope (Zeiss GmbH, Jena, Germany) at 10x magnification integrated with a Nikon Digital Sight DS-U1 camera. The images were observed and saved using the software NIS Elements F3.0 with a resolution of 1280 × 960 Normal.

3.3 Experiment 3

To determine if the choice of fixative caused the shrinkage of the ICS, Experiment 3 was done with brown trout (average weight of 350 g) at NTNU Sealab which mainly focused on morphological analysis of muscle samples. The method used was similar to the previous experiments. However, small pieces of fillets of approximately $7 \times 1.5 \times 0.5$ cm^3 were used instead of the whole fillets.

3.3.1 Fillet Contraction

The muscle samples were submerged in 0% NaCl, 0.9% NaCl, 2% NaCl and 50mg/L saponin solution with 0.9% NaCl (saponin concentration for cell permeabilization). Triplicate measurements were also done for each solution. A piece of dry muscle was used as a control throughout the experiment. Similar to Experiment 2, the average percentage change in mass, length and width for each sample were measured at 0, 2, 3, 4, 5, 6, 22 and 26 hours *post mortem* (Figure 3.3.1).

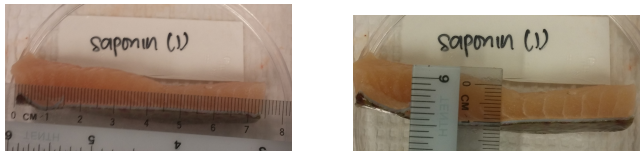

(a) length measurement (b) width measurement

Figure 3.3.1: Sample measurement for length and width measurement in Experiment 3.

3.3.2 Microstructure/Histology

For muscle histology, two small pieces of muscle (each around 3 mm thickness) were transversally cut from the control sample and samples in the various solutions at 0, 6 and 26 hours *post mortem*. The muscles taken at 0 hour were immersed in their respective solutions 10 minutes prior to cutting. The cut muscle pieces were placed

in cassettes and then immersed separately in two types of fixative: a solvent-free Clarke's solution (absolute ethanol and glacial acetic acid, 3:1), and 10% NBF solution. Clarke's solution was pre-cooled at 4°C for 24 hours before used as fixative.

The samples in Clarke's solution and NBF were processed, dehydrated after 24 and 48 hours respectively at room temperature and embedded in paraffin. Muscle fibres were cut transversally to 4 µm thick sections with a Leica RM2255 fully automated rotary microtome (Leica Biosystems, Wetzlar, Germany). One section from each tissue block per fish was used for histological analysis. Sections from the first replicate previously fixated with NBF were stained with H&E while those fixated with Clarke's solution were stained with Orange G and 1% aniline blue. As the method with Orange G-aniline blue gave an uneven staining, the other two replicates were stained only with H&E fixed in formalin.

A NanoZoomer SQ (Hamamatsu Photonics Norden, Kista, Sweden) was used for tissue examination connected to the software NanoZoomer Digital Pathology Scan Version 1.0.5. Only samples stained with H&E were analysed and scanned.

The scanned tissues were zoomed at 20x magnification, where 5 regions from the surface (furthest from the red muscle) and 5 regions from the centre of the muscle tissue were examined. From these images, morphological analysis was performed. Since triplicate muscle samples were done in each solution, the first replicates were first compared using different imaging software.

One of the software used for analysis is ImageJ, an open source Java-based image processing programme developed by the USA National Institute of Health. The scale was fixed at 2.42 pixels/µm. A uniform point grid frame of 7500 μm^2 was set on each image to estimate the area fraction of muscle tissue and extracellular spaces. Counts were made based on the number of points hitting the muscle tissue and ECS. BoneJ, an ImageJ plug-in for trabercular thickness (Tb.Th) in bone image analysis, was also used to define the mean thickness ECS of the tissue samples. This plug-in assumes that ECS are the foreground of a binarized image (Erikson et al., 2016). Its "Local Thickness" function defines the thickness at a point as the diameter of the greatest sphere that fits within the structure and which contains the point. The mean Tb.Th calculates the mean open space thickness from the pixel values in the resulting thickness map.

In comparison, Matlab (MATrix LABoratory) R2015b (The MathWorks Inc., Natick, Massachusetts, USA) was used to compare and calculate the cell area by image processing. The original image (Figure 3.3.2a) was first converted into a gray scale image (Figure 3.3.2b). To convert it further down to a binary image, a threshold needs to be found. A visual global threshold method was used to partition the image into a background pixel (black) and a foreground pixel (white). The binary image is shown in Figure 3.3.2c. Moreover, it can be seen from Figure 3.3.2c that the muscle fibres contain small white pixel holes. To reduce these holes an im-

age morphological operation called opening is used. The result after this operation can be seen in Figure 3.3.2d. A more detailed explanation is given in Appendix D.1.

These semi-automated scripts in Matlab identified the borders of cells in each image and calculated the average percentage ratio of ICS:ECS. This became the chosen software for further calculation on the other replicates as well as the inter-fibre distances (Appendix D.2) and cell angles (Appendix D.3).

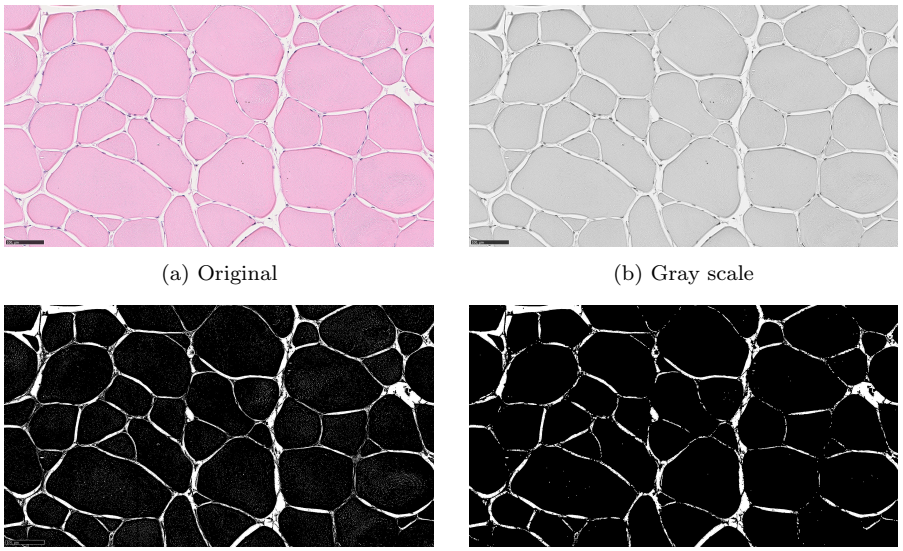

(a) Original

(b) Gray scale

(c) Binary without morphological operation

(d) Binary with morphological operation

Figure 3.3.2: Example of Matlab conversion of the (a) original image to (b) gray scale image, then to (c) binary without morphological operation and (d) binary with morphological operation.

Chapter 4

Results

This chapter presents the results of the three experiments. Dimension measurements are shown in all experiments while rigor index and texture analysis in Experiment 2. The morphological analysis of tissue samples done in Experiment 2 incurred artefacts so Experiment 3 was done. Experiment 3 shows a comparison of the fixative and staining method used, followed by imaging software comparison and morphological analysis. The respective numerical data for the obtained results are shown in the Appendix section.

4.1 Experiment 1

This section shows the results from Experiment 1, where brown trout muscle slices were used for dimension measurements in trials 1 and 2.

4.1.1 Trial 1

Figure 4.1.1 presents the results of percentage change in mass, length, and width. Based on one-way ANOVA, there was a significance in mass change (p=0.048), but insignificant length (p=0.528) and width change (p=0.251) among the different solutions. Furthermore, a general decrease in mass by 3% and a 24% contraction in length was observed when the slices were in the glucose solution, with an increase in width of 7%. Mass for slices in 0% NaCl gave an increase of 5% and a contraction of 13%, while width increased by 11%. Slices in 0.9% NaCl had a constant mass until 2 hours and had a rise of 4% afterwards with a contraction of 14%. The width had simultaneously increased by 20%. Lastly, slices in 1.5% NaCl had a steady decrease in mass by 2% with a contraction of 12%. The width decreased by 14% for the first 2 hours and then went back up to its initial width. To verify these results, another trial was carried out with more measurements.

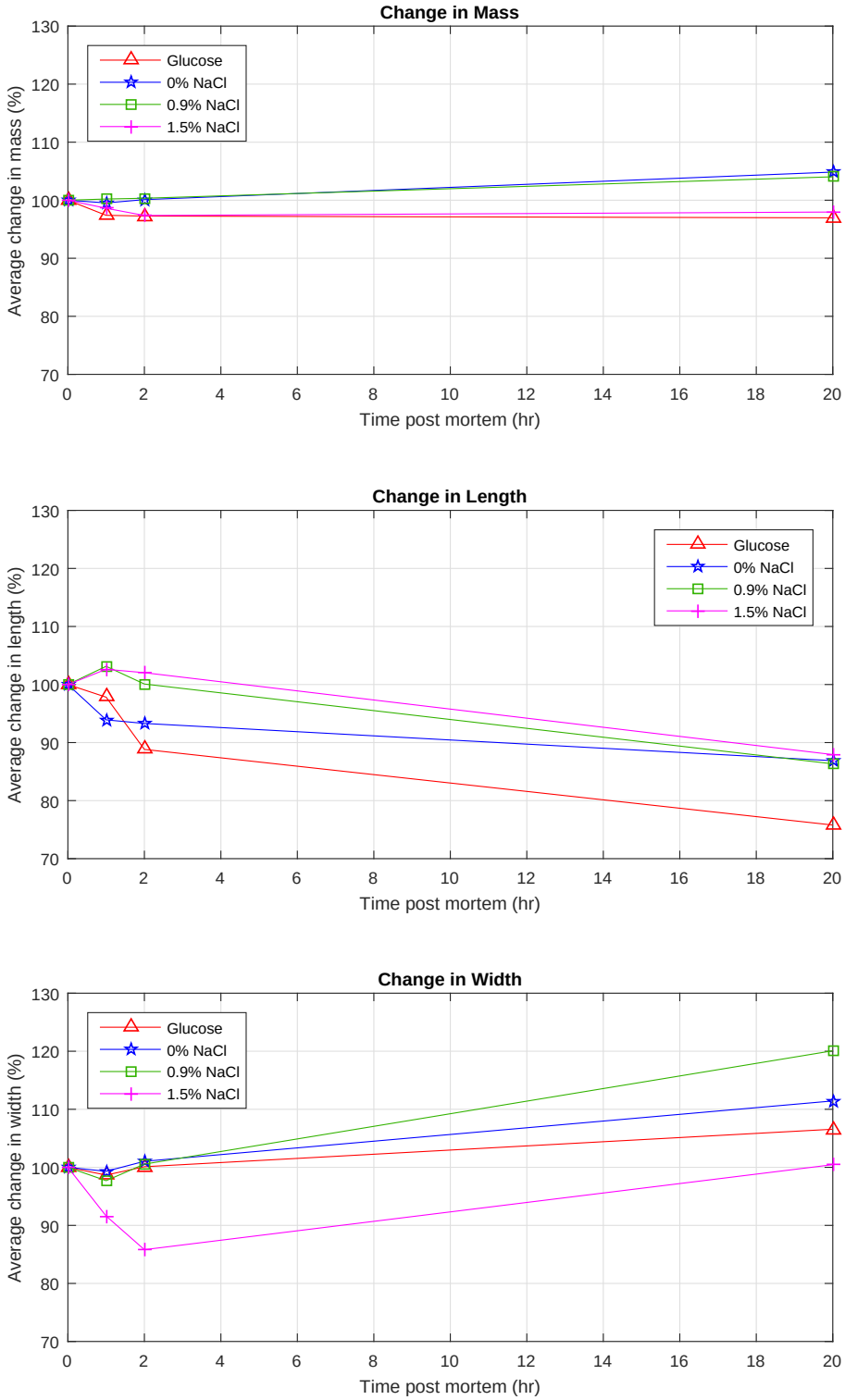

Figure 4.1.1: Average percentage change in mass, length and width for muscles in different solutions in trial 1. Standard deviation values can be found in Appendix A.1.

4.1.2 Trial 2

Figure 4.1.2 shows the dimension measurements of muscle samples in the various solutions for trial 2. One group of sample was kept dry throughout the trial as control. One-way ANOVA showed that there was a significant difference of change in mass ($p<0.001$), length ($p=0.003$) and width ($p<0.001$) among the solutions.

The dry samples had a steady decrease in all 3 measurements, where the strongest contraction occurred between 5 and 23 hours. This gave a total decline of 19% in length while having a 2% and 7% decrease in mass and width. The mass of samples in glucose only decreased by 1% while having a serious contraction of 22% and rise in width by 10%.

Mass increased steadily by 5% for samples in 0% NaCl solution while length heavily contracted by 26% and stabilised after 5 hours. To compensate for this contraction, the width increased by 5%. On the other hand, mass remained constant for 5 hours for tissues immersed in 0.9% NaCl. It was further observed that between 5 to 23 hours the mass had a significant increase of 8% and contracted by 15% throughout the whole period.

The samples in 2.0% NaCl showed water loss of 8% during the first 5 hours. After 5 hours, the opposite effect occurred and mass increased by 10% while having a total contraction of 13%. The width also decreased by 3%.

From the results obtained in both trials, there was a significant difference in mass between samples in different solutions. Therefore it was assumed that the osmotic pressure in cells does play a role in the movement of water during rigor.

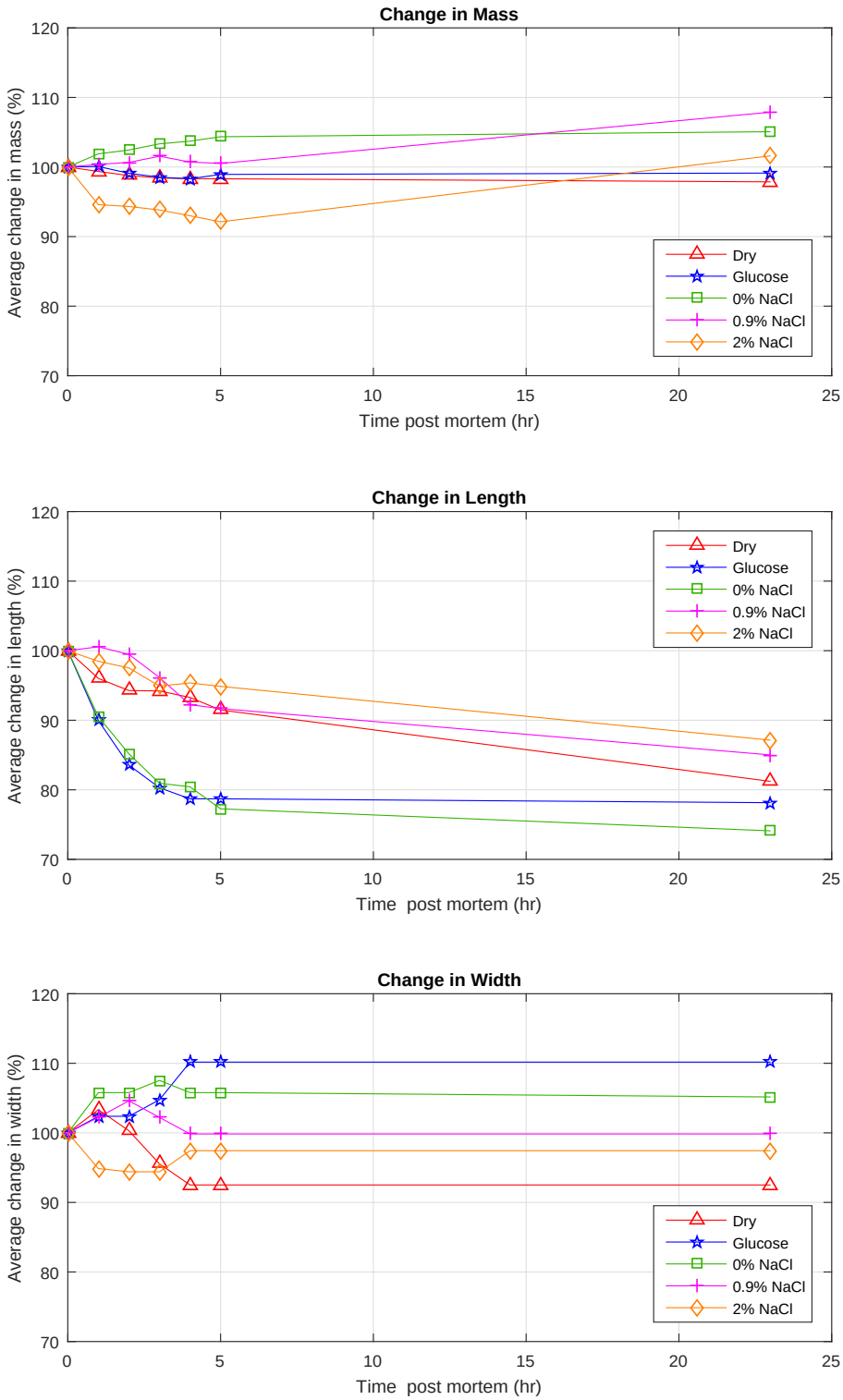

Figure 4.1.2: Average percentage change in mass, length and width for muscles in different solutions in trial 2. Standard deviation values can be found in Appendix A.1.

4.2 Experiment 2

Experiment 2 was done using whole fillets to further prove the hypothesis with texture analysis, morphological analysis and verify the results from Experiment 1. The right control fillets were left to dry on a surface while their corresponding left fillets were embedded in various solutions for comparison.

4.2.1 Dimension Measurements

The process of rigor development for the right and left fillets are presented in Figures 4.2.1 and 4.2.2. Since the right fillets were treated the same, their mass followed the same trend and decreased by 9-11 % at the end of 25 hours. Their lengths similarly decreased with a total contraction of 12-13 %, contracting most during the first 8 hours (9-12% contraction). Contraction rate decreased thereafter during the remaining period until 25 hours (1-4% contraction). The width of dry fillets decreased between 0 to 5 hours (1-3%) and had the greatest width increase from 5 to 8 hours (1-7%). This assumes that contraction leads to the increase in width to compensate for volume change. It was further observed that fillets became more dry in appearance and hard in texture.

On the other hand, the left fillets experienced faster contraction rate as compared to the dry fillets during the whole period. The fillets in 0% NaCl has totally increased by 4% in mass. They slowly appeared to be white, pale and bloated with a soft texture. The mass for fillets in 0.9% NaCl remained constant until 5 hours and then increased by 2%. For fillets in 1.5% NaCl solution, the mass initially decreased minimally by 1%, which then started to increase by 3%. Both fillets in 0.9% and 1.5% NaCl had slimy and slippery textures. All fillets in solution showed a similar trend for width change, where width decreased by 4-6% at the end of 25 hours. Gaping occurred in all fillets after 25 hours, especially for fillets in 0% NaCl.

The contraction rate for the left fillets were rapid during the first 5 hours (13-15% contraction). Maximum contraction was 15-16% lower than the initial fillet lengths at 8 hours. Contraction started to loosen afterwards. In general, the fillets in 1.5% NaCl gave a higher contraction than fillets in 0% and 0.9% NaCl.

Nonetheless, when results from both right and left fillets were combined, there was a statistical significant difference in mass ($p=0.001$) and width ($p=0.011$) but not contraction ($p=0.797$). The fillets in solutions seemed to give similar effects in length and width as compared to the dry ones. In contrast, the change in mass had opposite effects for the right and left fillets. This suggests that the movement of water may be independent of the contraction rate.

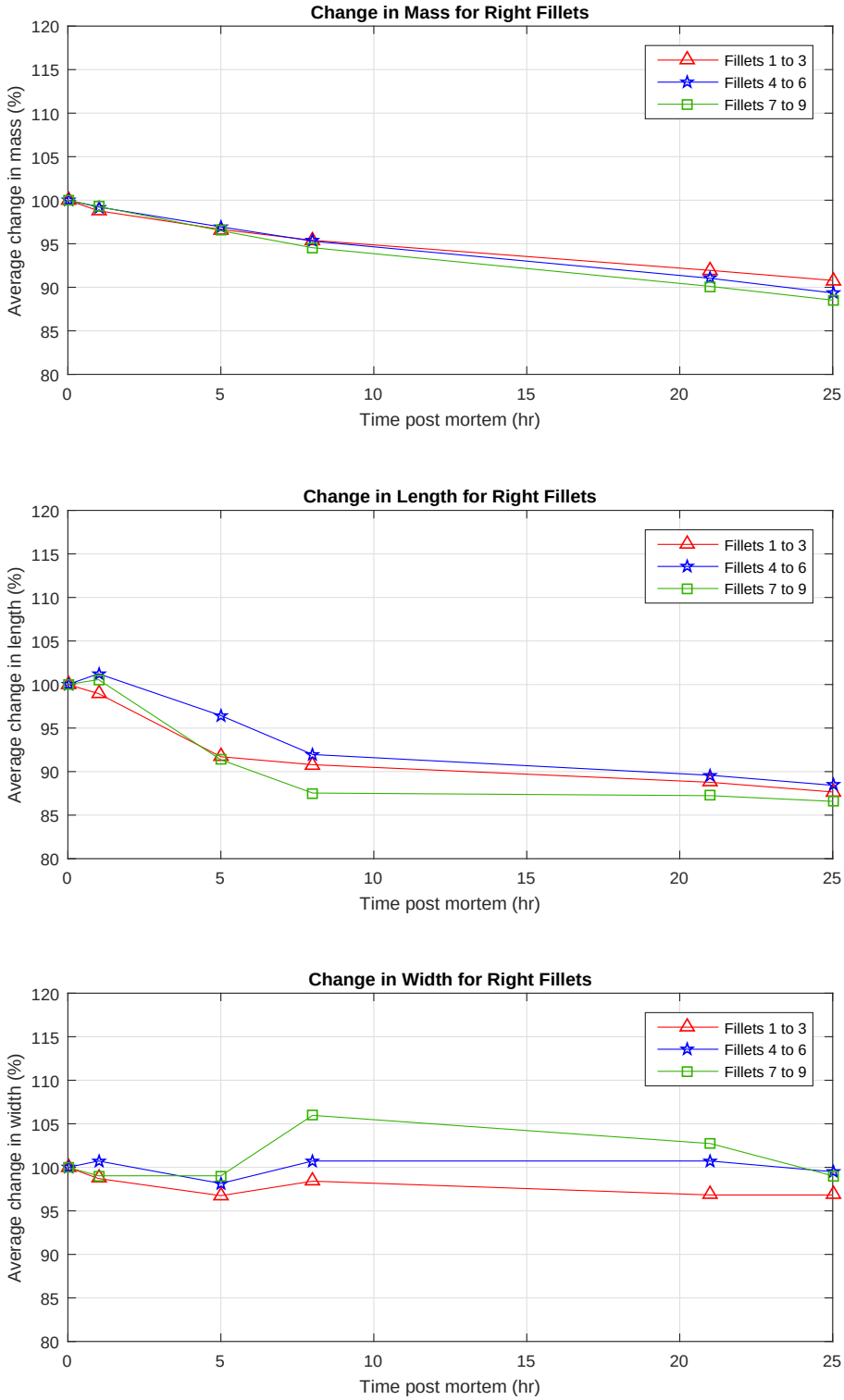

Figure 4.2.1: Average percentage change in mass, length and width of dry right fillets. Standard deviation values can be found in Appendix B.1.

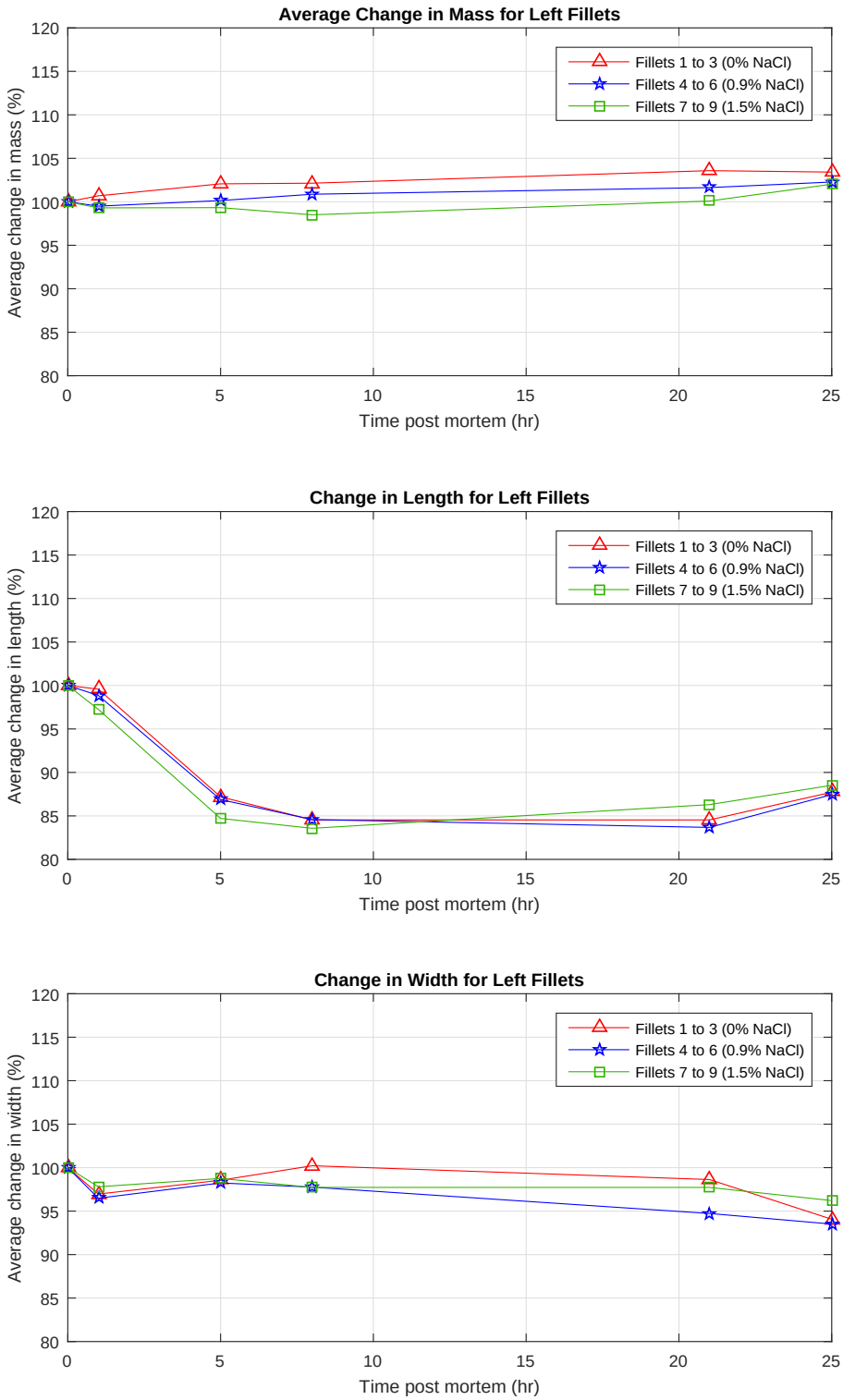

Figure 4.2.2: Average percentage change in mass, length and width of left fillets in various solutions. Standard deviation values can be found in Appendix B.1.

4.2.2 Rigor Index

The tail bend measurements that followed through the rigor development for 50 hours is shown in Appendix B.2.1. Rigor indices were further calculated and data plots with curve fitting are shown below (Figure 4.2.3).

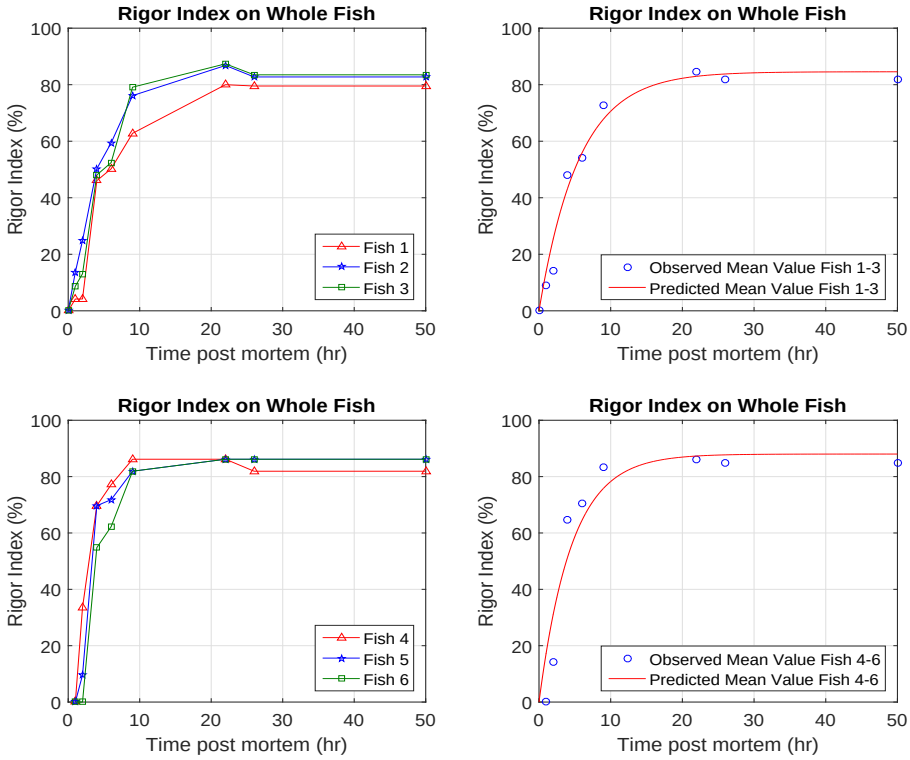

Figure 4.2.3: Rigor index on whole fish (left) and predicted rigor index (right).

From the predicted curve fitted model (see Section 3.2.2 for more details), Fish 1-3 was predicted to have $N_0 = 0$, $N_{max} = 84.58$ and $\mu_{max} = 0.18$. Furthermore, Fish 4-6 was predicted to have $N_0 = 0$, $N_{max} = 88.01$ and $\mu_{max} = 0.22$.

Hence for Fish 1-3 the time response is calculated to be

$$T = \frac{1}{\mu_{max}} = \frac{1}{0.18} \approx 5.5 \text{ hours}$$

while for Fish 4-6

$$T = \frac{1}{\mu_{max}} = \frac{1}{0.22} \approx 4.5 \text{ hours}$$

This means that Fish 4-6 had a faster rigor development than Fish 1-3. Fish 4-6 was an hour faster to reach 63.2 % of its maximum rigor than Fish 1-3. The average time constants of these two was $T = 5$ hours. Therefore histology samples were taken from the whole fillets at 5 hours since 63.2 % of the fish has undergone *rigor mortis*. Furthermore, it can be seen from the graphs that they gradually plateaued off at around 9 hours, and the rigor stabilised at around 22 hours where rigor was maximum. Resolution of rigor was not observed in any fish.

4.2.3 Texture Analysis

The average percentage breaking strength where shearing began were plotted at 0, 5, 8, 22 and 25 hours *post mortem* on each fillet (Figure 4.2.4). Results indicated that average breaking strength generally decreased with time for all fillets, meaning that the texture became softer. Overall, fillets immersed in solutions gave lower breaking strengths as compared to the dry samples. The breaking strength of fillets in varying salinity at 25 hours were similar at 25% (0% NaCl), 25% (0.9% NaCl) and 28% (1.5% NaCl). It was however expected that hardness should increase as the probe hits 80% down in the fillets when the fillets go from pre-rigor to rigor state at 5 hours. This phenomenon was not seen in the results. Moreover, the individual graphs (Appendix B.3.1) were difficult to give a general pattern due to high variations in the results obtained.

Figure 4.2.5 shows the average time used by the texture analyser to achieve this breaking strength. The time used for left fillets in 0% NaCl were higher than their corresponding dry fillets by 12-27%. For fillets in 0.9% NaCl, their time to breaking strength were 9-29% lower than the right fillets. Lastly, fillets in 1.5% NaCl were 6-14% lower than their right fillets left to dry.

Since there were individual variations obtained from the results, a new analysis was done by measuring force used when the probe was pressed at 5 seconds. This may give a more standardized comparison because at this time the breaking force started to elevate in all samples (Figure 4.2.6). Nonetheless it was still difficult to find a connection between the force used against time. Furthermore, the individual graphs (Appendix B.3.3) had again highly varying results.

A 3D plot with the axes breaking strength, time used to breaking strength and time *post mortem* is shown in Figure 4.2.7. It was found in this plot that there was a weak connection among these three variables. This can be explained by a number of factors, that is discussed later in the report.

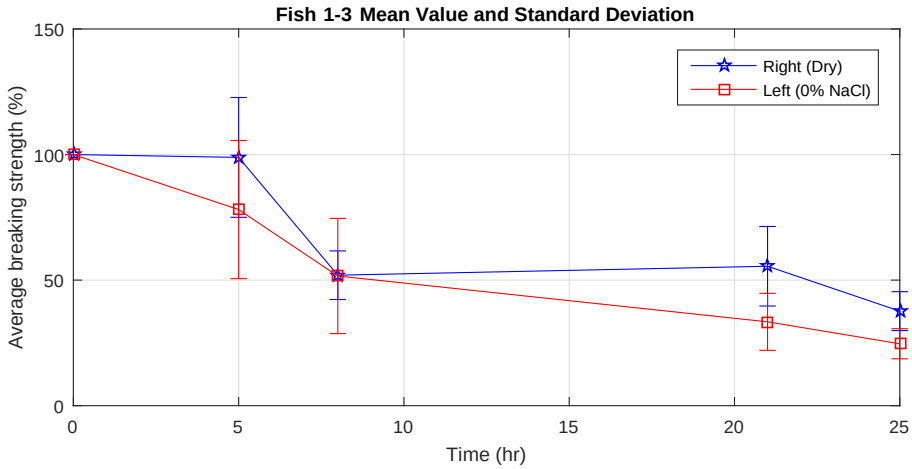

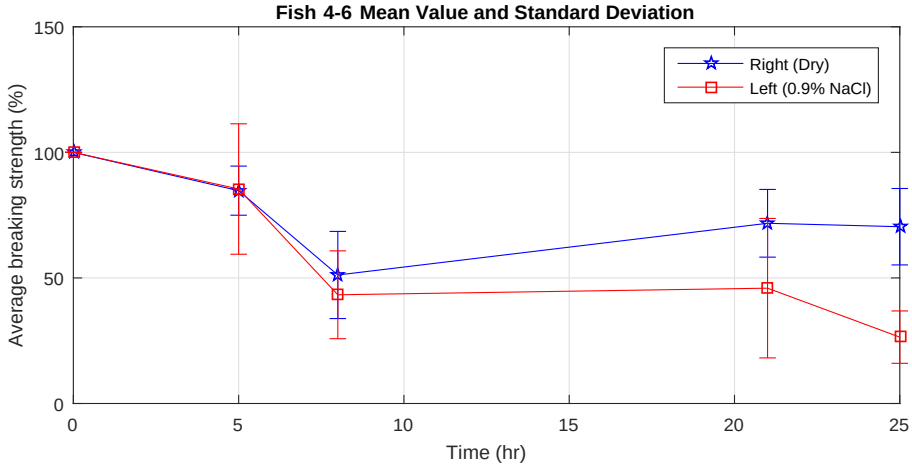

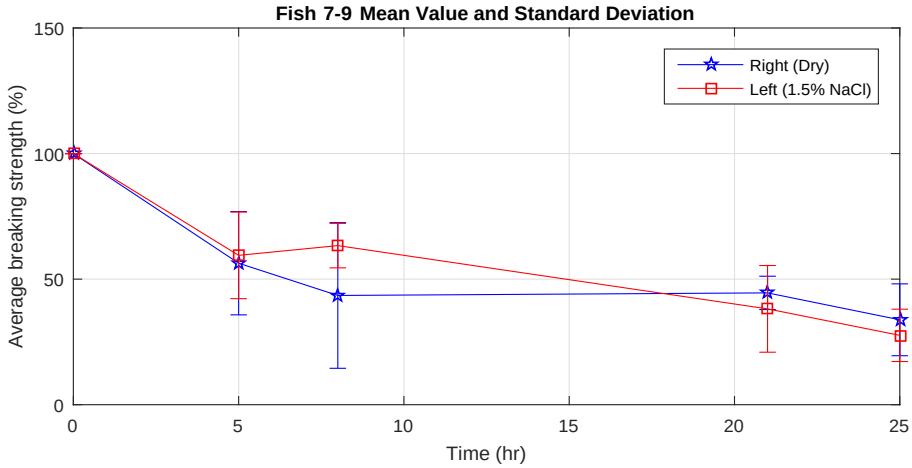

Figure 4.2.4: Graph of average breaking strength converted to percentage for fish 1-9, both dry (right fillets) and in various solutions (left fillets).

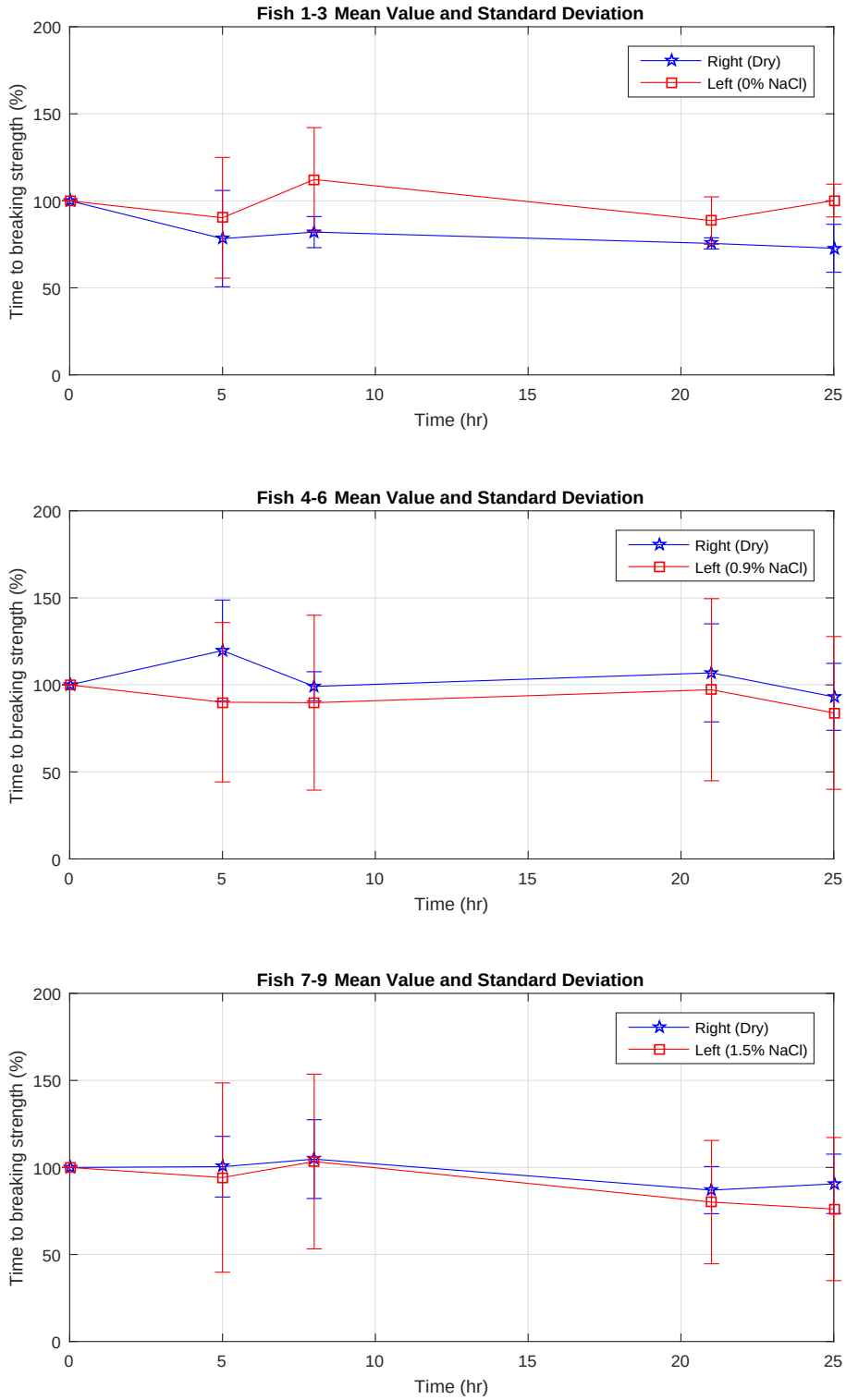

Figure 4.2.5: Graph of the average time used to reach breaking strength for fish 1-9, both dry (right fillets) and in various solutions (left fillets).

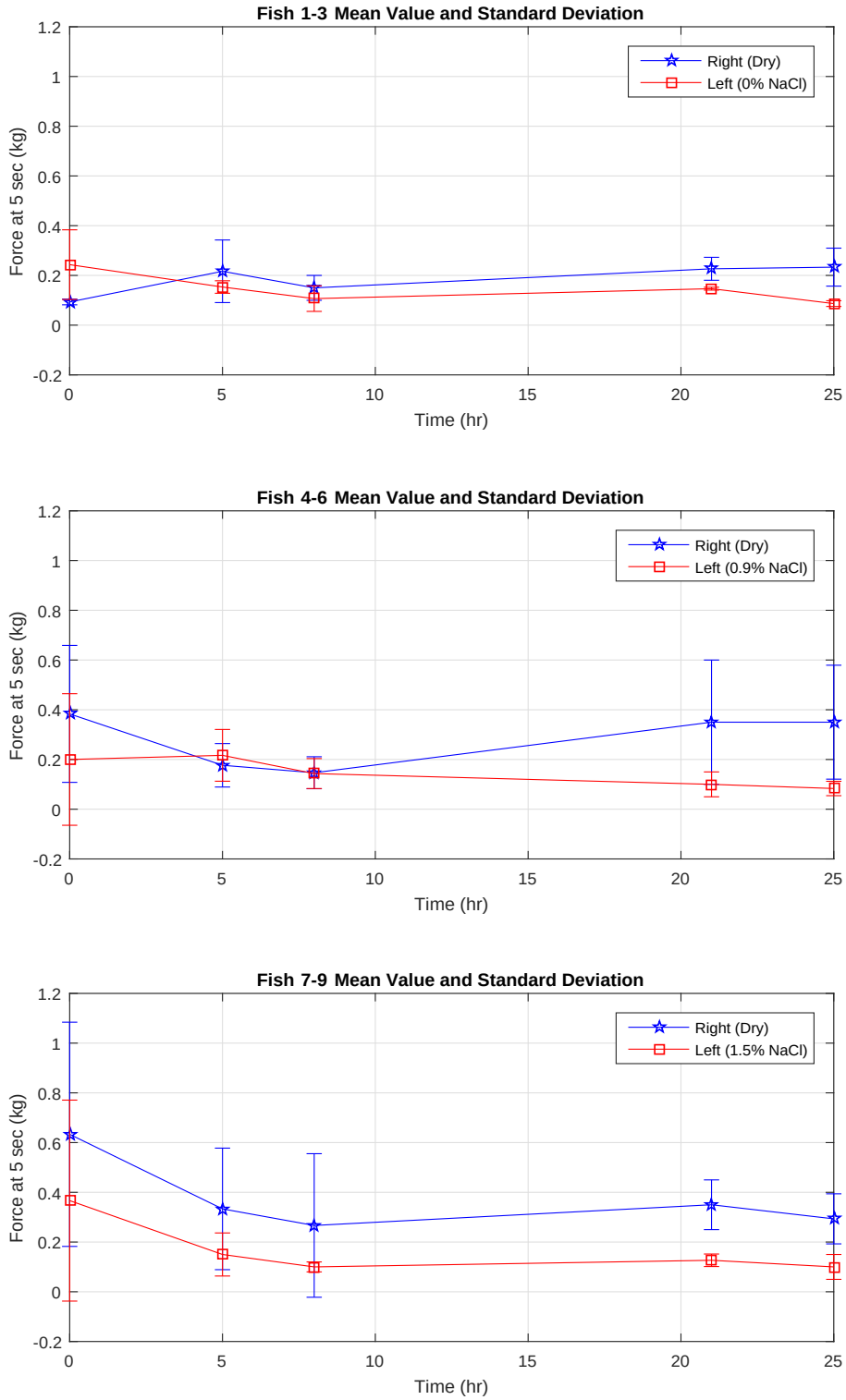

Figure 4.2.6: Graph of the average force used at time = 5 seconds for fish 1-9, both dry (right fillets) and in various solutions (left fillets).

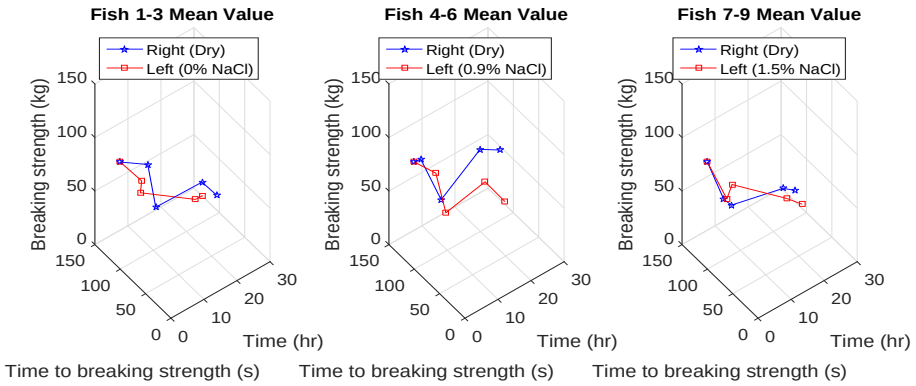

Figure 4.2.7: 3D graph of average breaking strength, time to breaking strength and time post mortem for fish 1-9, both dry (right fillets) and in various solutions (left fillets).

4.2.4 Morphological Analysis

Histological samples were collected from each fillet at 5 and 21 hours. A sample piece was also collected from a whole fish at 0 hour to serve as control. Morphological analysis was followed and the uppermost part of the muscle that were furthest away the red muscle, were observed.

Figure 4.2.8 shows the transverse sections of muscle taken from a whole fish used in the tail bending experiment. Figure 4.2.8a represents the control used in the whole experiment at 0 hour *post mortem*. The endomysium were nicely preserved but ICS of the fibres seemed to have shrank in size and nuclei detached from the sarcolemma. This was not an anticipated result as a fresh muscle taken immediately after death should occupy an ICS of around 60-70%. The ICS on fibres at 5 hours (Figure 4.2.8b) and 21 hours (Figure 4.2.8c) occupied a higher volume as compared to the control.

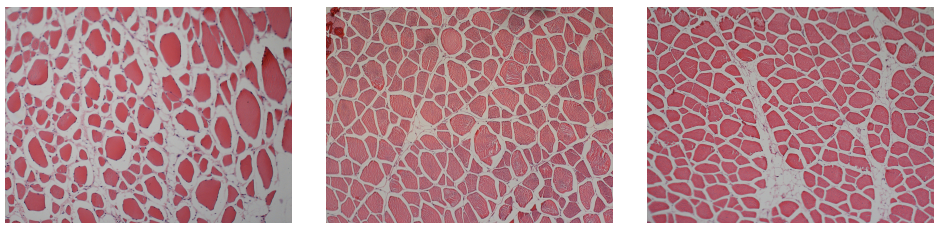

(a) 0 hour (b) 5 hours (c) 21 hours

Figure 4.2.8: Histologic cross-sections of Atlantic salmon white muscle at 0, 5 and 21 hours *post mortem*. The muscle samples were obtained from fish used in the tail bending experiment.

Transverse samples of the right and left fillets in 0% NaCl solution is presented

(Figure 4.2.9). By visual observation, the samples seemed homogeneous from the right fillets at 5 hours (Figure 4.2.9a). Fibre shrinkage was also observed which could be due to the formalin fixative used. The ICS of right fillets at 21 hours (Figure 4.2.9b) were higher than at 5 hours, which was assumed to be the time of rigor. On the other hand, fillets in the hypotonic solution have swelled up and became more compact after 5 hours (Figure 4.2.9c). The fibres were well-preserved, homogeneous with no cirrhosis and filled the area until the endomysium. One explanation could be that they have swelled before fixation. However the ICS decreased after 21 hours and the fibres shrank (Figure 4.2.9d), which did not coincide with the observed mass increase.

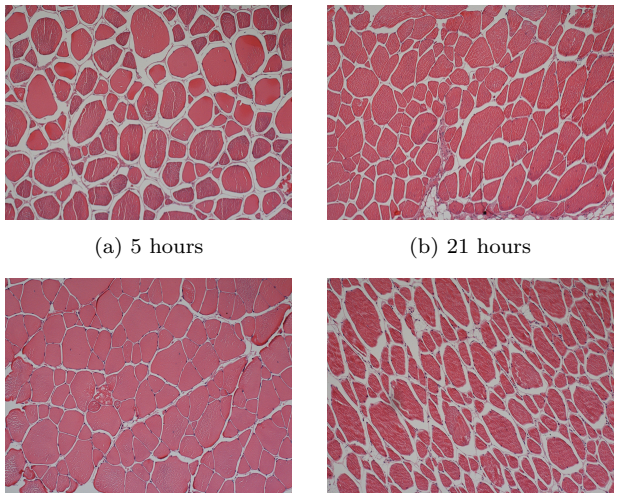

(a) 5 hours (b) 21 hours

(c) 5 hours (d) 21 hours

Figure 4.2.9: Histological cross section of Atlantic salmon white muscle (Fish 1) where (a) and (b) shows the the right fillet placed on surface at 5 and 21 hours *post mortem* respectively. (c) and (d) shows the corresponding left fillet immersed in 0% NaCl solution at 5 and 21 hours *post mortem*.

Figure 4.2.10 gives the sections for right and left fillets of fish kept dry and in 0.9% NaCl isotonic solution. Tissues from the right fillet seemed heterogeneous with some oblique incisions for sections at 5 hours (Figure 4.2.10a). There was also a higher ECS observed for right fillets at 21 hours (Figure 4.2.10b) than at 5 hours. In comparison, tissues from the left fillet at 5 hours (Figure 4.2.10c) were more heterogeneous, where some fibres looked more shrivelled than others and presumed to have less shrinkage than the other samples. At 21 hours, the section (Figure 4.2.10d) was expected to increase in ICS as osmolarity and mass increases. This was again not observed.

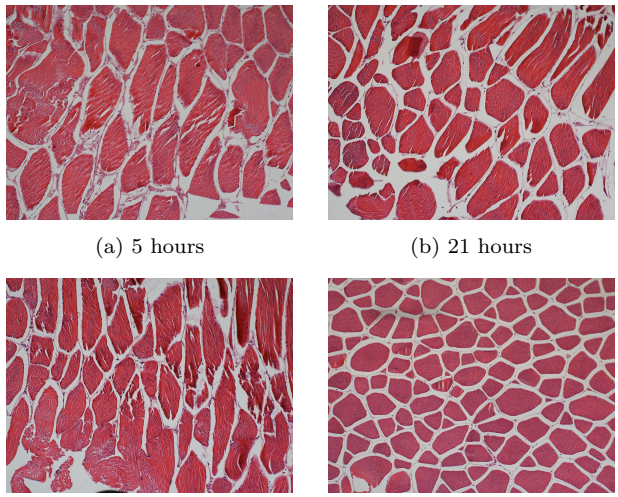

(a) 5 hours (b) 21 hours

(c) 5 hours (d) 21 hours

Figure 4.2.10: Histological cross section of Atlantic salmon white muscle (Fish 6) where (a) and (b) shows the the right fillet placed on surface at 5 and 21 hours *post mortem* respectively. (c) and (d) shows the corresponding left fillet immersed in 0.9% NaCl solution at 5 and 21 hours *post mortem*.

Lastly, Figure 4.2.11 shows the transverse section of right dry fillet and left fillet immersed in 1.5% NaCl. It was expected that the cells in salt water (Figure 4.2.11c) should have shrank in size as compared to the one left to dry (Figure 4.2.11a) at 5 hours. However, there was no obvious shrinkage observed despite the weight decrease. It was also expected that cells in salt water at 21 hour should have swelled due to increase in osmolarity and weight. Therefore it was speculated that the shrinkage seen could be due to prolonged fixation of tissue samples in formalin. This can significantly disturb the calculation of ICS and ECS considering that the spaces seen in the sections were artefacts. Hence another experiment was done on brown trout to verify this phenomenon, focusing on morphological analysis.

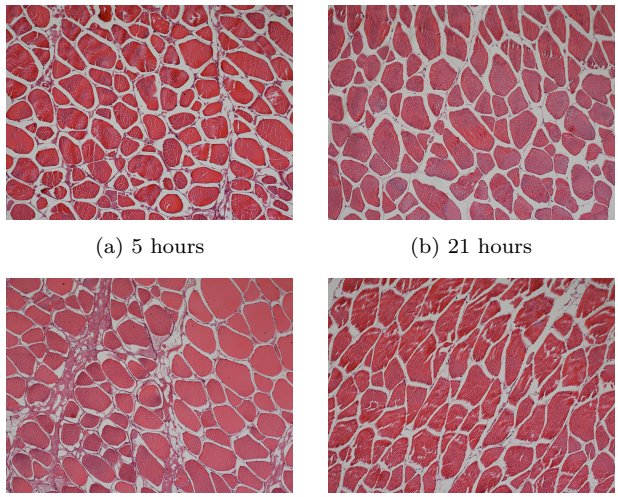

(a) 5 hours (b) 21 hours

(c) 5 hours (d) 21 hours

Figure 4.2.11: Histological cross section of Atlantic salmon white muscle (Fish 7) where (a) and (b) shows the the right fillet placed on surface at 5 and 21 hours *post mortem* respectively. (c) and (d) shows the corresponding left fillet immersed in 1.5% NaCl solution at 5 and 21 hours *post mortem*.

4.3 Experiment 3

Based on the previous experiment, the formalin fixative may have introduced cell shrinkage from the morphological results. Thus Experiment 3 was done to validate the effect of fixation.

4.3.1 Dimension Measurements

The average percentage change in mass, length and width is shown in Figure 4.3.1. Statistical results indicate that there were significant effects on mass ($p<0.001$), and width change ($p<0.001$), but not for contraction rate ($p=0.074$) for samples in the different solutions.

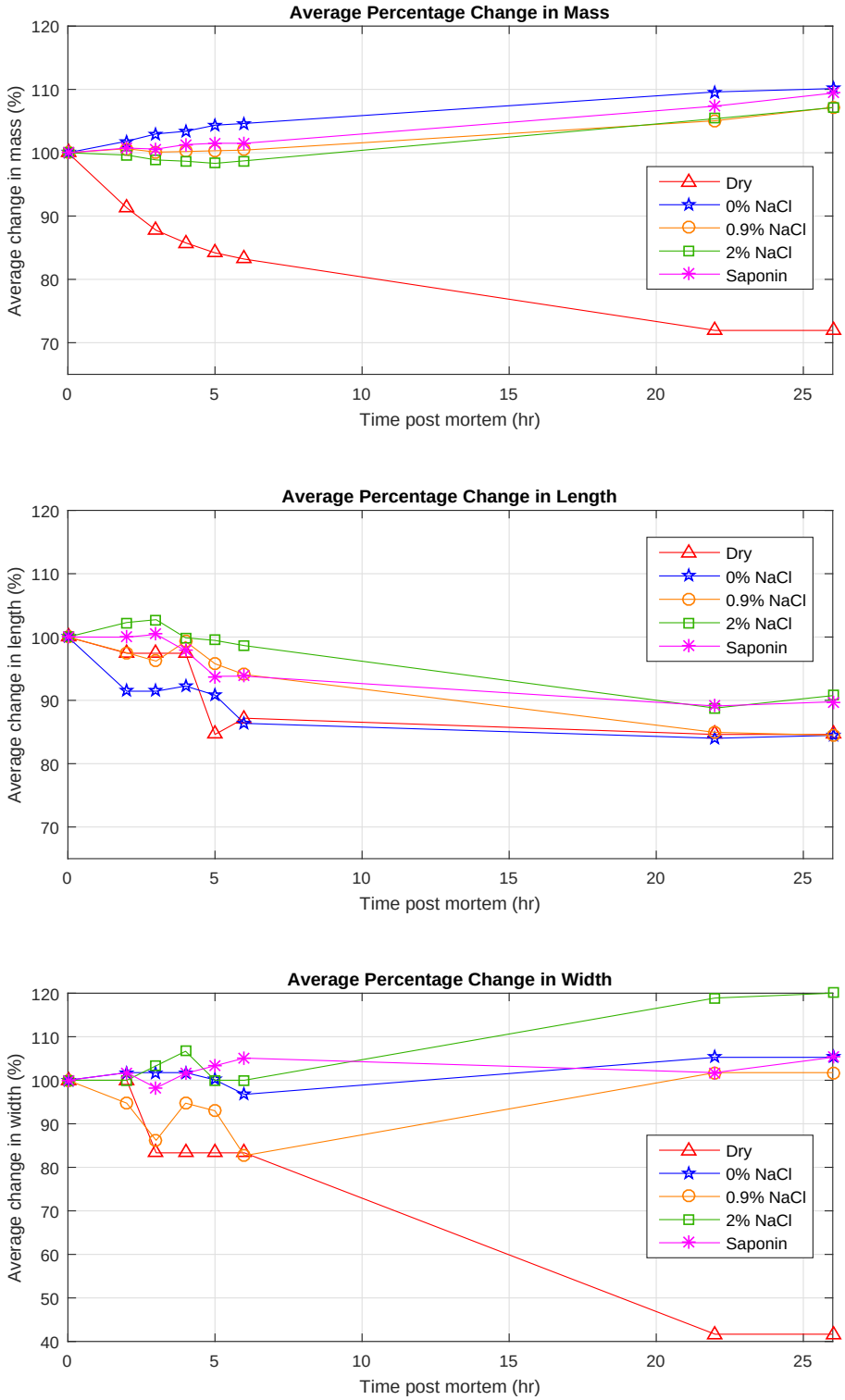

Figure 4.3.1: Average percentage change in mass, length and width of left fillets in various solutions. Standard deviation values can be found in Appendix C.1.

The dry sample, used as a control, had a steady mass decline by 28% and width by 58% while having a serious contraction in length by 15%. At the end of 26 hours, the tissues had a hard dry texture. Samples in 0% NaCl solution were in agreement with the previous experiments, where mass gained by 10% while contracting by 15%. Since the tissues contracted, the corresponding widths increased by 5% to accommodate this increase in mass.

The mass of muscle samples in 0.9% NaCl remained constant until 6 hours and started to ascend by 7% at the end of 26 hours, while length decreased steadily by 16%. Nevertheless, the width of the samples decreased by 17% for the first 6 hours and then increased by 19% from 6 to 22 hours. For 2% NaCl, the samples first decreased in mass by 2% and then increased by 9% while conjointly having a contraction of 9% and an increase in width of 20%. Lastly, samples in the saponin solution initially showed a stable mass and contraction rate but slowly increased in mass by 9% and had a contraction of 10% with an increase in width by 5%.

4.3.2 Fixative and Staining Method

Histological transverse sections of white muscle cut immediately after death and fixated in two fixations (Clarke's solution and NBF) are presented in Figure 4.3.2. Muscle specimens fixated in Clarke's solution and stained with Orange G-aniline blue were seen to have shrunk in size (Figure 4.3.2a). The staining method was inconsistent as certain parts were too dark and uneven (Figure 4.3.2c). On the other hand, the samples fixated in NBF and stained with H&E (Figures 4.3.2b and 4.3.2d) did not indicate any cell shrinkage. This staining method was more even and easy for observations. Therefore the muscle samples fixated in NBF were chosen for subsequent morphological analysis for all replicates.

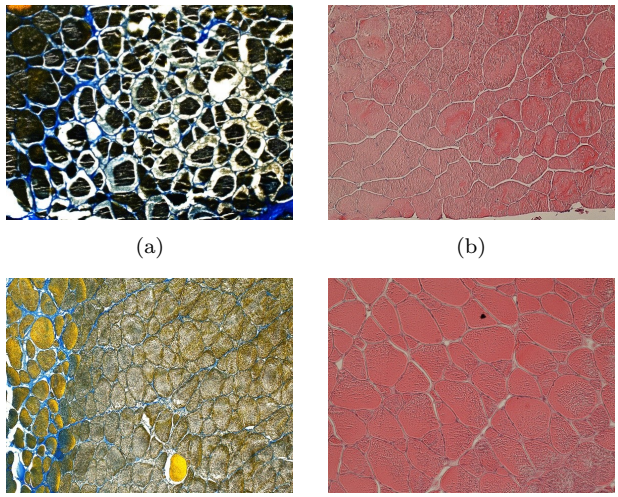

(a) (b)

(c) (d)

Figure 4.3.2: Histological cross-sections of Atlantic salmon white muscle all at 0 hour *post mortem*. (a) and (c) show samples fixated with Clarke's fixative stained with Orange G Aniline. (b) and (d) show samples fixated with NBF stained with H&E.

4.3.3 Matlab and ImageJ

The amount of ECS obtained from the surface and central regions of samples was compared using the BoneJ plug-in, ImageJ grid counting method and Matlab. The results are shown in Table 4.3.1.

Table 4.3.1: BoneJ, ImageJ and Matlab results on the extracellular space for the first sample in each groups of solutions at 0, 6 and 26 hours *post mortem*.

Samples	0 hour			6 hours			26 hours		
	BoneJ*	ImageJ	Matlab	BoneJ (µm)	ImageJ	Matlab	BoneJ (µm)	ImageJ	Matlab
Dry (surface)	12%	12%	16%	12%	9%	23%	15%	10%	21%
Dry (center)	11%	12%	15%	10%	5%	14%	20%	8%	23%
0% (surface)	10%	5%	12%	7%	5%	10%	16%	7%	21%
0% (center)	8%	2%	13%	10%	3%	9%	27%	25%	34%
0.9% (surface)	12%	9%	17%	10%	9%	21%	15%	6%	23%
0.9% (center)	10%	6%	16%	11%	3%	12%	26%	22%	37%
2% (surface)	11%	10%	16%	11%	4%	6%	20%	0%	3%
2% (center)	28%	22%	28%	32%	39%	46%	12%	5%	12%
Saponin (surface)	11%	4%	14%	18%	23%	37%	13%	9%	34%
Saponin (center)	10%	4%	17%	12%	4%	22%	12%	4%	17%

*Tb.Th (trabecular thickness) mean is the unit for thickness from BoneJ plug-in.

The Local Thickness application used in BoneJ gave the mean trabecular thickness (Tb.Th), calculating the mean thickness open space from the ECS in µm. This value was then converted to percent of ECS occupied in the whole image. Both BoneJ and ImageJ grid counting generally gave lower estimations in the amount

of ECS as compared to Matlab. ImageJ only gave rough estimations through grid counting. On the contrary, the program coded in Matlab used image processing to calculate the black and white area of every pixel in the image. This gave a better estimation on the ICS and ECS, covering the whole image. Therefore, the method used in Matlab was more accurate and chosen as the software for further calculations for rest of the samples.

4.3.4 Morphological Analysis

Matlab calculated the amount of ICS:ECS, inter-fibre (cell-to-cell) distance and cell angle from the scanned histological images (Appendix D). Images from the surface and central part of the sample were taken for comparison.

Dry sample

The histological cross-sections of dry samples and percentage of ICS:ECS are seen in Figures 4.3.3 and 4.3.4. Newly slaughtered, fresh trout muscle at 0 hour had a homogeneous muscle fibre distribution. The muscle had a narrow ECS of 16% from the tissue surface (Figure 4.3.3a) and 15% from the tissue center (Figure 4.3.3d).

The fibres began to shrink at 6 hours at the tissue surface by 7%, increasing the amount of ECS in correspondence with 7%. The contour of the cells became more angular. The ECS at the tissue center remains unchanged at 15%. This indicated an evaporation gradient that starts from the tissue surface and moves slowly to the center.

Further shrinkage by 12% and compression of cells took place at 26 hours especially at the surface (Figure 4.3.3c). Disorganization became more visible and fibres fragmentation were numerous as the endomysium were damaged. The fibres appeared scattered and more contoured with sharp edges. The amount of ECS at the central part only increased by 8% due to fillet thickness.

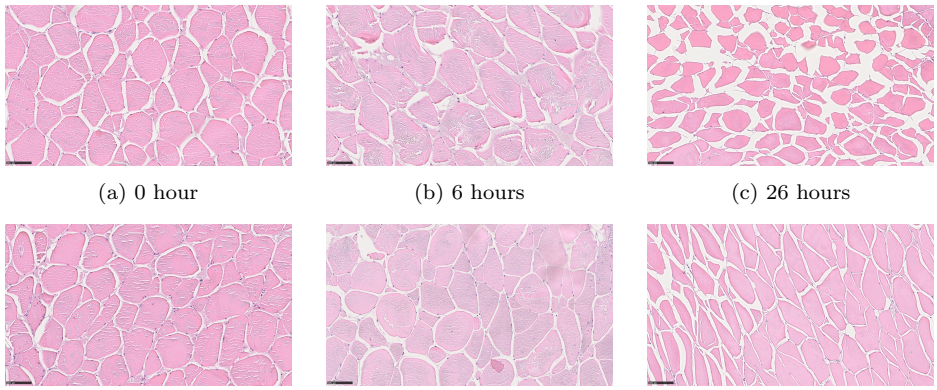

(a) 0 hour (b) 6 hours (c) 26 hours

(d) 0 hour (e) 6 hours (f) 26 hours

Figure 4.3.3: Histological cross-sections of dry samples at 0, 6 and 26 hours *post mortem*. (a), (b) and (c) were taken from the surface while (d), (e) and (f) were taken from the central part of the tissue section.

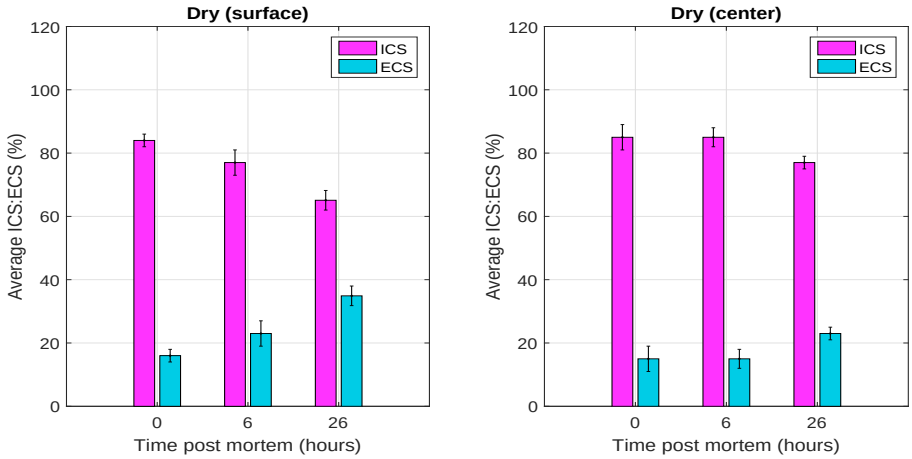

Figure 4.3.4: Average percentage of ICS:ECS of muscle fibres kept dry at 0, 6 and 26 hours *post mortem*. The left graph depicts the surface while right graph the center of the tissue samples.

0% NaCl Solution

By visual glance, the ICS of samples in freshwater occupied more space than the dry samples. This coincides with the calculations as ECS of the hypotonic samples were in general 4% lower than the dry ones. Muscle fibres at 0 hour occupied nearly the same amount of ICS at the surface (Figure 4.3.5a) and center (Figure 4.3.5d) at 88% and 87% respectively (Figure 4.3.6). The shape and contours of the fibres were distinct with little ECS in between fibres.

Although there were variations in cell size, the cells appeared bloated at 6 hours as water was absorbed. The ICS from surface muscle cells remained constant while those at the center increased by 5%. The cells were more spherical in shape, with less distinct contours and expanded towards the endomysium. In contrast, fibres at 26 hours had shrank from the surface by 1% (Figure 4.3.5c) and center by 25% (Figure 4.3.5f). The space between fibres increased and contours of the cells became more defined.

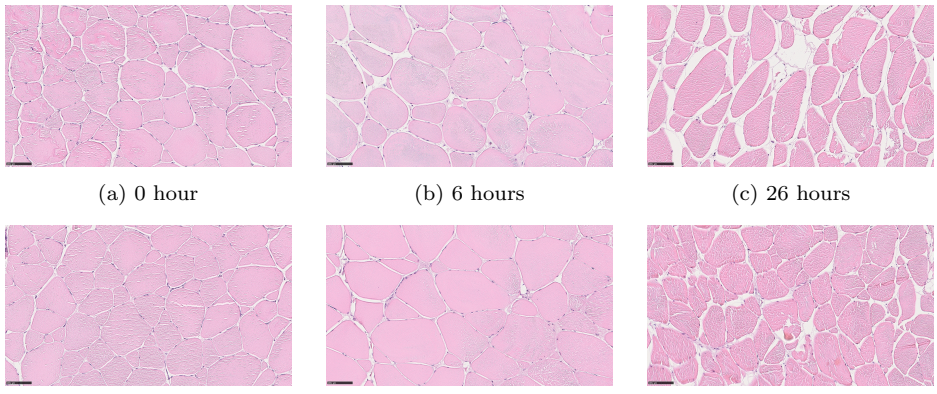

(a) 0 hour (b) 6 hours (c) 26 hours

(d) 0 hour (e) 6 hours (f) 26 hours

Figure 4.3.5: Histological cross section of samples in 0% NaCl at 0, 6 and 26 hours *post mortem*. (a), (b) and (c) were taken from the surface while (d), (e) and (f) were taken from the central part of the tissue section.

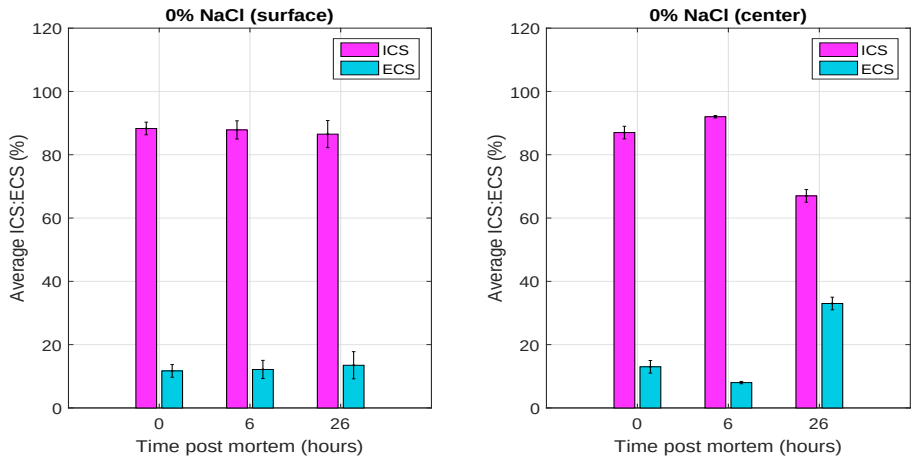

Figure 4.3.6: Average percentage of ICS:ECS of muscle fibres at 0% NaCl at 0, 6 and 26 hours *post mortem*. The left graph depicts the surface while right graph the center of the tissue samples.

0.9% NaCl Solution

Muscle fibres in 0.9% solution resembled the dry samples at 0 hour, occupying 79% and 86% of ICS at the tissue surface and center (Figures 4.3.7a and 4.3.7d). Their contours were also distinct. Nevertheless, fibres from the surface started to disintegrate at 6 hours (Figure 4.3.7b). This expedited the disruption of the endomysium, causing an increase in ECS by 9%. There were empty spaces between the myofibrils where intracellular material may have leaked. The fibres from the center on the contrary remained intact, with an increase in ECS by 4%.

The ECS of the center samples further increased by 14% as the fibres started to disintegrate at 26 hours (Figure 4.3.7f). Muscle cells on the surface have further disintegrated and lost its internal cell structure, leading to a decrease in ECS by 5% (Figure 4.3.7c).

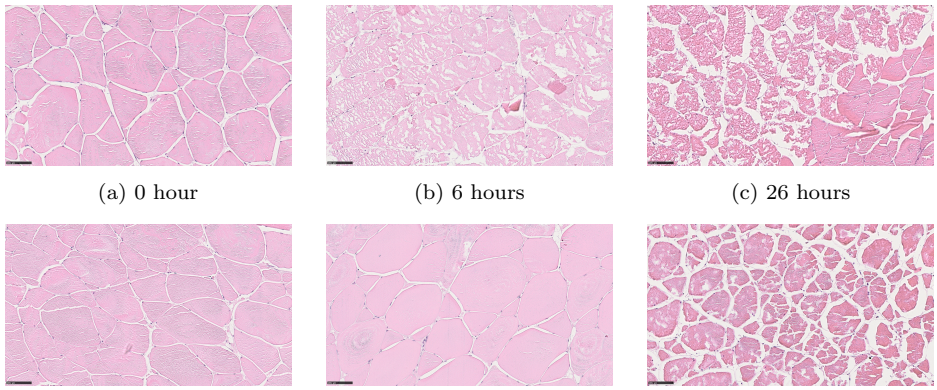

(a) 0 hour (b) 6 hours (c) 26 hours

(d) 0 hour (e) 6 hours (f) 26 hours

Figure 4.3.7: Histological cross section of samples in 0.9% NaCl at 0, 6 and 26 hours *post mortem*. (a), (b) and (c) were taken from the surface while (d), (e) and (f) were taken from the central part of the tissue section.

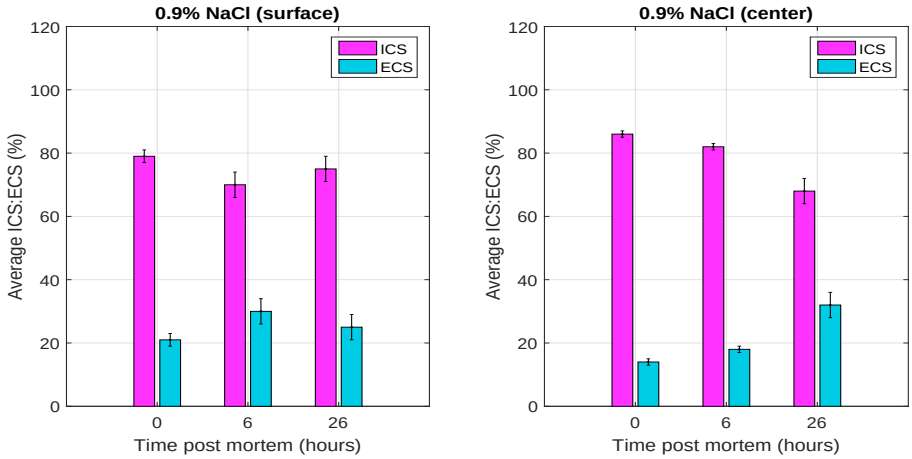

Figure 4.3.8: Average percentage of ICS:ECS of muscle fibres at 0.9% NaCl at 0, 6 and 26 hours *post mortem*. The left graph depicts the surface while right graph the center of the tissue samples.

2% NaCl Solution

At 0 hour, the ECS from the tissue surface and center occupied 13% and 30% of the total area (Figure 4.3.10). An obvious gradient was observed were the central region of the muscle have shrank significantly more than the surface fibres (Figure 4.3.9a). The centre fibres were heterogeneous but the endomysium were preserved nicely (Figure 4.3.9d). It was clear that the fibres were immersed in a hypertonic solution since the contours became notably sharper due to the shrinkage. There was little or no fixed arrangements of the cells in the tissue, with a variety of triangular and squarish shapes. On the contrary, muscle fibres from the surface immediately swelled up after immersing the muscle in solution for around 10 minutes. They were compressed together with little space within the pericellular layer[1], extending towards the endomysium.

The pericellular layer of tissue surface was disturbed and swelled up immensely at 6 hours (Figure 4.3.9b). Fibres were very squeezed together around surrounding cells. The ECS from the surface remained at 13% while the central region began to swell up and occupied more space, decreasing its ECS by 9% (Figure 4.3.9e).

Surface muscle fibres (Figure 4.3.9c) remained swollen at 26 hours and ECS declined by 3%. The central fibres have likewise swelled at 26 hours (Figure 4.3.9f) as ECS fell by 3%.

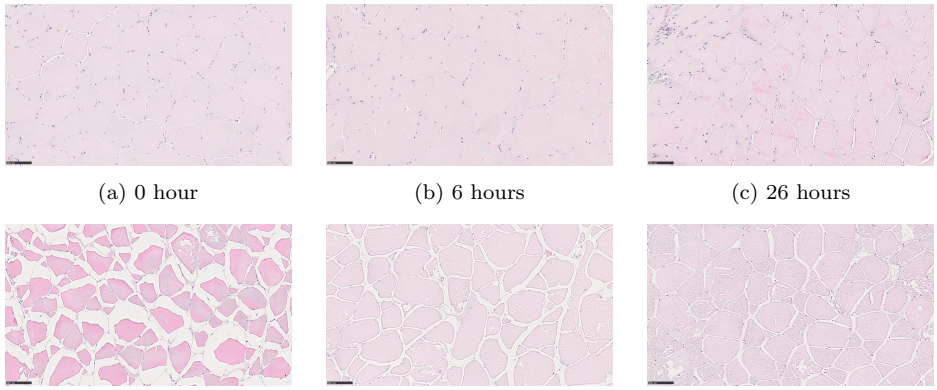

(a) 0 hour (b) 6 hours (c) 26 hours

(d) 0 hour (e) 6 hours (f) 26 hours

Figure 4.3.9: Histological cross section of samples in 2% NaCl at 0, 6 and 26 hours *post mortem*. (a), (b) and (c) were taken from the surface while (d), (e) and (f) were taken from the central part of the tissue section.

[1]The pericellular layer is a thin, threadlike sheet surrounding the cells

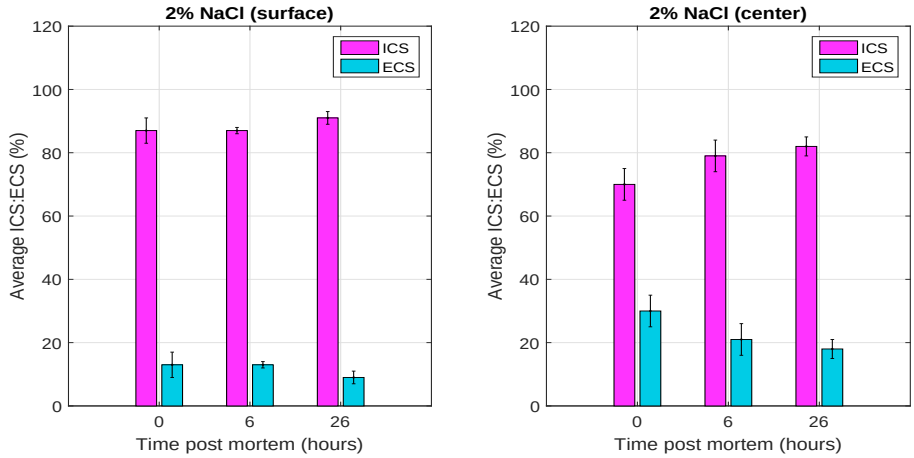

Figure 4.3.10: Average percentage of ICS:ECS of muscle fibres at 2% NaCl at 0, 6 and 26 hours *post mortem*. The left graph depicts the surface while right graph the center of the tissue samples.

Saponin with 0.9% NaCl Solution

For muscle specimens in saponin solution, the appearance of the tissue surface and centre looked similar where fibres were compact with small volumes of ECS (Figures 4.3.11a and 4.3.11d). The tissue surface and center covered 17% and 25% of ECS respectively (Figure 4.3.12).

At 6 hours, cells began to disintegrate from the surface as the saponin solution punctured the cell membrane. The overall shape of the fibres can still be observed but the ICS has decreased by 10% from the surface (Figure 4.3.11b). The tissue center did not disintegrate as much and had a lower ECS of 2% (Figure 4.3.11e).

Muscle fibres at 26 hours appeared more disintegrated both at the tissue surface (Figure 4.3.11c) and center (Figure 4.3.11f). There was a delayed effect of saponin at the center of the tissue. The peripheral nuclei were scattered and intracellular components were leaked out, losing their cell structure and shape. ICS from the surface and center has further decreased by 3% and 6%.

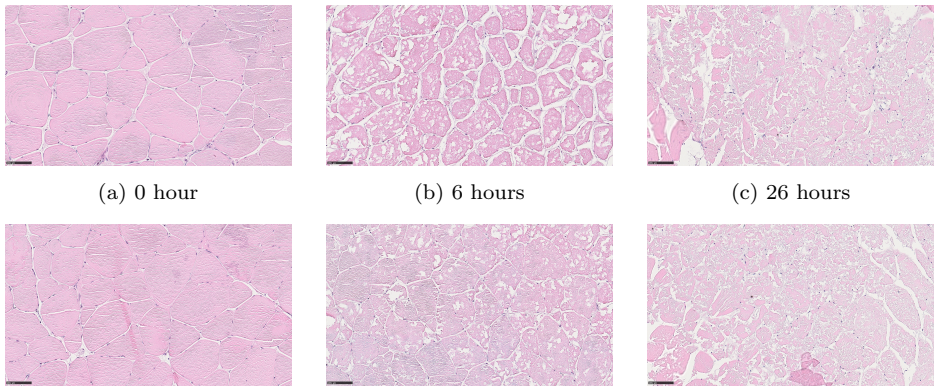

(a) 0 hour (b) 6 hours (c) 26 hours

(d) 0 hour (e) 6 hours (f) 26 hours

Figure 4.3.11: Histological cross section of samples in saponin solution at 0, 6 and 26 hours *post mortem*. (a), (b) and (c) were taken from the surface while (d), (e) and (f) were taken from the central part of the tissue section.

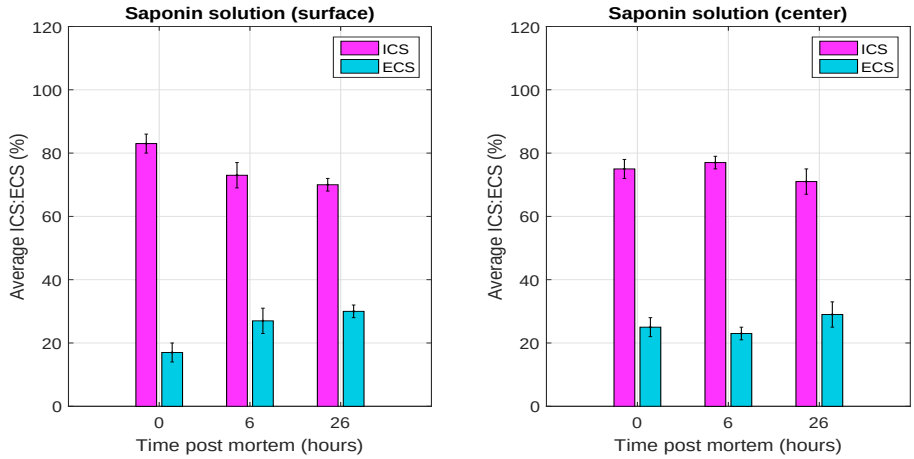

Figure 4.3.12: Average percentage of ICS:ECS of muscle fibres in saponin solution at 0, 6 and 26 hours *post mortem*. The left graph depicts the surface while right graph the center of the tissue samples.

Inter-Fibre Distance and Angle

The average distance between cells and angles for the various groups of samples are given in Figures 4.3.13 and 4.3.14.

The distance from the surface and center part of the dry samples increased by 2 μm and 5 μm over time, indicating an increase in the ECS that was depicted in Figure 4.3.4. Since the cells became more edged in shape as rigor progress, the cell angles had a general decrease in trend of 46°.

For muscle samples in freshwater, cell-to-cell distance from the surface increased gradually by 3 μm, which was in agreement with the observed increase in the amount of ECS. Likewise, images from the central section decreased in fibre distance by 1 μm at 6 hours then elevated by 7 μm at 26 hours and this was also consistent with the change in the ECS. In contrast, the cell angles decreased by 26° and 12° at the tissue surface and center respectively. This did not coincide with the fibre distance and volume since the fibres appeared to swell up at 6 hours, giving a more obtuse value in angle.

Fibre distance from the tissue surface and center in 0.9% salt solution raised by 2 μm and 6 μm respectively. This result also corresponds with the volume occupied by the ECS, with a greater increase in the calculated ECS from the center than surface of the muscle. Cell angles from the tissue surface reduced by 15° while the tissue center rose by 10°.

In the case of samples in 2% salt water, the average inter-fibre distance were higher at the central region than the surface. There was a descending trend of fibre distance for both at the surface and center by 4 μm and 8 μm. This was in conjunction with the ECS volume where it was higher in the tissue center since the cells have shrank. Nevertheless, the cell angles increased by 21° and 11° in both tissue surface and center.

Both fibre distances from surface and centre regions of muscle in saponin increased by 6 μm. This trend was also similar to the ECS volume that increased over time, except for a slight decrease at 6 hours for the central region. The cell angles calculated showed that they remained nearly constant throughout the process.

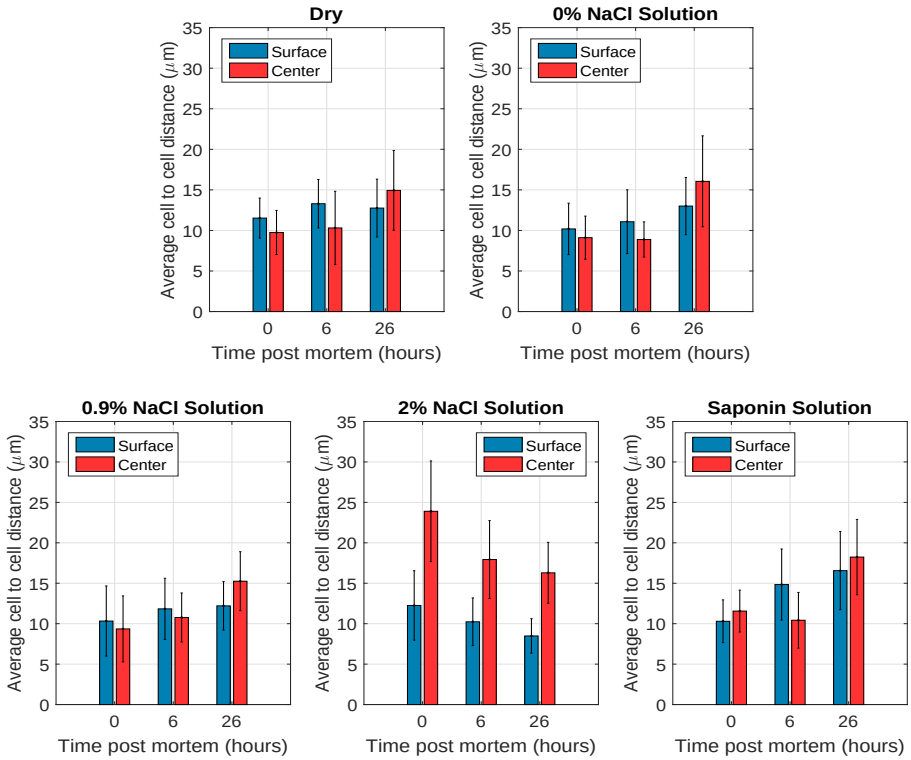

Figure 4.3.13: Average distance between muscle fibres in different solutions at 0, 6 and 26 hours *post mortem*.

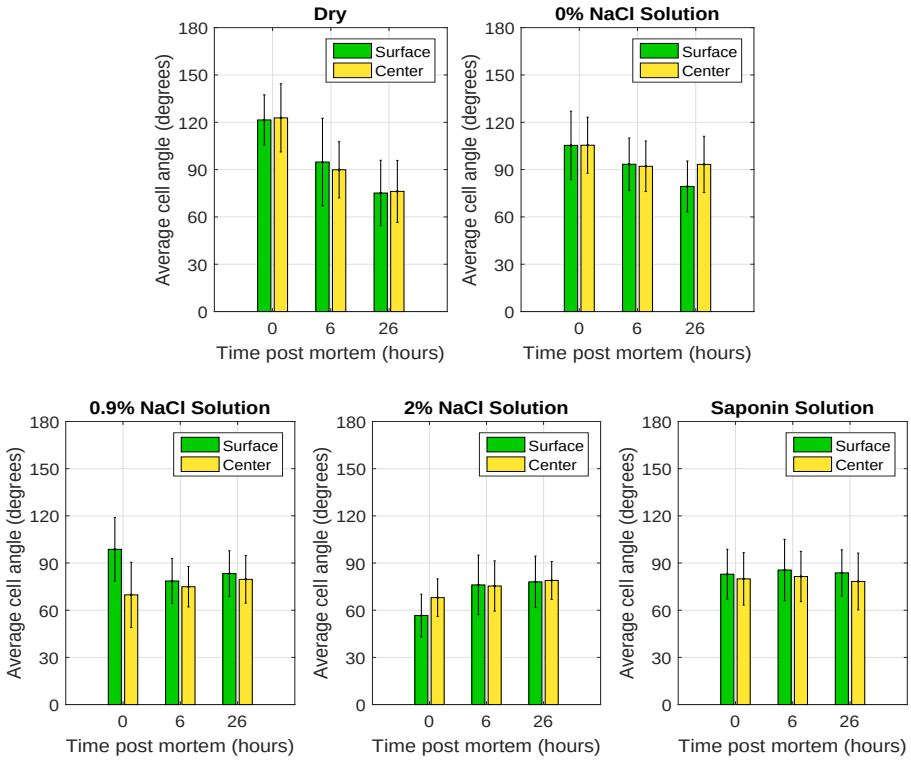

Figure 4.3.14: Average angle of muscle fibres in different solutions at 0, 6 and 26 hours *post mortem*.

Chapter 5

Discussion

This chapter is divided into six sections and discusses the results attained from the three experiments. The first section compares the dimension measurements from the experiments while the second section focuses on the rigor index and texture analysis results from Experiment 2. The third section explains the observed effect of formalin fixative, whereas the fixative and staining method used in Experiment 3 is examined in the fourth section. Next, the fifth section compares the different software used for morphological studies in Experiment 3. Lastly, morphological analysis done in the last experiment is further discussed.

5.1 Comparison of Dimension Measurements

In the experiments, the flow of water to and from a muscle immersed in a given solution was conveniently determined by weighing the muscle on a mass balance at successive time intervals. Although some errors may have occurred during drying when samples were immersed each time, they were dried consistently to impel off water before each measurement. By adopting a constant routine of gentle wiping and weighing, the errors of observation were reduced to a minimum.

It was seen that the change in mass, length and width measurements from Experiment 2 were lesser than the other two experiments. This was likely caused by the relatively thicker fillets used, thus having a lower surface-to-mass ratio. The surface area of the whole fillets in Experiment 2 were higher as compared to the thinner tissue slices. Hence a longer time was needed for water movement from the sample surface to the central region in Experiment 2.

The dry control samples in all three experiments uniformly indicated mass and width reductions accompanied by heavy contractions. These were the only group of samples with a steady mass decline compared to other groups in solutions. An

explanation for this mass decline is that diffusion of water occurred from the muscles and skin to the exposed surface. This caused the muscles to appear rough and dry. As time increased, the muscle surfaces gradually dried up and rate of water loss falls. Moreover, it was observed that muscles immersed in freshwater contracted faster than the control samples in all experiments. This implied that the movement of water in and out of the cell can affect the rate of *rigor mortis*.

The osmolarity of glucose in muscle tissues is around 60 mOsm/L. For tissues immersed in the 350 mOsm/L glucose solution (Experiment 1), the idea was that glucose influx into muscle cells will increase lactate production. Glucose was converted to pyruvic acid then to lactate by the enzyme lactate dehydrogenase. This process caused a hike in ionic strength within the ICS and an influx of water into the cells to achieve osmotic equilibrium. Therefore mass increased after some time with a serious rigor contraction, as actomyosin bridges were formed. To compensate for this contraction, width expanded. However the expansion in width did not correlate to the contracted length, depicting a possible volume change during rigor.

The results for tissues in hypotonic solution (0 mOsm/L) were consistent among all experiments as mass progressively increased immediately after immersion. For isotonic solution (350 mOsm/L), the mass for all samples initially remained constant but gradually increased with time. Samples immersed in hypertonic 1.5% NaCl (500 mOsm/L) and 2% NaCl (680 mOsm/L) had a decrease in mass during the initial hours followed by an increase. This was similar to that of 0.9% NaCl, except that mass decreased initially due to osmotic properties. It was observed that mass for all experiments had the greatest increase when fillets were in hypotonic solution. As the solution was hypoosmotic, muscle fibres had a higher osmotic pressure. Water movement, which is osmotic driven, caused water to move fromt he surroundings into the cells. Hence the cells took up water, expanded in size and appeared bloated during rigor.

Samples in isotonic solution had an initial delay since there was no net movement of water. As the muscle entered rigor, osmolarity and ionic concentration in the cells increased, resulting in the uptake of water into the cells. When the solution is hyperosmotic, water is drawn out from the ICS to the ECS and surrounding to maintain osmotic equilibrium. Nonetheless, the mass did not change in direct proportion to the tonicity of the bathing solution. As time after death increased, ion concentration increased intra-cellularly and the reverse phenomenon occured, allowing water to flow into the ICS. Apart from Experiment 3, samples in 2% NaCl had changed more in mass than those in 1.5% NaCl since it had a higher osmolarity.

Saponin solution was used in Experiment 3 to perforate the cell membranes and prevent build-up of intracellular pressure. This solution was isotonic so there was initially no change in mass. Saponin fell into effect with time as it gradually disintegrated the membranes. This induced a leakage of intracellular components to the surroundings. The effect of saponin weakened as the depth deepened into the

tissue center. Hence mass increased and width expanded as water entered the cells, while having a contraction.

In general, the change in mass was calculated to be significant among the various treatments in all experiments. Contraction rates did not differ among the groups, showing that actomyosin contraction still occurred, dry or in solutions regardless of salinity. The greatest contraction rate occurred for samples in hypotonic solution. From this it is induced that the change in mass is independent with contraction rate, which can be explained by the change in osmotic pressure in cells.

5.2 Rigor Index and Texture Analysis

One of the main aspects of this thesis was to study the impact of fillets in different solutions to flesh firmness (texture). In Experiment 2, the breaking force used to penetrate the fillets was chosen as a firmness determinant for texture analysis. The rigor index method done in the study served as a guide to follow the rigor progess for the whole fillets, so texture and morphological analysis can be done. This method is an easy and practical method to observe rigor development. It is however important to note that the whole fish and fillet samples used in the experiment may have entered and exited rigor at different times. (Cappeln and Jessen, 2002) stated that during rigor development, contents of glycogen and ATP decreased differently depending on the fillet location. Hence this might render the rigor index method as an indication of rigor for the fillet samples to be inaccurate.

The rigor index results obtained in this study were consistent with previous findings until 26 hours (Toyohara and Shimizu, 1988; Wang et al., 1998; Ando et al., 1991; Balevik, 2004). Wang et al. (1998) and Balevik (2004) stated that rigor resolution began after 30 hours when fish were kept at 4°C. In contrast, the rigor index measurements of Toyohara and Shimizu (1988) and Ando et al. (1991) plateaued after the maximum stiffness even after 72 hours at higher temperatures. In this study, rigor resolution was also not observed at 50 hours although the fish were kept at 14°C. Therefore the time of rigor resolution fluctuates among various researches. This can be due to muscle fibres in each individual fish having its own time for rigor maximum and resolution due to different metabolic and physiological status.

It is generally accepted that the hardness of fish is at its highest when the fish is in rigor, and reduces as rigor decreases (Dikeman and Devine, 2014). The contraction and rigor index measurements illustrated that stiffness was high at around 4 to 6 hours *post mortem*, so the breaking force was also expected to be high at this time. However, the breaking force results gave a general reduction with time despite that rigor being at its highest. Such observations were also found in other studies (Toyohara and Shimizu, 1988; Roth et al., 2002; Slinde et al., 2003). These results suggest that the stiffness in the fish muscle is independent of *rigor mortis* and there may be another factor in addition to actomyosin bond that causes the

rigidity.

The results for time to breaking strength, shear force where the probe was pressed at 5 seconds, and the 3D plots did not give an obvious relationship with time *post mortem*. Moreover, when individual texture analysis results were compared (Appendix B.3), it was difficult to correlate the shear force used for muscle penetration to rigor. These high standard deviations among individuals reflected high variations between samples. Generally a high standard deviation reflects a disadvantage for the method but perhaps it may be more descriptive on textural analysis because it reflects high variations between samples.

Many factors could have contributed to this high individual variations from the texture analysis results. During the experiment, handling was a main problem as fillets were moved back and forth from the texture analyser to the various solutions or left to dry. This may have possibly affected the muscle structure and the original characteristics of the samples, so the fillets have gone quickly out of rigor. It would be more desirable to use an established method that does not require extensive handling of the fillets. In addition, there is currently no universal method nor an agreement on which method is best for measuring the textural properties in fish (Hyldig and Nielsen, 2001; Hultmann, 2003). The fillet temperature during textural measurements is also crucial as fish softens when temperature increases. Small temperature fluctuations have been proven to influence the measurements (Mørkøre, 2002), so the fillets should have as equal temperature as possible. During the experiment, the texture analyzer was located at another room so the temperature was difficult to keep constant and monitor.

Furthermore, the instrumental method used in the experiment may not be optimal. The instrumental set-up and cylindrical probe were chosen based on the availability of equipment. It may be possible that the geometry of the 10 mm cylindrical probe or testing device was not the best device to use in detecting small changes in textural properties. Mørkøre and Einen (2003) has compared different systems for instrumental texture determination between salmon fillets. There were significant differences observed with the two cylinders and sphere, but not with the Warner-Bratzler blade. Veland and Torrisen (1999) also compared the Warner Brazler blade test with a spherical probe (25 mm diameter) in salmon fillets and found that the shear test detected a slightly more sensitive result than the compression test in differentiating the texture. In contrast, Mørkøre (2002) recommended using a 12.5 mm diameter flat-ended cylinder with a 90% compression force for objective texture analysis in raw salmon. Therefore there are conflicting opinions as to which instrument is optimal to use as each instrument has both pros and cons in determining textural properties.

Sigurgisladottir et al. (1999) suggested that the area under the dorsal fin is suitable for measuring textural properties in fish. It was however difficult to place the plunger on the sample fillets without hitting some part of the bone structure or

connective tissues during the experiment. The heterogenic orientation of structural elements like fat distribution, pigments and collagen within the flesh varied and could have interrupted with the parameters. The geometry of the samples (i.e. fillet thickness) was also be considered as a source of variation when a compression test was applied directly to the fillet. The fillets used had different thickness from head to tail, so the comparison became more uncertain and its textural properties varied. Besides, there is no conclusive evidence as to which region rigor actually starts. (Casas et al., 2006) found that muscle from the tail part were firmer than the rest of the salmon fillet. In contrast, Sigurgisladottir (2001) revealed that hardness and shear force required increased from head to tail when fillets of natural thickness were used.

Nevertheless, an increase in fillet gaping was observed during the experiment especially for the fillets in solutions. The myosepta eventually separated from one other as time increased. Gaping is frequently accompanied by tissue softening (Einen et al., 1999), but can occur even if the flesh is firm (Mørkøre and Rørvik, 2001). This lead to an increased deformation of muscle fibres which made the texture measurements even more challenging. Fish diet could have also influenced the texture analysis and rigor index measurements (Kiessling et al., 1990; Einen et al., 1998). Some studies showed a positive correlation between softness to a high fat content in diet (Andersen et al., 1997). Therefore, all the above mentioned factors are credible reasons that could explain the high variations from the obtained results.

5.3 Effect of Formalin Fixative

In Experiment 2, the histological samples might have been too thick prior to trimming which influenced the rate of fixative penetration. Formalin fixation is dependent on diffusion of fixative into the specimen. The thicker the tissue, the more time is needed to achieve complete penetration and cross-linking of tissue proteins. The center of the tissue could also suffer from autolysis or incomplete fixation. Hence, tissues should be cut no thicker than 3 mm and soaked in NBF immediately after.

10% NBF is the most widely used fixative for tissue preparation in histological examinations that provides the best preservation for tissue morphology (Travlos, 2006). It is also inexpensive and easy to use without any adverse effects. Formalin fixes by introducing cross-linkage to the side chains of basic amino acids and to the amide nitrogen atoms of peptide linkages (Nowacek, 2010). Thus cross-linking methylene bridges are formed when two formaldehyde binding sites are in close proximity.

The total effect of formalin in the tissues were assessed after the samples have been processed, sectioned and stained in Experiment 2. It was seen that the nuclei

remained attached with the sarcolemma while the ICS seemed to have shrunk in size. The ECS was greater than expected especially for the control sample at 0 hour as the ICS:ECS ratio was expected to be 60-70%:30-40%. This high amount of ECS observed can possibly be explained by the effect of the formalin fixative. Tissues frequently change in volume during fixation (Chatterjee, 2014). Most fixatives can cause some degree of shrinkage or give inadequate protection so tissue shrinkage occurs during dehydration and clearing. The mechanisms involved are not fully understood, but different factors have been suggested like change in membrane permeability and ion transport through membranes.

Most studies have concluded that tissues should be fixed in NBF for 24-48 hours. After 24-48 hours, the samples should be extracted from NBF and transferred immediately for tissue processing and paraffin embedding. If this cannot be performed after the 48 hour fixation period, the samples should be transferred to 70% ethanol (Werner et al., 2000). The histology samples used in the experiment were transported from Matre to Trondheim and morphological studies only started a week later. The transportation process, unstable temperature and excessive fixation time could have jointly caused the shrinkage of muscle fibres. Chatterjee (2014) suggested that tissues fixed in formalin and embedded in paraffin wax could shrink by 20-30% of its volume. Prolonged fixation in formalin can lead to further shrinkage and hardening during subsequent processing in paraffin wax. NBF may further give poor cellular detail and lose certain staining characteristics. Therefore as the tissue samples were fixated in formalin for over 48 hours, this lead to tissue shrinkage and presence of tissue artefacts, affecting the calculation of ICS and ECS. Shrinkage not only occurs to the overall tissue piece becoming smaller in dimensions. It also occurs at a cellular level where cells and fibres separate from each other, introducing spaces that were non-existed before.

Muscle growth is a dynamic process in fish. Enlargement of existing fibres (hypertrophy) and recruitment of new fibres (hyperplasia) within a muscle mass still continues even past the age of sexual maturity. Another explanation for the high amount of ECS observed is that the samples may have been taken from these recruitment areas. Recently recruited fibres are relatively small in size and these fibres increase in cross sectional area through hypertrophic growth (Karahmet et al., 2014). Hence the empty spaces seen in the ECS is to give the intracellular components a sufficient space for growth and increase in fibre size.

As morphological studies from Experiment 2 gave inconclusive data, the tissues were deemed unsuitable for further examination. These results were not followed up due to the presence of artefacts that could be introduced by formalin, transportation, handling, staining method or others. Morphological studies was again done in Experiment 3 to confirm the effect of formalin by comparing it with Clarke's solution.

5.4 Fixative and Staining Method Comparison

There is currently no consensus on the best fixation method ideal for preserving all tissue components. The tissues fixated in Clarke's solution was expected to contribute to a more uniform tissue fixation with minimal loss of tissue components due to its low molecular weight and rapid tissue penetration. Since it contains no water, the Clarke's solution can almost completely dehydrate the specimen, thus has a shorter processing time than NBF. However, multiple studies revealed that noncross-linking alcoholic reagents are not suitable for morphological studies due to shrinkage (Srinivasan et al., 2002). The orange G-aniline blue staining method used with Clarke's fixative was also expected to provide good contrast between muscle fibres (orange), connective tissues (blue) and fat cells (white). But uneven staining and shrinkage of tissue sections were observed in the image results. This solution is more recommended for frozen tissues, preserving the nucleic acids while lipids are extracted. Therefore this fixation and staining method was not chosen for further morphological analysis.

In comparison, tissues fixated in NBF and stained with H&E in Experiment 3 gave more promising results than Experiment 2 as they were processed immediately after 2 days. This eliminated the chance of shrinkage and presence of non-existing artefacts with a more even staining. Hence this method was chosen for further morphological analysis in Experiment 3. Matlab and ImageJ software were used to analyse the tissue sections and compared.

5.5 Matlab and ImageJ Comparison

In Experiment 3, it was challenging to decide the area per point via ImageJ grid counting method to ensure that an overall representation was achieved while having an appropriate numbers of grids. Too many grids can affect the manual counting method due to human error. These grids only served as a representation on the amount of ICS and ECS and did not cover the whole image area. There were instances that the grids failed to hit the ECS, leading to a lower value obtained even though visual observation presented otherwise.

BoneJ is more suited for bone image analysis by calculating its trabecular geometry and whole bone shape. In comparison, Matlab gave a more precise calculation of the ICS and ECS. Matlab provides accurate solutions to problems, producing graphics easily and code efficiently. Image thresholding is a simple yet effective segmentation method of separating an image into a foreground and background (Verma et al., 2013). It is also more flexible to set and standardize the image threshold for image segmentation to reduce the error seen as white pixels in the ICS. Therefore, this software gave better estimations on the amount ICS and ECS, calculating the black and white pixels numerically.

5.6 Morphological Analysis

This section discusses the morphological results from Experiment 3. The biggest challenge in morphological studies is to find the property of cells that can accurately explain the differences. There is currently no standard way of quantifying morphological images. It was found challenging to measure muscle fibre angles without any errors incurred due to the high variations of angle measurements in each cell. In addition, the time selected for post rigor fixation at 26 hours might have not been the best time for observing all the differences.

The research of Slinde et al. (2003) and Balevik et al. (2004) cited that *post mortem* reactions cause the osmotic pressure to increase in the cells, resulting in movement of water from the ECS to ICS to achieve equilibrium. However, results from the dry control samples did not match with these findings. Samples used in the experiment of Balevik (2004) were left with the skin on and wrapped in aluminium foils to prevent dehydration. In contrast, the dry samples used in this project were exposed to the surrounding air especially at the tissue surface. Consequently, dehydration slowly occurred while the muscles were undergoing rigor. During rigor development, the WHC of muscle fibres were drastically altered. The membrane flexibility may have deteriorated as a result of enzymatic degradation processes, inducing water to move out from the fibre into the ECS.

The process that occurred in the experimental dry samples were basically the preservation method of air drying under open surroundings. It was speculated that the thermodynamic activity of water in the muscle fibre was a significant contributing factor to the tensile and adhesive properties of muscle (Oplatka, 1994). Most water in the muscle are located in structures of the cell, at the ICS. Previous observations showed that changes occur in the ECS from *post mortem* reactions (Huff-Lonergan and Lonergan, 2005). This causes protein denaturation, specifically myosin denaturation and results in myofibrillar lattice shrinkage. This shrinkage reduces spaces between myofibrils and forces water out from the ICS. The disintegration of cellular membranes also contributes to water leakage out of the ICS during the same process. This rapid rate of change in WHC in muscle results in the transport of intrafibre water in and out of the ECS in the form of drip (Huff-Lonergan and Lonergan, 2005; Zayas, 1997; Currie and Wolfe, 1980; Heffron and Hegarty, 1974). Therefore major changes in the intracellular architecture of the cell during rigor affects the ability of muscle cells to retain water. This negatively influences meat quality and gives significant drip loss. The evaporation of water observed in the tissues uses the principle of the first law of thermodynamics and this has preceded the movement of water to achieve Donnan equilibrium ($\Pi = cRT$) in the samples. Hence the muscle cells shrank in size and became sharper in the edges while the ECS increased, even if the osmotic pressure increased in the ICS.

Moreover, WHC is high after slaughter and decreases rapidly during rigor. This decreases the fibre diameter over time and at the same time, increases the amount

of ECS. As muscle pH drops, ECS of the samples become hyperosmotic, causing migration of water from the fibre into the ECS through the sarcoplasmic membrane (Bonnet et al., 1992). Heffron and Hegarty (1974) found changes in intracellular diameter *post mortem*, which decreased with 18.5% from pre- to rigor state. This finding correlated to the experimental results as interfibre space increased from pre-rigor to rigor state, which is likely the result of lateral shrinkage of the myofibrils to the entire cell. A study by Bertram et al. (2002) found that a higher fraction of water is held in the I-bands of the myofibrils than the more protein dense A-bands. Thus during rigor and I-band shortening, the volume loss in myofibrils combined with the pH-induced lateral shrinkage expel water into the extramyofibrillar spaces in the muscle cell, and ultimately out of the muscle and into the ECS. As a result the overall volume is constricted (Huff-Lonergan and Lonergan, 2005).

Another plausible explanation for fibre shrinkage could be that the experimental fish used were stressed prior to slaughter. This phenomenon is similar to PSE in pork which suffers from excessive drip loss due to poor water binding capacity. This lead to the meat losing water with an undesirable appearance, lacking firmness. But the dry samples observed in this project had a firm texture with a dark orange colour. Thus muscle fibre shrinkage is most likely caused by dehydration.

For hypoosmotic solutions, Hall (2016) stated that both the intracellular and extracellular volumes increase with the addition of hypotonic fluids. The intracellular volume increases to a greater extent than the extracellular space (Figure 5.6.1). In the experiment, the swelling of muscle was due to the diffusion of water into the cell. Hypotonic solutions tend to lose pressure as they have lower concentration of impermeable solutes. If a hypotonic solution is added to muscle fibres, the osmolarity of the extracellular fluid decreases and some extracellular water diffuses into the cells. This dilutes the ICS while also concentrating the ECS until both places have about the same osmolarity to achieve osmotic equilibrium. This further explains the increase in mass and decrease in ECS, inter-fibre distance and cell angle observed during rigor as cells take up water and gain in mass. At 26 hours, the decrease in ICS volume seen that resulted in the increase of inter-fibre distance may indicate the damage of cell membranes associated with the loss of salts. This allowed the penetration of water into the cells. According to a study by Brading and Setekleiv (1968) in guinea pig muscles, cells at 0.5 tonicity had an increase in ECS due to damage of the cell membranes which permit solutes to enter the cell, suffering a certain loss of intracellular electrolyte. The increase in ECS volume seen in the results could be due to the continuous influx of water into the ECS, accompanied by the damage to membranes, resulting in the continuous mass increase.

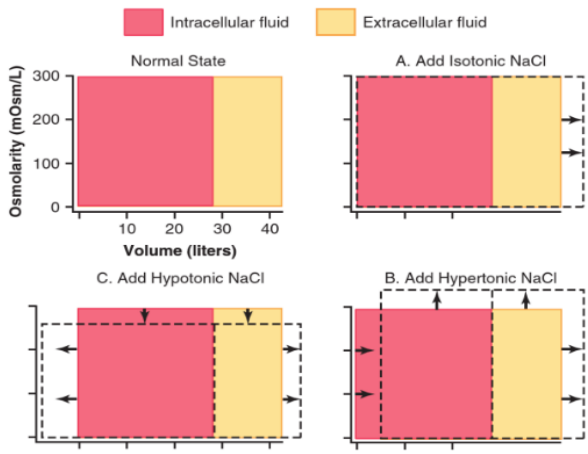

Figure 5.6.1: Effect of different salinities to the intra and extracellular fluid after osmotic equilibrium. The normal state is depicted by the solid lines, and the shifts shown by dashed lines (Hall, 2016).

There was initially no net movement of water through the sarcoplasmic membranes when the samples were in isotonic solution. If isotonic saline is added to the tissue, the osmolarity of the extracellular fluid does not change. An osmotic gradient was found in the morphological studies where the fibres started to disintegrate from the surface of the samples. As osmotic pressure increases over time, water flows into the fibres that resulted in the slow mass increment and disintegration of intracellular components. Hall (2016) explained that ECS increases in isotonic salinity (Figure 5.6.1) and this was observed in this experiment. The Na^+ and Cl^- remain largely in the extracellular fluid as the sarcolemma behaves as though it is impermeable to NaCl.

Hypertonic solutions have osmolarities greater than 350 mOsm/L, so osmotic pressure is unequal inside and outside the compartments. The extracellular osmolarity should initially increase which draws water out from the ICS, inducing cell shrinkage and expansion of ECS (Figure 5.6.1). Almost all the added NaCl should remain in the ECS and this net effect gives an increase in extracellular volume while a decrease in intracellular volume as osmolarity increases in both compartments (Hall, 2016). However, this phenomenon was however not observed from the tissue surface of the morphological samples in Experiment 3. A possible explanation is that fibres have already shrunk shortly after immersion. Carroll (1969) found that wet weight decreased rapidly during the initial 20 minutes of immersion in various hypertonic solutions and steadily increased afterwards. As time increases, the osmotic pressure inside the fibres builds-up as a result of catabolic reactions. Therefore water from the surroundings flows into the cells and swell up. This could explain the difference in gradient from the surface to the center of the tissue as it takes a longer amount of time for the solution to enter the center region. Another possibility is that the

muscle fibres have collapsed when immersed in the solution. Hence the swelling of cells observed was actually a consequence of this collapse, making the fibres packed very tightly together.

Lastly, the function of saponin is to permeabilize cell membranes without destroying them. The muscle fibres disintegrated early hence the difference in osmotic pressure between intra and extracellular fluid were eliminated. Water moved into the compartments freely, accounting for the mass increase. Its effect decreased as depth of penetration increased towards the center of the tissue.

By combining the dimension measurements with the morphology results, it is concluded that there are significant changes in the ICS and ECS as water moves through muscle fibres during rigor development. More research has to be conducted in order to uncover more details regarding the alternative hypothesis and further prove its validity.

Chapter 6

Conclusion

There are still contrasting opinions as to what really is causing the rigor phenomenon. The present study was conducted to provide an overview of mass, contraction and width change that associates with textural and morphological properties. The different saline solutions used in this study showed significant changes in mass as contraction proceeded. This demonstrated that the inflow of water into the muscle cellular structures does play a role in rigor development. Therefore, cross-linkages formed between actin and myosin alone cannot explain the stiffness that occurs during *rigor mortis*.

The breaking force required to shear the fillets was found rather challenging to relate with the dimension measurements due to several contributing factors. However, based on morphological analysis there were obvious differences in intra and extracellular spaces for fillets in varying salinities. Hence it is conceded that osmolarity changes in *post mortem* muscle. Since osmosis leads to water and ion movement between compartments, it is proposed that water displacement intra and extracellularly could be an important factor causing the rigidity during rigor.

A number of limitations was encountered during this study to fully utilize the results, but it presented results which can serve as guidelines for further works in the future. There is a need for further characterization of different methods to determine textural properties and better associate texture with muscle stiffness. There can perhaps be a standard agreement between international researchers on recommended method(s) to analyse textural properties. It would also be interesting to follow the muscle fillets more closely and add in more measuring parameters like pH, lactate, glucose, glycogen and electrical conductivity measurements to strengthen the alternative hypothesis. The volume difference can be observed to accurately conclude whether there is a volume change as water moves in and out of the solution.

Considering that the reduction of quality and weight directly translates to economic loss, the rigor process is of great interest to fisheries and meat industry to prevent huge water loss during slaughter. *Rigor mortis* happens to all animals after death. An increase in the understanding of rigor can overcome the practical problems during early processing, PSE, DFD as well as in forensic science. It can also increase the concept of meat texture, water binding properties and affect different preservations techniques like drying and salting.

To conclude, the alternative hypothesis of *rigor mortis* has proven to be true to a certain extent. Further research that is well-substantiated, unified and verified are required for this hypothesis to be developed into a theory.

Appendix A

Experiment 1

A.1 Dimension Measurements

Table A.1.1: Average percentage change in mass at increasing time *post mortem* for trial 1.

Solution	0 hour	1 hour	2 hours	20 hours
Glucose	100%	97±2%	97±1%	97±2%
0% NaCl	100%	100±1%	100±1%	105±4%
0.9% NaCl	100%	100±1%	100±1%	104±3%
1.5% NaCl	100%	99±0%	97±1%	98±1%

Table A.1.2: Average percentage change in length at increasing time *post mortem* for trial 1.

Solution	0 hour	1 hour	2 hours	20 hours
Glucose	100%	98±1%	89±2%	76±7%
0% NaCl	100%	94±4%	93±6%	87±11%
0.9% NaCl	100%	103±4%	100±3%	86±3%
1.5% NaCl	100%	103±4%	102±4%	88±6%

Table A.1.3: Average percentage change in width at increasing time *post mortem* for trial 1.

Solution	0 hour	1 hour	2 hours	20 hours
Glucose	100%	99±6%	100±10%	107±10%
0% NaCl	100%	99±14%	101±20%	111±24%
0.9% NaCl	100%	98±8%	101±6%	120±14%
1.5% NaCl	100%	92±7%	86±15%	100±13%

Table A.1.4: Average percentage change in mass at increasing time *post mortem* for trial 2.

Solution	0 hour	1 hour	2 hours	3 hours	4 hours	5 hours	23 hours
Dry	100%	99±0%	99±0%	98±0%	98±0%	98±1%	98±1%
Glucose	100%	100±0%	99±1%	99±1%	98±1%	99±2%	99±4%
0% NaCl	100%	102±0%	102±1%	103±0%	104±0%	104±0%	105±3%
0.9% NaCl	100%	100±0%	101±0%	102±0%	101±1%	101±0%	108±1%
2.0 % NaCl	100%	95±1%	94±0%	94±0%	93±1%	92±0%	102±2%

Table A.1.5: Average percentage change in length at increasing time *post mortem* for trial 2.

Solution	0 hour	1 hour	2 hours	3 hours	4 hours	5 hours	23 hours
Dry	100%	96±4%	94±5%	94±6%	93±5%	91±8%	81±2%
Glucose	100%	90±2%	84±2%	80±5%	79±4%	79±4%	78±5%
0% NaCl	100%	91±8%	85±12%	81±10%	80±9%	77±11%	74±9%
0.9% NaCl	100%	101±1%	99±3%	96±4%	92±1%	92±2%	85±3%
2.0 % NaCl	100%	98±1%	98±2%	95±3%	95±4%	95±4%	87±2%

Table A.1.6: Average percentage change in width at increasing time *post mortem* for trial 2.

Solution	0 hour	1 hour	2 hours	3 hours	4 hours	5 hours	23 hours
Dry	100%	103±6%	100±10%	96±13%	93±15%	93±15%	93±15%
Glucose	100%	102±4%	102±4%	105±4%	110±4%	110±4%	110±4%
0% NaCl	100%	106±10%	106±10%	108±7%	106±10%	106±10%	105±5%
0.9% NaCl	100%	102±4%	105±4%	102±4%	100±7%	100±7%	100±7%
2.0 % NaCl	100%	95±13%	94±5%	94±5%	97±4%	97±4%	97±4%

Appendix B

Experiment 2

B.1 Dimension Measurements

Table B.1.1: Average percentage change in mass at increasing time *post mortem* for dry right fillets.

Solution	0 hour	1 hour	5 hours	8 hours	21 hours	25 hours
1-3	100%	99±1%	97±1%	95±1%	92±1%	91±1%
4-6	100%	99±1%	97±1%	95±1%	91±1%	89±2%
7-9	100%	99±1%	96±1%	95±1%	90±1%	89±1%

Table B.1.2: Average percentage change in length at increasing time *post mortem* for dry right fillets.

Solution	0 hour	1 hour	5 hours	8 hours	21 hours	25 hours
1-3	100%	99±2%	92±2%	91±5%	89±6%	88±5%
4-6	100%	101±2%	96±2%	92±5%	90±3%	88±4%
7-9	100%	101±1%	91±4%	88±6%	87±3%	87±2%

Table B.1.3: Average percentage change in width at increasing time *post mortem* for dry right fillets.

Solution	0 hour	1 hour	5 hours	8 hours	21 hours	25 hours
1-3	100%	99±1%	97±3%	98±3%	97±3%	97±3%
4-6	100%	101±5%	98±8%	101±5%	101±5%	99±7%
7-9	100%	99±2%	99±2%	106±6%	103±7%	99±2%

Table B.1.4: Average percentage change in mass at increasing time *post mortem* for left fillets in varying salinity.

Solution	0 hour	1 hour	5 hours	8 hours	21 hours	25 hours
1-3 (0% NaCl)	100%	101±0%	102±1%	102±1%	104±1%	103±1%
4-6 (0.9% NaCl)	100%	99±0%	100±0%	101±1%	102±1%	102±0%
7-9 (1.5% NaCl)	100%	99±0%	99±1%	99±2%	100±2%	102±2%

Table B.1.5: Average percentage change in length at increasing time *post mortem* for left fillets in varying salinity.

Solution	0 hour	1 hour	5 hours	8 hours	21 hours	25 hours
1-3 (0% NaCl)	100%	99±4%	87±1%	85±2%	85±2%	88±2%
4-6 (0.9% NaCl)	100%	99±5%	87±1%	85±2%	84±1%	87±2%
7-9 (1.5% NaCl)	100%	97±1%	85±2%	84±2%	86±3%	89±2%

Table B.1.6: Average percentage change in width at increasing time *post mortem* for left fillets in varying salinity.

Solution	0 hour	1 hour	5 hours	8 hours	21 hours	25 hours
1-3 (0% NaCl)	100%	97±3%	99±3%	100±5%	99±6%	94±7%
4-6 (0.9% NaCl)	100%	96±5%	98±7%	98±3%	95±4%	94±2%
7-9 (1.5% NaCl)	100%	98±2%	99±3%	98±2%	98±2%	96±2%

B.2 Rigor Index

Table B.2.1: Measured tail bend in cm at increasing time *post mortem* for fish 1-6.

Fish	Tail Bend (cm)								
	0 hour	1 hour	2 hours	4 hours	6 hours	9 hours	22 hours	26 hours	50 hours
1	21.5	20.6	20.6	11.6	10.7	8.0	4.3	4.4	4.4
2	19.7	17.0	14.8	9.8	8.0	4.7	2.6	3.4	3.4
3	20.6	18.8	17.9	10.7	9.8	4.3	2.6	3.4	3.4
4	-	18.8	12.5	5.7	4.3	2.6	2.6	3.4	3.4
5	-	18.8	17.0	5.7	5.3	3.4	2.6	2.6	2.6
6	-	18.8	18.8	8.5	7.1	3.4	2.6	2.6	2.6

The curve fitting of tail bend is done the same way as in Section 3.2.2, but with another exponential growth model. The growth model here is given as

$$\mathrm{TB(t)} = \mathrm{N_0} + \mathrm{N_{max}} e^{-\mu_{\mathrm{max}} \mathrm{t}}$$

where $\mathrm{N_0} = 3.27$, $\mathrm{N_{max}} = 18.37$ and $\mu_{\mathrm{max}} = 0.19$ for Fish 1-3, and $\mathrm{N_0} = 2.64$, $\mathrm{N_{max}} = 24.80$ and $\mu_{\mathrm{max}} = 0.38$ for Fish 4-6.

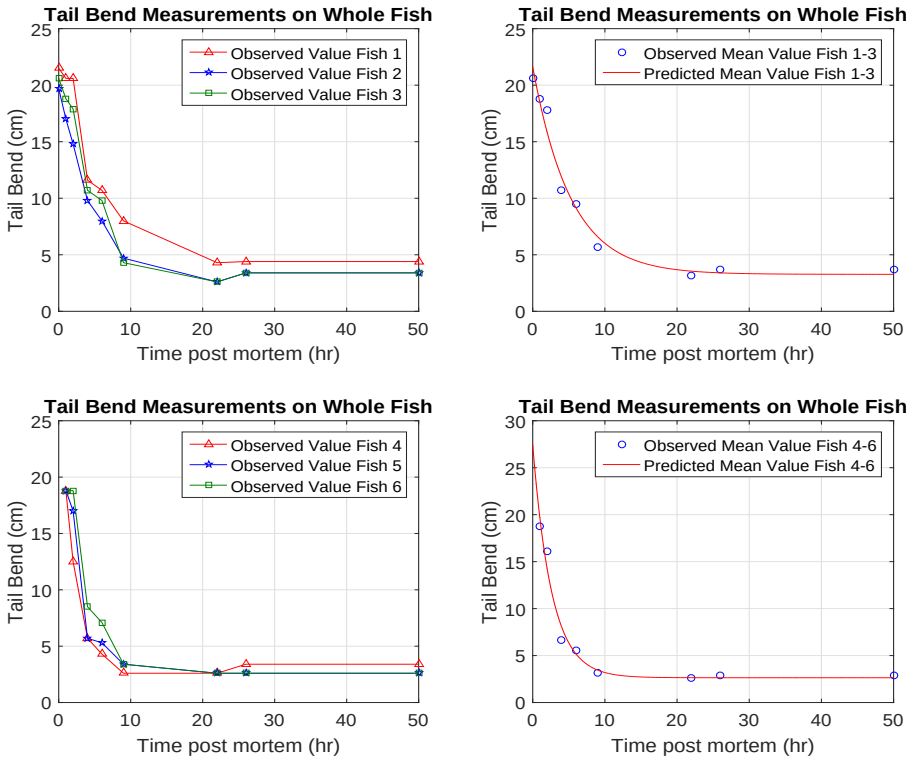

Figure B.2.1: Tail bend measurements on whole fish (left) and predicted tail bending model (right).

Table B.2.2: Calculated rigor index at increasing time *post mortem* for fish 1-6.

Fish	Rigor Index								
	0 hour	1 hour	2 hours	4 hours	6 hours	9 hours	22 hours	26 hours	50 hours
1	0%	4%	4%	46%	50%	63%	80%	80%	80%
2	0%	14%	25%	50%	59%	76%	87%	83%	83%
3	0%	9%	13%	48%	52%	79%	87%	83%	83%
4	-	0%	34%	70%	77%	86%	86%	82%	82%
5	-	0%	10%	70%	72%	82%	86%	86%	86%
6	-	0%	0%	55%	62%	82%	86%	86%	86%

mu_max	0,18
No	0,00
Nmax	84,58

RSS (Residual sum of squares): 218,43

RMSE (Root mean square error): 6,03

Observed Data		Predictive Data	
Time (h)	Sample	Sample	(Residual)^2
0,00	0,00	0,00	0,00
1,00	8,88	13,61	22,37
2,00	14,06	25,02	120,29
4,00	48,12	42,64	30,00
6,00	54,02	55,05	1,07
9,00	72,69	67,13	30,88
22,00	84,73	82,79	3,74
26,00	81,92	83,69	3,13
50,00	81,92	84,56	6,97

E4 = SUM(E11:E19)
E11 = (C11-D11)^2
D11 = C$5+C$6*(1-EXP(-C$4*B11))

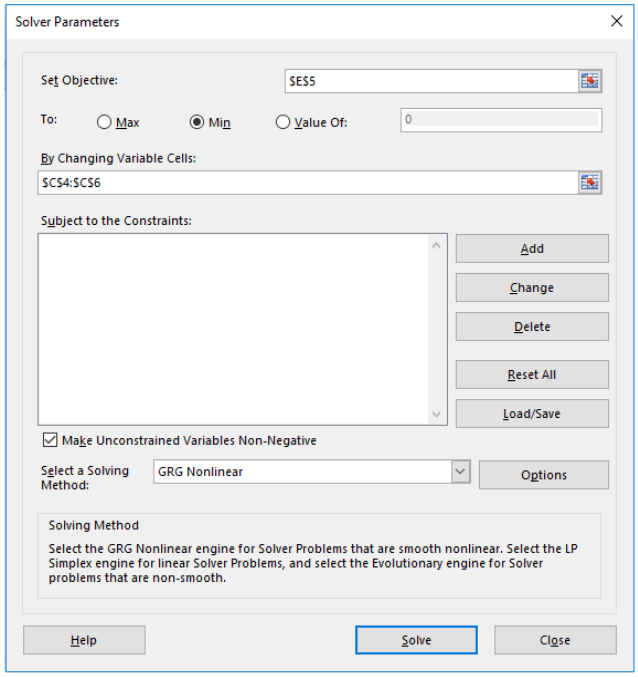

Figure B.2.2: An example of curving fitting using the non-linear in-build solver in Microsoft Excel.

B.3 Texture Analysis

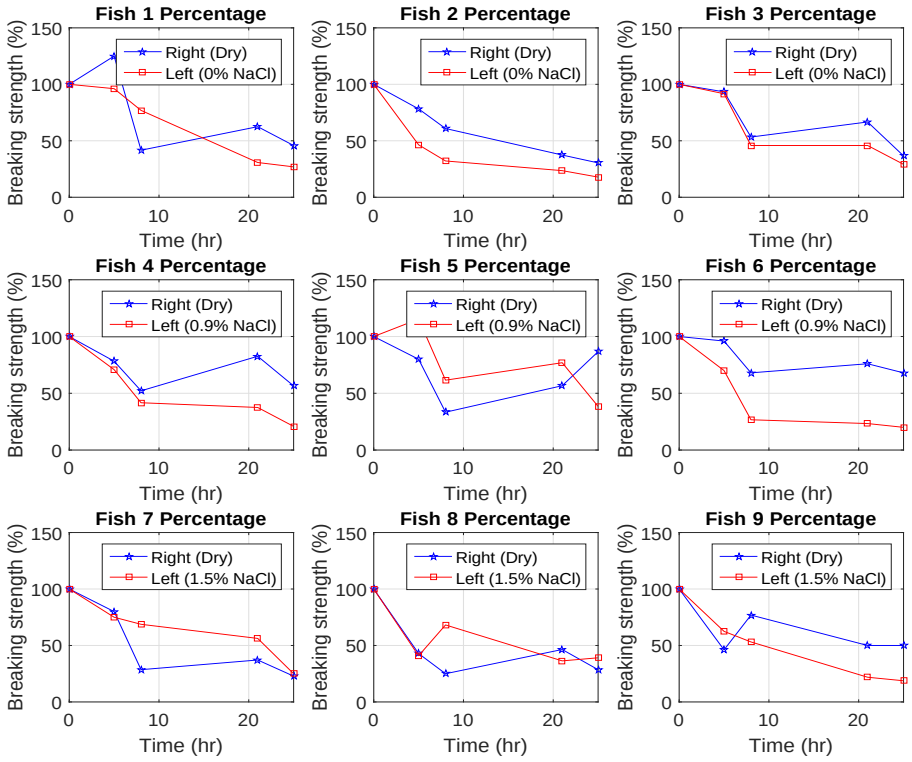

Figure B.3.1: Individual graphs of breaking strength converted to percentage for fish 1-9, both dry (right fillets) and in various solutions (left fillets).

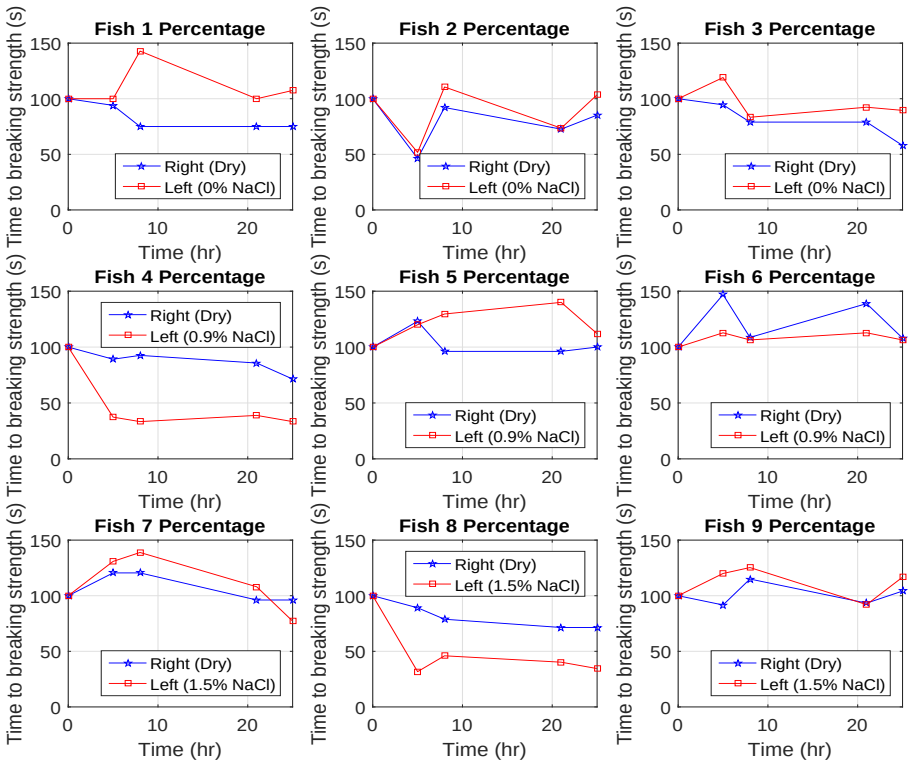

Figure B.3.2: Individual graphs of the time to breaking strength converted to percentage for fish 1-9, both dry (right fillets) and in various solutions (left fillets).

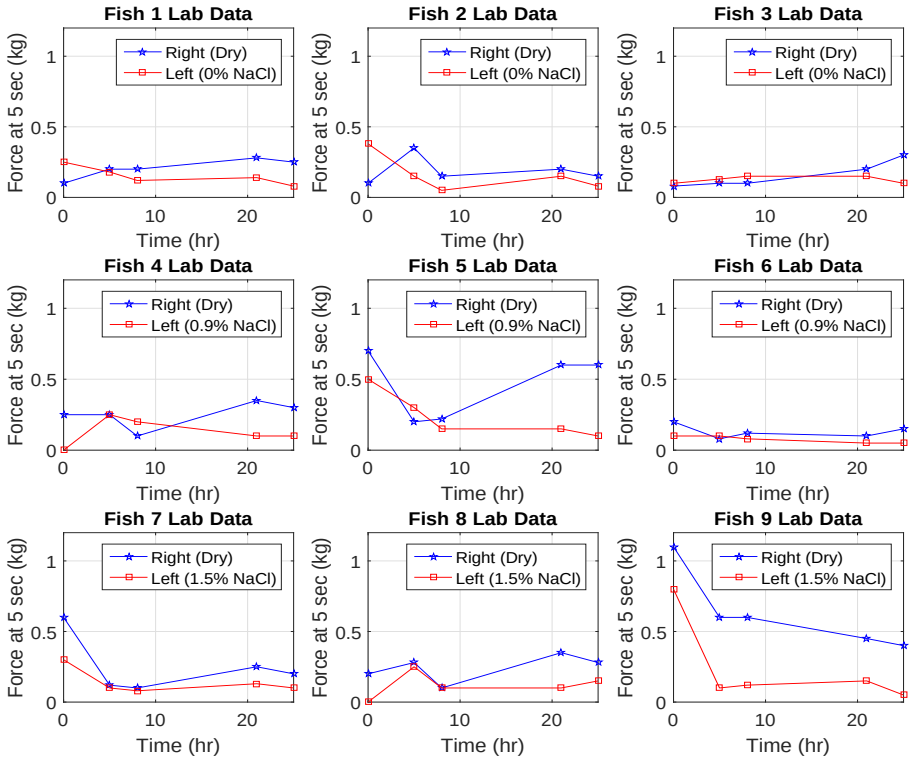

Figure B.3.3: Individual graphs of the force used at time = 5 seconds for fish 1-9, both dry (right fillets) and in various solutions (left fillets).

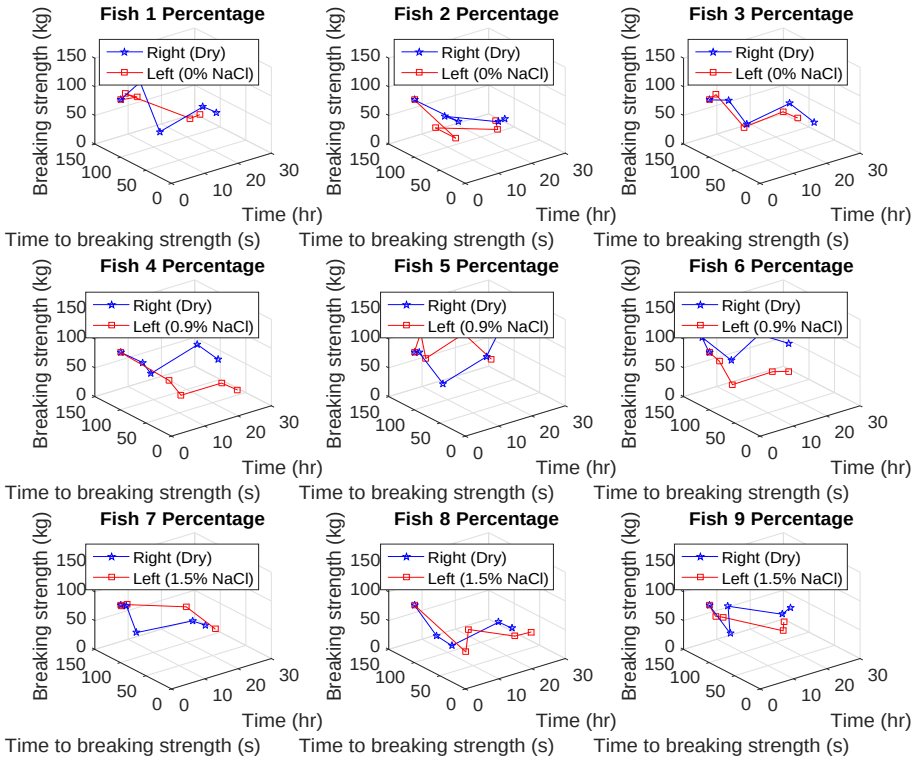

Figure B.3.4: Individual 3D graphs of the breaking strength, time to breaking strength and time *post mortem* for fish 1-9, both dry (right fillets) and in various solutions (left fillets).

Appendix C

Experiment 3

C.1 Dimension Measurements

Table C.1.1: Average percentage change in mass at increasing time *post mortem* for various fillets.

Solution	0 hour	2 hour	3 hours	4 hours	5 hours	6 hours	22 hours	26 hours
Dry	100%	91±0%	88±0%	86±0%	84±0%	83±0%	72±0%	72±0%
0% NaCl	100%	102±1%	103±1%	103±0%	104±0%	105±0%	110±2%	110±2%
0.9% NaCl	100%	101±1%	100±0%	100±1%	100±1%	100±1%	105±1%	107±1%
2% NaCl	100%	100±0%	99±0%	99±1%	98±1%	99±0%	105±1%	107±1%
Saponin	100%	101±0%	101±0%	101±0%	101±0%	102±0%	107±1%	109±1%

Table C.1.2: Average percentage change in length at increasing time *post mortem* for various fillets.

Solution	0 hour	2 hour	3 hours	4 hours	5 hours	6 hours	22 hours	26 hours
Dry	100%	97±0%	97±0%	97±0%	85±0%	87±0%	85±0%	85±0%
0% NaCl	100%	91±1%	91±1%	92±2%	91±1%	87±1%	84±1%	85±1%
0.9% NaCl	100%	97±3%	96±2%	99±4%	96±4%	94±4%	85±7%	84±7%
2% NaCl	100%	102±4%	103±5%	100±6%	100±6%	99±7%	89±10%	91±9%
Saponin	100%	100±1%	100±1%	98±3%	94±4%	94±6%	89±8%	90±3%

Table C.1.3: Average percentage change in width at increasing time *post mortem* for various fillets.

Solution	0 hour	2 hour	3 hours	4 hours	5 hours	6 hours	22 hours	26 hours
Dry	100%	100±0%	83±0%	83±0%	83±0%	83±0%	42±0%	42±0%
0% NaCl	100%	102±3%	102±3%	102±3%	100±5%	97±11%	105±9%	105±9%
0.9% NaCl	100%	95±9%	86±17%	95±9%	93±12%	83±11%	102±3%	102±3%
2% NaCl	100%	100±0%	103±6%	107±12%	100±0%	100±0%	119±27%	120±20%
Saponin	100%	102±3%	98±3%	102±8%	103±6%	105±5%	102±3%	105±9%

C.2 Morphology Analysis

Table C.2.1: Average ICS:ECS in percentage for dry samples (surface).

Dry (top)	Time *post mortem*		
	0 hour	6 hour	26 hours
ICS	84±2%	77±4%	79±8%
ECS	16±2%	23±4%	21±8%

Table C.2.2: Average ICS:ECS in percentage for dry samples (center).

Dry (top)	Time *post mortem*		
	0 hour	6 hour	26 hours
ICS	85±4%	85±3%	77±2%
ECS	15±4%	15±3%	23±2%

Table C.2.3: Average ICS:ECS in percentage for samples in 0% NaCl solution (surface).

Dry (top)	Time *post mortem*		
	0 hour	6 hour	26 hours
ICS	80±2%	82±1%	79±3%
ECS	20±2%	18±1%	21±3%

Table C.2.4: Average ICS:ECS in percentage for samples in 0% NaCl solution (center).

Dry (top)	Time *post mortem*		
	0 hour	6 hour	26 hours
ICS	81±3%	80±3%	67±2%
ECS	19±3%	20±3%	33±2%

Table C.2.5: Average ICS:ECS in percentage for samples in 0.9% NaCl solution (surface).

Dry (top)	Time *post mortem*		
	0 hour	6 hour	26 hours
ICS	79±2%	70±4%	75±4%
ECS	21±2%	30±4%	25±4%

Table C.2.6: Average ICS:ECS in percentage for samples in 0.9% NaCl solution (center).

Dry (top)	Time *post mortem*		
	0 hour	6 hour	26 hours
ICS	86±1%	82±1%	68±4%
ECS	14±1%	18±1%	32±4%

Table C.2.7: Average ICS:ECS in percentage for samples in 2% NaCl solution (surface).

Dry (top)	Time *post mortem*		
	0 hour	6 hour	26 hours
ICS	87±4%	87±1%	91±3%
ECS	13±4%	13±1%	9±3%

Table C.2.8: Average ICS:ECS in percentage for samples in 2% NaCl solution (center).

Dry (top)	Time *post mortem*		
	0 hour	6 hour	26 hours
ICS	70±5%	79±5%	82±3%
ECS	30±5%	21±5%	18±3%

Table C.2.9: Average ICS:ECS in percentage for samples in saponin solution in 0.9%NaCl (surface).

Dry (top)	Time *post mortem*		
	0 hour	6 hour	26 hours
ICS	83±3%	73±4%	70±2%
ECS	17±3%	27±4%	30±2%

Table C.2.10: Average ICS:ECS in percentage for samples in saponin solution in 0.9%NaCl (center).

Dry (top)	Time *post mortem*		
	0 hour	6 hour	26 hours
ICS	75±3%	77±2%	71±4%
ECS	25±3%	23±2%	29±4%

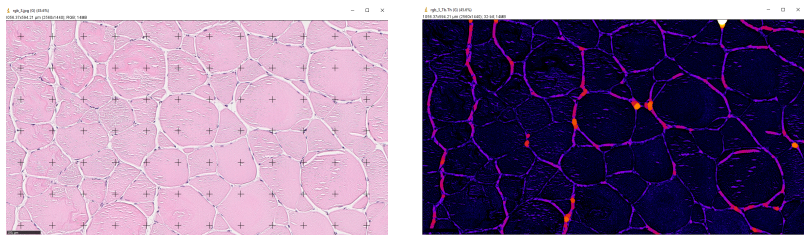

(a) (b)

Figure C.2.1: A graphic representation of using the (a) grid counting and (b) BoneJ plug-ins in ImageJ.

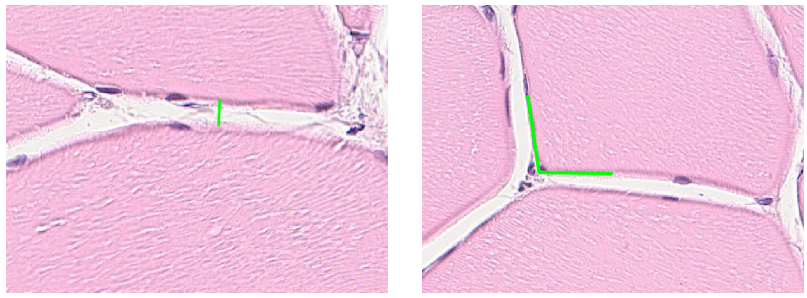

(a) (b)

Figure C.2.2: A graphic representation of using Matlab to calculate (a) cell to cell distance and (b) cell angle.

Appendix D

MatLab Codes

In this Appendix, MatLab codes used in morphology analysis and one-way ANOVA are presented. The code is divided in four different programs. The first program finds the area of ICS:ECS in the image while the next program calculates the cell-to-cell distance in the image. The third program calculates the cell angles in the image, while the last explains how one-way ANOVA statistics work. A brief explanation of the idea behind the code is given first and then the code used is shown.

D.1 Program 1: Finding the Area of ICS:ECS

This program first reads in the image as RGB (R = Red, G = Green, B = Blue) (Figure D.1.1a) and transforms it into gray scale image (Figure D.1.1b).

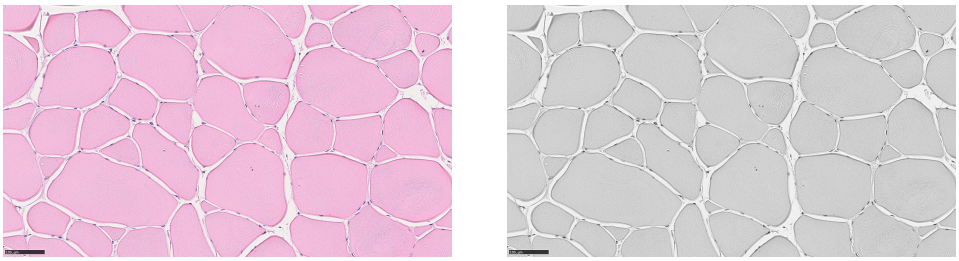

(a) RGB image (b) Gray scale image

Figure D.1.1: RGB image transformed to gray scale image.

Since only the area of ICS:ECS is calculated, it means that only two pixel intensities are needed (0 and 1). Therefore the gray scale image can be further reduced to a

binary image. To do so some few steps need to be done. The next step is to plot the gray scale image into an intensity histogram. The intensity value of the gray scale image is from 0 to 255. A function in MatLab called `imhist` makes this plot, where the x-axis is intensity of the gray pixels while the y-axis is the frequency of intensity of the gray pixel. The intensity histogram is shown in Figure D.1.2.

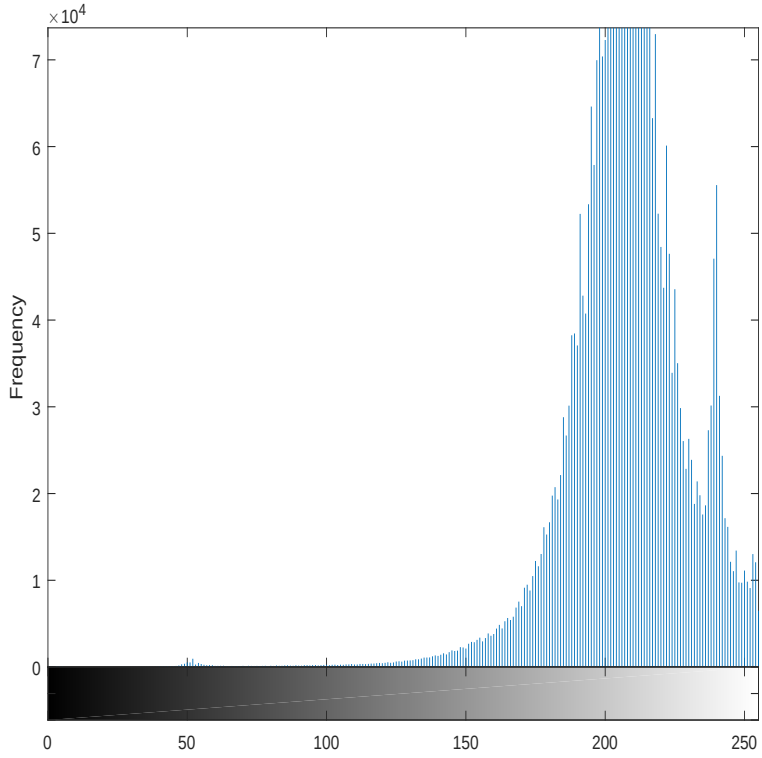

Figure D.1.2: Intensity histogram of the gray scale image.

As it can be seen from Figure D.1.2, there are two clear peaks and a valley with a bottom at around intensity 234. So a good threshold for separating the background pixel (the black pixels) and foreground pixel (the white pixel) will be at around intensity 234 in this image. The method used is a visual global threshold of the image. Furthermore, the background pixels are the ICS and foreground pixels ECS. The intensity histogram in Figure D.1.3 shows where the threshold line is set.

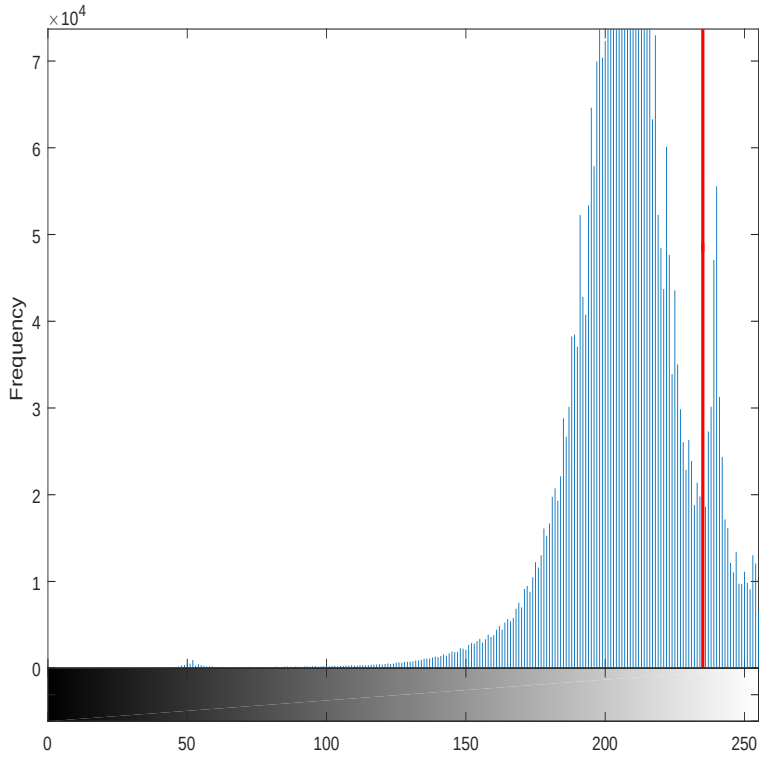

Figure D.1.3: Intensity histogram of the gray scale image with threshold line.

The gray scale image has its threshold at intensity 234, where the intensity from 0 to 234 are background pixel (black = 0, ICS) and intensity from 235 to 255 are foreground pixel (white = 1, ECS). The resulting binary is shown in Figure D.1.4a.

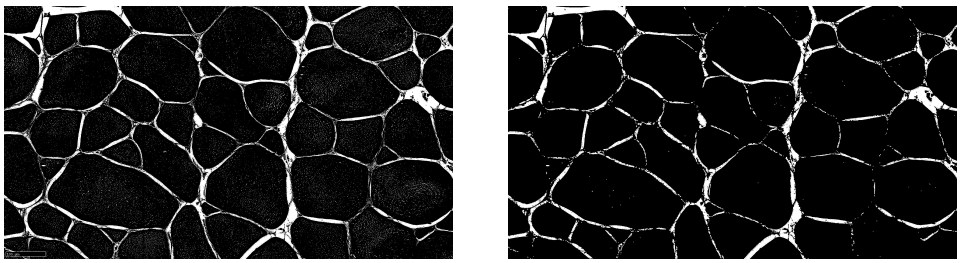

(a) Binary image without morphology

(b) Binary image with morphology

Figure D.1.4: Binary images with and without morphology

As it can be seen in Figure D.1.4a, the image contains of small white pixel holes within the cells. To reduce these holes inside the cell, an image morphology opera-

tion called opening is used. The morphology opening operation is mathematically expressed as follow

$$I \circ S = (I \ominus S) \oplus S$$

where I is the image and S is the structure element. The opening first does erosion on the image followed by dilation on the already eroded image. The result of the opening operation is shown in Figure D.1.4b. It can clearly be seen that the small white pixel holes has been reduced in the cells while the white ECS spaces around the cells remain. The structure element used for erosion and dilation is as follow

$$S = \begin{array}{|c|c|c|} \hline 1 & 1 & 1 \\ \hline 1 & \textcircled{1} & 1 \\ \hline 1 & 1 & 1 \\ \hline \end{array}$$

where the circled center pixel is the origin. Erosion makes the center pixel to 0 if the structure element does not fit with a 1 in the image pixel. Dilation changes the center pixel to 1 if the structure element hits a 1 in the image pixel.

The implemented code in MatLab for finding area of ICS:ECS is given below

```
clear; close all; clc; warning off;

% Display the plot as full screen
scrsz = get(groot, 'ScreenSize');
fig = figure('OuterPosition', [scrsz(1) scrsz(2) scrsz(3) scrsz(4)], 'PaperUnits', 'in', 'PaperPosition
      ', [0 0 10 10]);

% Initialize the values
array_output_one = 0; array_output_two = 0;

% Loop through the number of images
for i = 1:11

    % Make filename i
    filename = 'rgb_'; filename = strcat(filename, num2str(i)); filename = strcat(filename, '.jpg');

    RGB = imread(filename);    % Read in the image into MatLab (RGB = Red, Blue, Green)
    figure; imshow(RGB);       % Show the RGB image in MatLab

    % Make the RGB image into gray scale image
    gray_scale = 0.3*RGB(:,:,1) + 0.59*RGB(:,:,2) + 0.11*RGB(:,:,3);

    figure; imshow(gray_scale);   % Show the gray scale image in MatLab
    figure; imhist(gray_scale);   % Show intensity histogram of gray scale

    % Make the intesity histgram full screen
    ScrSize = get(0,'ScreenSize'); set(gcf,'Units','pixels','Position',ScrSize);

    % ginput is an in-build function in MatLab where points can be selected with the mouse on the image
    % and the function returns the position in x-direction and y-direction. In this case one position
    % will be returned due to ginput(1). Only the x-position is interesting since this gives the
    % threshold value and will be selected between 0-255. Put the threshold value between to valleys
    [threshold,~] = ginput(1);

    % Make filename for storing the gray scale image
    output = 'gray_'; output = strcat(output, num2str(i)); output = strcat(output, '.jpg');

    % Store the gray scale image
    imwrite(gray_scale, output); hold on;

    % Draw threshold line
    t = 0:255; plot(threshold+0*t, 1000*t, 'r', 'linewidth', 2); ylabel('Frequency'); hold on;

    % Make filename for storing the intensity histogram plot of the gray scale image
    output = 'gray_histogram_'; output = strcat(output, num2str(i));
```

```
    % Store the intensity histogram plot of the gray scale image
    print(output, '-depsc', '-r300');

    [row, col, colour] = size(RGB);  % Find the size of RGB image
    bw = false(row,col);             % Initialize an empty binary matrix

    % Loop through the row and column of the RGB image to make it into a binary image. The threshold
    % is found from intensity histogram of gray scale with MatLab in-build function ginput(1)
    for y = 1:1:row
        for x = 1:1:col
            if 0.3*RGB(y,x,1) + 0.59*RGB(y,x,2) + 0.11*RGB(y,x,3) < threshold
                bw(y,x) = 0;
            else
                bw(y,x) = 1;
            end
        end
    end

    [w1, b1] = count_muscle(bw);    % Function counting the white and black pixels
    figure; imshow(bw);             % Shows the binary image in MatLab

    % Store the counted percentage of white and black pixels
    if array_output_one == 0;
        array_output_one = [w1; b1];
    else
        tmp = [w1; b1]; array_output_one = [array_output_one tmp];
    end

    % Make filename for storing the binary image
    output = 'bw1_'; output = strcat(output, num2str(i)); output = strcat(output, '.jpg');

    % Store the binary image
    imwrite(logical(bw), output);

    % Use a technique morphology in image processing called opening
    % which contains of erosion with following dilation

    s = ones(3,3);          % Making structuring element for erosion and dilation
    bw = imerode(bw, s);    % Using the in-build function in MatLab imerode
    bw = imdilate(bw,s);    % Using the in-build function in MatLab imdilate

    [w2, b2] = count_muscle(bw);    % Function counting the white and black pixels
    figure; imshow(bw);             % Show the binary image after morphology operations

    % Store the counted percentage white and black pixels after morphology operations
    if array_output_two == 0;
        array_output_two = [w2; b2];
    else
        tmp = [w2; b2]; array_output_two = [array_output_two tmp];
    end

    % Make filename for storing the binary image after morphology operations
    output = 'bw2_'; output = strcat(output, num2str(i)); output = strcat(output, '.jpg');

    % Store the binary image after morphology operations
    imwrite(logical(bw), output);

end

% Store the counted white and black pixel of all images in an excel file
filename = 'data.xlsx'; out = [array_output_one; array_output_two];
xlswrite(filename, out);
```

```
function [percent_white, percent_black] = count_muscle(bw)

    % Take a binary image as input
    % Count the number of white and black pixels in the binary image
    % Return the percent of white pixels and percent of black pixels

    [row, col] = size(bw);

    count = 0;

    for y = 1:row
        for x = 1:col
            if bw(y,x) == 1
                count = count + 1;
            end
        end
    end

    total = row*col;
    white_pixels = count;
    black_pixels = total - white_pixels;

    percent_white = (white_pixels / total) * 100;
    percent_black = (black_pixels / total) * 100;

end
```

D.2 Program 2: Finding the Cell-to-Cell Distance

This program first reads in the image as RGB (Figure D.2.1a) and the user manually crops the image (Figure D.2.1b) to make it easier to select two points for measuring the distance.

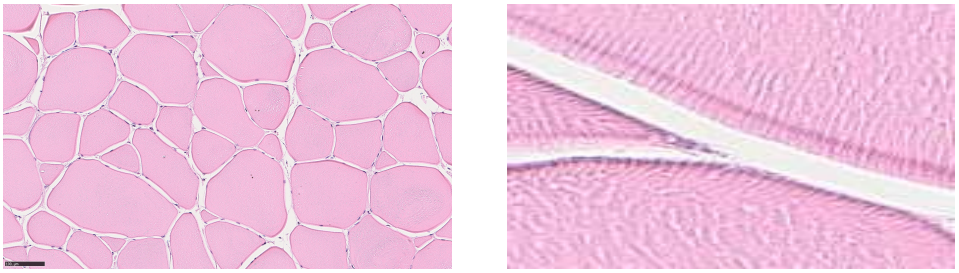

(a) Original image (b) Cropped image

Figure D.2.1: Original and cropped image to find inter-fibre distance

MatLab's in-build function `ginput(2)` makes it possible to pick two points in the image. The function returns the x-direction and y-direction for the two points. The distance is drawn into the image as a green line and can be shown in Figure D.2.2a. Furthermore two points (x_1, y_1) and (x_2, y_2) are made in to easier illustrate how the distance is calculated.

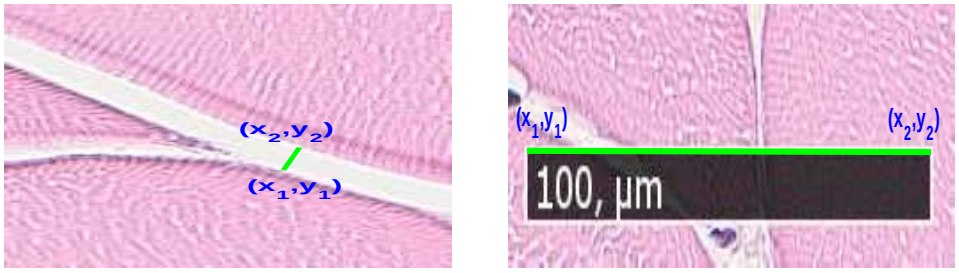

(a) Pick two point and draw a line (b) Measuring the distance of 100 µm

Figure D.2.2: Matlab procedure to measure inter-fibre distance

The Euclidean distance is calculated with the following formula

$$d = \sqrt{(x_2 - x_1)^2 + (y_2 - y_1)^2}$$

where d is the distance. To measure the distance in micro meter the distance of 100 µm was found to be around 228 with the formula above. This gives 1 µm $\approx$ 2.3. So to get the distance in micro meter the original length is divided by 2.3 µm.

The implemented code in MatLab for finding distance between the cells is given below

```
clear; close all; clc; warning 'off';

% Initialize the value
store_dis_micro_meter = 0; all_distance = 0;

% Read in the RGB image into MatLab (R = Red, B = Blue, G = Green)
RGB = imread('rgb_5.jpg');

% Loop through the image five times to find different distance
% First crop the image and then click with the mouse two times on the image
% where the distance would like to be measured
for i = 1:5

    figure; imshow(RGB);            % Show the RGB image
    im = imcrop(RGB); imshow(im);   % Crop the RGB image smaller

    % Make the cropped picture full screen
    ScrSize = get(0,'ScreenSize'); set(gcf,'Units','pixels','Position',ScrSize);

    % ginput is an in-build function in MatLab where points can be selected with the mouse on the image
    % and the function returns the position in x-direction and y-direction. In this case two
    % different positions will be returned due to ginput(2).
    [x,y] = ginput(2);

    % Calculate the Euclidean distance between the two points
    distance = sqrt( (x(2)-x(1))^2 + (y(2)-y(1))^2 );

    % Plot the distance line on the image
    hold on; plot(x, y, 'g', 'linewidth', 3);

    % Store all the distances that is found during the five iterations
    if all_distance == 0
        all_distance = distance;
    else
        all_distance = [all_distance distance];
    end

end

% Print the five distances found
all_distance

% Calculate the mean and standard deviation of the five distances
avg_dis = mean(all_distance)
std_dis = std(all_distance)

% One micro meter was measured as distance 2.3 and
% that gives the following micro meter distance
avg_micro_meter = avg_dis / 2.3
std_micro_meter = std_dis / 2.3
```

D.3 Program 3: Finds the Angle of Cells

This program first reads in the image as RGB (Figure D.3.1a) and then the user manually crops the image (Figure D.2.1b) to make it easier to select three points for measuring the angle.

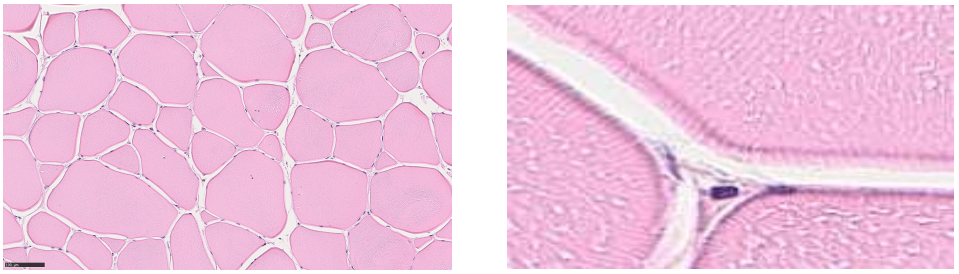

(a) Original image (b) Cropped image

Figure D.3.1: Original and cropped image to find cell angles

MatLab's in-build function `ginput(3)` makes it possible to choose three points in the image. The function returns the x-direction and y-direction for the three selected points. The angle is drawn into the image as a green lines and can be seen in Figure D.3.2.

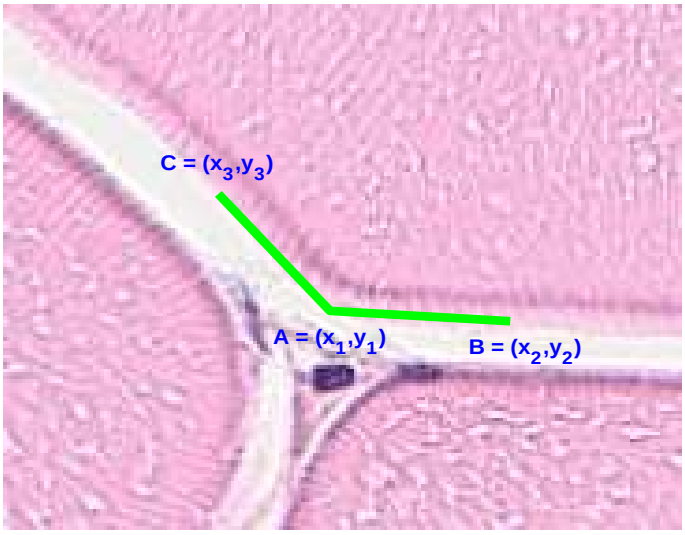

Figure D.3.2: Matlab procedure to measure cell angle

The interested angle to measure is the angle marked A and it can be seen in Figure D.3.2 and is equivalent to Figure D.3.3. From Figure D.3.3, it is possible to find the

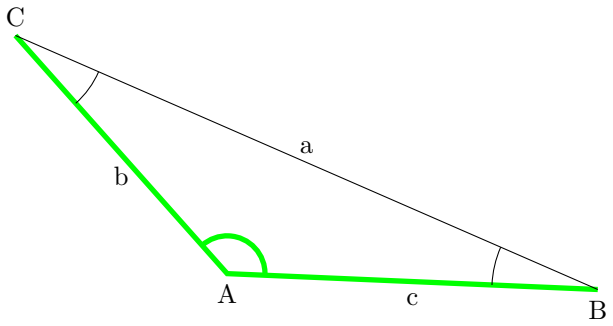

Figure D.3.3: A sketch to simplify the use of the law of cosines where the interesting angle A is emphasized with green angle sketch

distances a, b and c. Distances a, b and c are calculated by the Euclidean distance as follow

$$a = \sqrt{(x_3 - x_2)^2 + (y_3 - y_2)^2}$$
$$b = \sqrt{(x_3 - x_1)^2 + (y_3 - y_1)^2}$$
$$c = \sqrt{(x_2 - x_1)^2 + (y_2 - y_1)^2}$$

where (x_1, y_1), (x_2, y_2) and (x_3, y_3) are the points selected in the image and return by the function `ginput(3)`. Since all the distances are known, the law of cosines can be used as follow to find angle A

$$A = \arctan\left(\frac{b^2 + c^2 - a^2}{2bc}\right)$$

which is of interest. MatLab gives A in radians and therefore A has to be multiplied by (180 / π) to convert it to degrees. The two other angles are also calculated to check that the sum of the angles A, B and C adds up to 180 degrees. The formula used for calculating the two other angles are for angle B

$$B = \arctan\left(\frac{a^2 + c^2 - b^2}{2ac}\right)$$

and for angle C

$$C = \arctan\left(\frac{a^2 + b^2 - c^2}{2ab}\right)$$

The implemented code in MatLab for finding the angles of the cells is given on the next page.

```
clear; close all; clc; warning off;

% Initialize the value
store_angle = 0; all_angle = 0;

% Read in the RGB image into MatLab (R = Red, B = Blue, G = Green)
RGB = imread('rgb_5.jpg');

% Loop through the image five times to find different angles
% First crop the image and then click with the mouse three times on the image
% Important to place the first click at the corner and make the two next
% clicks away from the corner. The angle in between will be stored
for i = 1:5

    figure; imshow(RGB);            % Show the RGB image
    im = imcrop(RGB); imshow(im);   % Crop the RGB image smaller

    % Make the cropped picture full screen
    ScrSize = get(0,'ScreenSize'); set(gcf,'Units','pixels','Position',ScrSize);

    % ginput is an in-build function in MatLab where points can be selected with the mouse on the image
    % and the function returns the position in x-direction and y-direction. In this case three
    % different position will be returned due to ginput(3).
    [x,y] = ginput(3);

    dx = [x(2) x(1) x(3)];  % Store the coordinate point in x-direction in an array
    dy = [y(2) y(1) y(3)];  % Store the coordinate point in y-direction in an array

    % Plot the angle lines on the image
    hold on; plot(dx, dy, 'g', 'linewidth', 4);

    % Calculate the Euclidean distance between the two points
    a = sqrt( (x(3)-x(2))^2 + (y(3)-y(2))^2 );
    b = sqrt( (x(3)-x(1))^2 + (y(3)-y(1))^2 );
    c = sqrt( (x(2)-x(1))^2 + (y(2)-y(1))^2 );

    % Use the law of cosines to calculate the angles and times with (180/pi) to get angles in degrees
    A = acos((b^2 + c^2 - a^2) / (2*b*c)) * (180/(pi));
    B = acos((a^2 + c^2 - b^2) / (2*a*c)) * (180/(pi));
    C = acos((a^2 + b^2 - c^2) / (2*a*b)) * (180/(pi));

    % Output the angles
    out = [A B C]

    % Store all the angles that is found during the five iterations
    % Note that it is only the angle between the shown lines that will be stored
    if all_angle == 0
        all_angle = A;
    else
        all_angle = [all_angle A];
    end

end

% Print the five angles found
all_angle

% Find the mean and standard deviation between the five angles
avg_angle = mean(all_angle)
std_angle = std(all_angle)
```

D.4 Program 4: One-Way ANOVA

Analysis of variance (ANOVA) is useful to compare three or more means for statistical significance. This statistical analysis is relevant to this thesis since there were more than two groups of samples. One-way ANOVA is used as there was only one independent variable analysed each time in the dimension measurements.

Algorithm for One-Way ANOVA

Step 1: Set up one way ANOVA hypotheses

- $\mathrm{H}_0 : \mu_1 = \mu_2 = \mu_3 = \cdots = \mu_k$
- H_a : At least one difference among the means

Step 2: Find the degrees of freedom (df)

- $\mathrm{df}_{\mathrm{between}} = \mathrm{k} - 1$, where k are the amount of sample groups
- $\mathrm{df}_{\mathrm{within}} = \mathrm{N} - \mathrm{k}$, where N are the total amount of samples and k is as above
- $\mathrm{df}_{\mathrm{total}} = \mathrm{df}_{\mathrm{between}} + \mathrm{df}_{\mathrm{within}}$

Step 3: Calculate $\mathrm{SS}_{\mathrm{total}}$, $\mathrm{SS}_{\mathrm{within}}$ and $\mathrm{SS}_{\mathrm{between}}$

- $\mathrm{SS}_{\mathrm{total}} = \sum_{i=1}^{M} \sum_{j=1}^{N} (x_{ij} - \bar{\bar{x}}))^2$, where $\bar{\bar{x}}$ is the mean of all samples
- $\mathrm{SS}_{\mathrm{within}} = \sum_{i=1}^{M} \sum_{j=1}^{N} (x_{ij} - \bar{x}_i))^2$, where $\bar{x}_i$ are the group mean of the samples
- $\mathrm{SS}_{\mathrm{between}} = \mathrm{SS}_{\mathrm{total}} - \mathrm{SS}_{\mathrm{within}}$

Step 4: Calculate $\mathrm{MS}_{\mathrm{within}}$ and $\mathrm{SS}_{\mathrm{between}}$

- $\mathrm{MS}_{\mathrm{within}} = \frac{\mathrm{SS}_{\mathrm{within}}}{\mathrm{df}_{\mathrm{within}}}$
- $\mathrm{MS}_{\mathrm{between}} = \frac{\mathrm{SS}_{\mathrm{between}}}{\mathrm{df}_{\mathrm{between}}}$

Step 5: Calculate F

- $\mathrm{F} = \frac{\mathrm{MS}_{\mathrm{between}}}{\mathrm{MS}_{\mathrm{within}}}$

Step 6: Find $\mathrm{F}_{\mathrm{critical}}$ and $\mathrm{P}_{\mathrm{value}}$ from tables

- Find $\mathrm{F}_{\mathrm{critical}}(\alpha, \mathrm{df}_{\mathrm{between}}, \mathrm{df}_{\mathrm{within}})$, where $\alpha = 0.05$
- Find $\mathrm{P}_{\mathrm{value}}(\mathrm{F}, \mathrm{df}_{\mathrm{between}}, \mathrm{df}_{\mathrm{within}})$

Step 7: Check for significance

- If $\mathrm{F} < \mathrm{F}_{\mathrm{critical}}$, the null hypothesis H_0 fails to be rejected and there is no significant difference between the means $\mu_1 = \mu_2 = \mu_3 = \cdots = \mu_k$.

– Else the null hypothesis H_0 can be rejected and the alternative hypothesis H_a is significant.

Step 8: Print out to screen

– $F_{critical}$, F and p-value

The implemented code of one-way ANOVA in MatLab is shown below.

```
clear; close all; clc;

% Reads in the data from Excel
data = xlsread('p_value.xlsx', 'trial 1 mass');
samples = data(1:4,2:5);

[row, col] = size(samples);

%% Step 1: Set up one way ANOVA hypotheses
str1 = 'H_0: \mu_1 = \mu_2 = \mu_3 = \mu_4';
str2 = 'H_a: At least one difference among the means';

%% Step 2: Find the degrees of freedom (df)
df_between = col-1;
df_within = row*col - col;

df_total = df_between + df_within;

%% Step 3: Calculate SS_total, SSwithin and SS_between
mean_groups = mean(samples);        % group mean of the samples
mean_total = mean(mean(samples));   % the mean of all samples

SS_total = 0;

for i = 1:col
    for j = 1:row
        SS_total = SS_total + (samples(j,i) - mean_total)^2;
    end
end

SS_within = 0;

for i = 1:col
    for j = 1:row
        SS_within = SS_within + (samples(j,i) - mean_groups(i))^2;
    end
end

SS_between = SS_total - SS_within;

%% Step 4: Calculate MS_within and MS_between
MS_between = SS_between / df_between;
MS_within = SS_within / df_within;


%% Step 5: Calculate F
F = MS_between / MS_within;

%% Step 6: Find F_critical and P_value from tables
F_critical = finv(0.95,df_between,df_within);
p = 1-fcdf(F,df_between,df_within);

%% Step 7: Sum up hypotheses
if F < F_critical
    str3 = 'Fail to reject null hypotheses and there are no significant among the means';
else
    str3 = 'Reject null hypotheses. There are significant among the means';
end

%% Print result
str4 = '                    df          SS                  MS';
str5 = ['Between      ' num2str(df_between)  '       ' num2str(SS_between) '      ' num2str(MS_between)];
str6 = ['Within         ' num2str(df_within) '      ' num2str(SS_within) '      ' num2str(MS_within)];
str7 = ['Total           ' num2str(df_total) '      ' num2str(SS_total)];

str8 = 'F_{critical}            F               P';
str9 = [num2str(F_critical) '      ' num2str(F) '      ' num2str(p)];

annotation('textbox', [0 0 1 1], 'String',{str1, str2, '', str3, '', str4, ...
            str5, str6, str7, '', str8, str9}, 'FontSize',11, 'FontName','Arial', ...
            'EdgeColor',[1 1 1], 'LineWidth',2, 'BackgroundColor',[1 1 1], 'Color',[0 0 0]);
```

Comparing the Matlab program with Excel in-build one-way ANOVA gives the same results (Figure D.4.1).

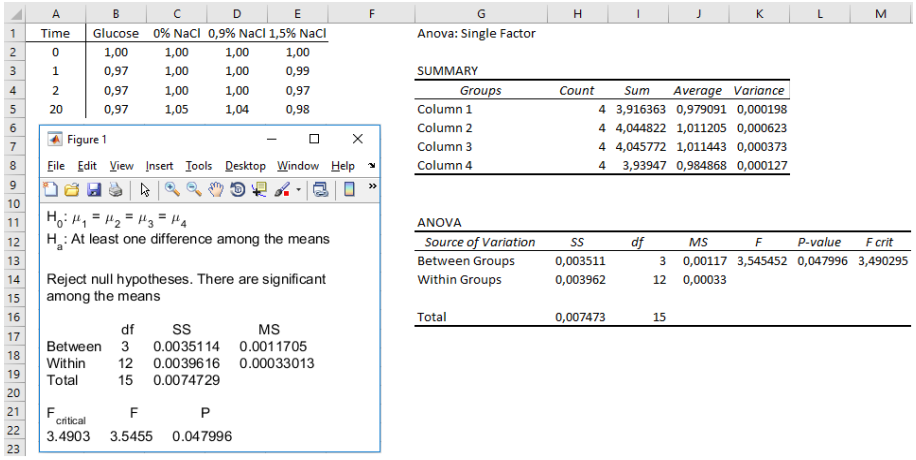

Time	Glucose	0% NaCl	0,9% NaCl	1,5% NaCl
0	1,00	1,00	1,00	1,00
1	0,97	1,00	1,00	0,99
2	0,97	1,00	1,00	0,97
20	0,97	1,05	1,04	0,98

Figure 1

File Edit View Insert Tools Desktop Window Help

H_0: $\mu_1 = \mu_2 = \mu_3 = \mu_4$

H_a: At least one difference among the means

Reject null hypotheses. There are significant among the means

	df	SS	MS
Between	3	0.0035114	0.0011705
Within	12	0.0039616	0.00033013
Total	15	0.0074729	

$F_{critical}$	F	P
3.4903	3.5455	0.047996

Anova: Single Factor

SUMMARY

Groups	*Count*	*Sum*	*Average*	*Variance*
Column 1	4	3,916363	0,979091	0,000198
Column 2	4	4,044822	1,011205	0,000623
Column 3	4	4,045772	1,011443	0,000373
Column 4	4	3,93947	0,984868	0,000127

ANOVA

Source of Variation	*SS*	*df*	*MS*	*F*	*P-value*	*F crit*
Between Groups	0,003511	3	0,00117	3,545452	0,047996	3,490295
Within Groups	0,003962	12	0,00033			
Total	0,007473	15				

Figure D.4.1: Comparison of one-way ANOVA with MatLab code and Excel in-build solver.

Bibliography

Abbott, J., Lu, R., Upchurch, B., and Stroshine, R. (1997). Technologies for non-destructive quality evaluation of fruits and vegetables. *Horticulture Reviews*, 20:1–120.

Andersen, U., Strømsnes, A., Steinsholt, K., and Thomassen, M. (1994). Fillet gaping in farmed atlantic salmon (*Salmo salar*). *Norwegian Journal of Aquaculture Sciences*, 8:165–179.

Andersen, U., Thomassen, M., and Rora, A. (1997). Texture properties of farmed rainbow trout (*Oncorhynchus mykiss*): Effect of diet, muscle fat content and time of storage on ice. *Journal of Food Agriculture*, 74:347–353.

Ando, M., Toyohara, H., Shimizu, Y., and Sakaguchi, M. (1991). Post-mortem tenderization of fish muscle proceeds independently of resolution of rigor mortis. *Nippon Suisan Gakkaishi*, 57(6):1165–1169.

Andreassen, I. (2012). Gentle and rapid handling gives best salmon fillet. `http://nofima.no/en/nyhet/2012/11/gentle-and-rapid-handling-gives-best-salmon-fillet/`. Accessed: 22 February 2016.

Astruc, T. (2014). Connective tissue: structure, function and influence on meat quality. *Encyclopedia of Meat Science*, pages 321–328.

Balevik, S. B. (2004). Slaktetemperaturens innvirkning på drypptap og muskelforkorting i filet fra oppdrettet atlantisk laks (*Salmo salar L.*) og hvite muskelfibrer sin morfologi før og under rigor. Master's thesis, University of Bergen.

Balevik, S. B., Botha, S., Hoffman, L., and Slinde, E. (2004). The effect of intramuscular water fluid transport on rigor mortis. In *50th International Congress of Meat Science and Technology*. ICoMST.

Baumgarten, C. and Feher, J. (2001). *Cell Physiology Source Book (Third Edition) A Molecular Approach*. Elsevier Inc.

Bear, R. and Rintoul, D. (2014). Musculoskeletal system. `http://cnx.org/contents/emTaI81m@7/Musculoskeletal-System#fig-ch38_04_05`. Accessed: 21 February 2016.

Bendall, J. (1973). Post mortem changes in muscle. *Structure and function of muscle*.

Bertram, H., Purslow, P., and Andresen, H. (2002). Relationship between meat structure, water mobility and distribution: A low-field nuclear magnetic resonance study. *Journal of Agricultural and Food Chemistry*, 50(4):824–829.

Bito, M., Yamada, K., Mikumo, Y., and Amano, K. (1983). Studies on rigor mortis of fish: I. difference in the mode of rigor mortis among some varieties of fish by modified cutting's method. *Bulletin of Tokai Regional Fisheries Research Laboratory*, 109:89–96.

Bonnet, M., Ouali, A., and Kopp, J. (1992). Beef muscle osmotic pressure as assessed by differential scanning calorimetry (dsc). *International Journal of Food Science and Technology*, 27:399–408.

Brading, A. and Setekleiv, J. (1968). The effect of hypo- and hypertonic solutions on volume and ion distribution of smooth muscle of guinea pig taenia coli. *Journal of Physiology (Oxford, United Kingdom)*, 195:107–118.

Cappeln, G. and Jessen, F. (2002). Atp, imp and glycogen in cod muscle at onset and during development of rigor mortis depend on the sampling location. *Journal of Food Science*, 67(3):991–995.

Carroll, P. (1969). The effect of hypertonic solution on the wet weight and contractions of rat uterus and vas deferens. *Journal of General Physiology*, 53(5):590–607.

Casas, C., Martinez, O., Guillen, M. D., Pin, C., and Salmeron, J. (2006). Textural properties of raw atlantic salmon (*Salmo salar*) at three points along the fillet, determined by different methods. *Food Control*, 17:511–515.

Chatterjee, S. (2014). Artefacts in histopathology. *Journal of Oral and Maxillofacial Surgery*, 18:111–116.

Cheng, J. H., Sun, D. W., Han, Z., and Zeng, X. A. (2014). Texture and structure measurements and analyses for evaluation of fish and fillet freshness quality: A review. *Comprehensive Reviews in Food Science and Food Safety*, 13:52–61.

Currie, R. and Wolfe, F. (1979). Relationship between ph fall and initiation of isotonic contraction in post mortem beef muscle. *Canadian Journal of Animal Science*, 59:639–647.

Currie, R. W. and Wolfe, F. H. (1980). Rigor related changes in mechanical properties (tensile and adhesive) and extracellular space in beef muscle. *Journal of Meat Science*, 4:123–143.

Deike, J. (2014). Is farmed salmon safe to eat? *EcoWatch*.

Devine, C., Wahlgren, N., and Tornberg, E. (1999). Effect of rigor temperature on muscle shortening and tenderisation of restrained and unrestrained beef *m. longissimus thoracicus et lumborum*. *Meat Science*, 51:61–72.

Dikeman, M. and Devine, C. (2014). *Encyclopedia of Meat Sciences*. Elsevier Inc.

Einen, O., Mørkøre, T., Rørå, A., and Thomassen, M. (1999). Feed ration prior to slaughter - a potential tool for managing product quality of atlantic salmon (*Salmo salar*). *Aquaculture*, 178:149–169.

Einen, O., Waagan, B., and Thomasse, M. (1998). Starvation prior to slaughter in atlanic salmon (*Salmo salar*) i. effects on weight loss, body shape, slaughter-and fillet-yield, proximate and fatty acid composition. *Aquaculture*, 166:85–104.

ElMasry, G., Barbin, D., Sun, D. W., and Allen, P. (2012). Meat quality evaluation by hyperspectral imaging technique: an overview. *Critical Reviews in Food Science and Nutrition*, 52(8):689–711.

Erikson, U., Kjørsvik, E., Bardal, T., Digre, H., Schei, M., Søreide, T. S., and Aursand, I. G. (2016). Quality of atlantic cod frozen in cell alive system, air-blast and cold storage freezers. *Journal of Aquatic Food Product Technology*.

FAO (2014). Report highlights growing role of fish in feeding the world. *Food and Agriculture Organization of the United Nations*.

Gonzalez-Fandos, E., Villarino-Rodriguez, A., Garcia-Linares, M., Garcia-Arias, M., and Garcia-Fernandez, M. (2005). Microbiological safety and sensory characteristics of salmon slices processed by the sous vide method. *Food Control*, 16:77–85.

Guignot, F., Vignon, X., and Monin, G. (1993). Post mortem evolution of myofilament spacing and extracellular space in veal muscle. *Meat Science*, 33:333–347.

Haard, N. (1992). Control of chemical composition and food quality attributes of cultured fish. *Food Research International*, 25 (4):289–307.

Hall, J. (2016). *Guyton and Hall Textbook of Medical Physiology, 13th Edition*. Elsevier Inc.

Heffron, J. and Hegarty, P. (1974). Evidence for a relationship between atp hydrolysis and change in extracellular space and fibre diameter during rigor development in skeletal muscle. *Comparative Biochemistry and Physiology*, 49A:43–56.

Høgåsen, H. R. (1998). *Physiological Changes Associated with the Diadromous Migration of Salmonids*. National Research Council of Canada.

Hill, R. W., Wyse, G. A., and Anderson, M. (2012). *Animal Physiology: Third Edition*. Sinauer Associates, USA.

Honikel, K., Roncales, P., and Hamm, R. (1983). The influence of temperature on shortening and rigor onset in beef muscle. *Meat Science*, 8:221–241.

Huff-Lonergan, E. and Lonergan, S. (1999). Postmortem mechanisms of meat tenderization: The roles of the structural proteins and the calpain system. *Quality Attributes of Muscle Foods*, pages 229–251.

Huff-Lonergan, E. and Lonergan, S. (2005). Mechanisms of water-holding capacity of meat: The role of postmortem biochemical and structural changes. *Meat Science*, 71:194–204.

Hultin, H. O. (1984). Postmortem biochemistry of meat and fish. *Journal of Chemical Education*, 61(4):289.

Hultmann, L. (2003). *Endogenous proteolytic enzymes - Studies of their impact on fish muscle proteins and texture*. PhD thesis, Norwegian University of Science and Technology.

Hultmann, L. and Rustad, T. (2002). Textural changes during iced storage of salmon (*Salmo salar*) and cod (*Gadus morhua*). *Journal of Aquatic Food Product Technology*, 11 (3/4):105–123.

Hyldig, G. and Nielsen, D. (2001). A review of sensory and instrumental methods used to evaluate the texture of fish muscle. *Journal of Texture Studies*, 32(3):219–242.

Johnston, I. A. (2001). *Muscle Development and Growth*. Gulf Professional Publishing.

Karahmet, E., Viles, A., Katica, A., Mlaco, N., and Toroman, A. (2014). Differences between white and red muscle fibers diameter in three salmon fish species. *Biotechnology in Animal Husbandry*, 30(2):349–356.

Kent, M., Oehlenschlager, J., Mierke-Klemeyer, S., Manthey-Karl, M., Knochel, R., Daschner, F., and Schimmer, O. (2004). A new multivariate approach to the problem of fish quality estimation. *Food Chemistry*, 87:531–535.

Kiessling, A., Johansson, L., and Kiessling, K. (1990). Effects of starvation on rainbow trout muscle. *Acta Agriculturae Scandinavica*, 40:309–324.

Kiessling, A., Larsson, L., Kiessling, K.-H., Lutes, P., Storebakken, T., and Hung, S. (1995). Spawning induces a shift in farmed rainbow trout white muscle energy metabolism from a glucose to a lipid dependence. *Fish Physiology and Biochemistry*, 14:439–448.

Kiessling, A., Ruohonen, K., and Bjørnevik, M. (2006a). Muscle fibre growth and quality in fish. *Archives Animal Breeding, Dummerstorf*, 49:137–146.

Kiessling, A., Stien, L. H., Torslett, i., Suontama, J., and Slinde, E. (2006b). Effect of pre- and post-mortem temperature on rigor in atlantic salmon muscle as measured by four different techniques. *Aquaculture*, 259:390–402.

Kobayashi, M., Ikegaya, H., Takase, I., Hatanaka, K., Sakurada, K., and Iwase, H. (2001). Development of rigor mortis is not affected by muscle volume. *Forensic Science International*, 117(3):213–219.

Kobayashi, M., Takemori, S., and Yamaguchi, M. (2004). Differential rigor development in red and white muscle revealed by simultaneous measurement of tension and stiffness. *Forensic Science International*, 140:79–84.

Korhonen, R. W., Lanier, T. C., and Giesbrecht, F. (1990). An evaluation of simple methods for following rigor development in fish. *Journal of Food Science*, 55(2):346–348.

Koteng, D. (1992). Markedsundersokelse, norsk laks. *Fiskerinæringsens Landsforening (FNL), Norway.*

Kristoffersen, S., Tobiassen, T., Esaiassen, M., Olsson, G. B., Godvik, L. A., Seppola, M., and Olsen, R. L. (2006). Effects of pre rigor filleting on quality aspects of atlantic cod (*Gadus morhua L.*). *Aquaculture Research*, 37:1556–1564.

Kristoffersen, S., Vang, B., Larsen, R., and Olsen, R. (2007). Pre rigor filleting and drip loss from fillets of farmed atlantic cod (*Gadus morhua L.*). *Aquaculture Research*, 38(16):1721–1731.

Listrat, A., Lebret, B.and Louveau, I., Astruc, T., Bonnet, M., Lefaucheur, L., Picard, B., and Bugeon, J. (2016). How muscle structure and composition influence meat and flesh quality. *The Scientific World Journal*, 2016:1–14.

Lucas, J. and Southgate, P. (2012). *Aquaculture: Farming Aquatic Animals and Plants, 2nd Edition.* Wiley-Blackwell.

Lynum, L. and Rustad, T. (2005). *Fisk som råstoff : holdbarhet og kvalitetssikring.* Tapir, Trondheim, Norway.

Macagano, A., Careche, H., Herrero, A., Paolesse, R., Martinelli, E., Pennazza, G., Carmona, P., D'Amico, A., and Di Natale, C. (2005). Model to predict fish quality from instrumental features. *Sensors and Actuators B: Chemical*, 111:293–298.

Marine Harvest, . (2015). Salmon farming industry handbook 2015. Technical report, Marine Harvest.

Martin, R. E. and Flick, G. J. (1990). *The Seafood Industry.* Springer Science Business Media New York.

Martinez, I., Bang, B., Hatlen, B., and Blix, P. (1993). Myofibrilar proteins in skeletal muscle of parr, smolt and adult atlantic salmon (*Salmo salar L.*) – comparision with another salmonid, the arctic charr, *Salvelinus alpinus L. Comparative Biochemistry and Physiology*, 106B:1021–1028.

Martinez, I., Christiansen, J., Ofstad, R., and Olsen, R. (1991). Comparison of myosin isoenzymes present in skeletal and cardiac muscle of the arctic charr, salvelinus alpinus, (l.). sequential expression of different myosin heavy chains during development of fast white skeletal muscles. *European Journal of Biochemistry*, 195:743–753.

Mascheroni, R. (2012). *Operations in Food Refrigeration.* Taylor and Francis Group LLC.

McCormick, R. and Phillips, A. (1999). Muscle extracellular matrix: Role in

growth, development and meat tenderness. *Quality Attributes of Muscle Foods*, pages 219–227.

McCormick, S. D., Farrel, A. P., and Brauner, C. (2013). *Fish Physiology: Euryhaline Fishes, 1st Edition*. Academic Press.

Möller, A. (2007). Seafood proceedings - local sources, global markets. In *Globalisation and Fisheries: Proceedings of an OECD-FAO Workshop*, pages 87–92.

Mørkøre, T. (2002). *Texture, fat content and product yield of salmonids*. PhD thesis, Agricultural University of Norway.

Mørkøre, T. and Einen, O. (2003). Relating sensory and instrumental texture analyses of atlantic salmon. *Journal of Food Science*, 68(4):1492–1497.

Mørkøre, T. and Rørvik, K. A. (2001). Seasonal variations in growth, feed utilization and product quality of farmed atlantic salmon (*Salmo salar*) transferred to seawater as 0+ smolts or 1+ smolts. *Aquaculture*, 199:145–157.

Mørkøre, T., Ruohonen, K., and Kiessling, A. (2009). Variation in texture of farmed atlantic salmon (*Salmo salar L.*). relevance of muscle fibre cross-sectional area. *Journal of Texture Studies*, 40:1–15.

Nowacek, J. (2010). *Special Stains and H&E*. Dako North America.

Nuss, J. and Wolfe, F. (1981). Effect of post mortem storage temperatures on isometric tension, ph, atp, glycogen and glucose-6-phosphate for selected bovine muscles. *Meat Science*, 5:201–213.

Oplatka, A. (1994). The role of water in the mechanism of muscular contraction. *FEBS Letters*, 355:1–3.

Ouali, A. (1990). Meat tenderization: Possible causes and mechanisms. *Journal of Muscle Foods*, 1:129–165.

Rahman, M. S. (2007). *Handbook of Food Preservation, Second Edition*. CRC Press.

Rehbein, H. and Oehlenschlager, J. (2009). *Fishery Products: Quality, Safety and Authenticity*. Wiley Blackwell.

Riley, P. (2005). *Food Policy, Control and Research*. Nova Biomedical Books, New York.

Roth, B., Møller, D., Veland, J., and Slinde, E. (2002). The effect of stunning methods on rigor mortis and texture properties of atlantic salmon (salmo salar). *Journal of Food Science*, 67:1462–1466.

Sen, D. P. (2005). *Advances in Fish Processing Technology*. Allied Publishers.

Sigurgisladottir, S. (2001). *Textural and structural properties of fresh and smoked salmon (Salmo salar)*. PhD thesis, University of Bergen.

Sigurgisladottir, S., Hafsteinsson, H., Jonsson, A., Lie, O., Nortvedt, R., Thomassen, M., and Torrissen, O. (1999). Textural properties of raw salmon fillets as related to sampling method. *Journal of Food Science*, 64(1):99–104.

Sigurgisladottir, S., Torrisen, O., Lie, ., Thomassen, M., and Hafsteinsson, H. (1997). Salmon quality: Methods to determine the quality parameters. *Reviews in Fisheries Science*, 5(3):223–252.

Skare, E. (2015). Effect of ploidy and temperature on quality attributes of diploid versus triploid atlantic salmon (*Salmo salar L.*), and the effect of locality (north-south) and season (spring-autumn) for quality attributes under commercial protection. Master's thesis, Norwegian University of Life Sciences.

Skjervold, P. O., Fjæraa, S., Østbya, P., and Einenb, O. (2001). Live chilling and crowding stress before slaughter of atlantic salmon (*Salmo salar*). *Aquaculture*, 192(2-4):265–280.

Slinde, E., Roth, B., Balevik, S. B., Suontama, J., Stien, L., and Kiessling, A. (2003). The influence of intracellular osmorality on rigor mortis. In *49th International Congress of Meat Science and Technology., 2nd Brazilian Congress of Meat Science and Technology*, pages 135–136.

Slinde, E., Roth, B., and Torrissen, O. (2001). *Cold shortening and drip loss in Atlantic salmon (Salmo salar), Rainbow Trout (Oncorhynchus mykiss), Halibut (Hippoglossus hippoglossus), Cod (Gadus morhua), Haddock (Melanogrammus aeglefinus) and Saithe (Pollachius virens)*. Farmed Fish Quality.

Sänger, A. and Stoiber, W. (2001). *Muscle fibre diversity and placticity. In: Muscle developemnet and growth*. Academic Press, London.

Sørensen, N., Brataas, R., Nyvold, T., and Lauritzen, K. (1997). *Influence of early processing (pre rigor) on fish quality*. Elvesier Science B.V.

Srinivasan, M., Sedmak, D., and Jewell, S. (2002). Effect of fixatives and tissue processing on the content and integrity of nucleic acids. *American Journal of Pathology*, 161(6):1961–1971.

Stead, S. M. and Laird, L. (2002). *The Handbook of Salmon Farming*. Praxis Publishing Ltd, Chichester, UK.

Sévon-Aimonen, M.-L., Honkavaara, M., Serenius, T., Mäki-Tanilla, A., and Puonti, M. (2007). Genetic variation of loin and ham quality in finnish landrace and large white pigs. *Agricultural and Food Science*, 16:89–102.

Torgersen, J. S., Koppang, E. O., Stien, L. H., Kohler, A., Pedersen, M. A., and Mørkøre, T. (2014). Soft texture of atlantic salmon fillets is associated with glycogen accumulation. *PLOS One*, 9 (1):1–7.

Toyohara, H. and Shimizu, Y. (1988). Relation of the rigor mortis of fish body and the texture of the muscle. *Nippon Suisan Gakkaishi*, 54:1795–1798.

Travlos, G. (2006). Normal structure, function, and histology of the bone marrow. *Toxicologic Pathology*, 34(5):548–565.

Tsuchimoto, M., Yamaga, T., Lee, K. H., Wu, Z., Misima, T., and Tachibana, K. (1998). The influence of Ca^{2+} concentration around myofibrillar Ca^{2+} -atpase on the speed and pattern of rigor mortis in fish species or cultured and wild fish. *Fisheries science*, 64(1):148–154.

Tsuchiya, H., Kita, S., and Seki, N. (1992). Postmortem changes in alpha-actinin and connectin in carp and rainbow trout muscles. *Bulletin of the Japanese Society of Scientific Fisheries (Japan).*

Veiseth, E., Shackelford, S., Wheeler, T., and Koohmaraie, M. (2004). Indicators of tenderization are detectable by 12 h postmortem in ovine longissimus. *Journal of Animal Science*, 82(5):1428–36.

Veland, J. and Torrisen, O. J. (1999). The texture of atlatic salmon (*Salmo salar*) muscle as measured instrumentally using tpa and warner-brazler shear test. *Journal of the Science of Food and Agriculture*, 79 (12):1737–1746.

Verma, S., Khare, D., Gupta, R., and Chandel, G. (2013). Analysis of image segmentation algorithms using matlab. *Proceedings of the Third International Conference on Trends in Information, Telecommunication and Computing*, pages 163–172.

Wang, D., Tang, J., Correia, L. R., and Gill, T. A. (1998). Postmortem changes of cultivated atlantic salmon and their effects on salt uptake. *Journal of Food Science*, 63 (4):634–637.

Werner, M., Chott, A., Fabiano, A., and Battifora, H. (2000). Effect of formalin tissue fixation and processing on immunohistochemistry. *The American Journal of Surgical Pathology*, 24(7):1016–1019.

Winger, R. and Pope, C. (1980). Osmotic properties of post-rigor beef muscle. *Meat Science*, pages 355–369.

Xiong, Y. L., Ho, C., and Fereidoon, S. (1999). *Quality Attributes of Muscle Foods.* Springer Science Business Media New York.

Zayas, J. F. (1997). *Functionality of Proteins in Food.* Springer-Verlag Berlin Heidelberg.